Power Assist Robot Design Inspired by Biological Control and Actuation Mechanisms

生物の制御と操作メカニズムに学ぶ パワーアシストロボットの設計

A Doctoral Dissertation Submitted to
The Department of Electrical Engineering
for the Degree of Doctor of Philosophy

by

Valerio Salvucci

Supervisors

Professor Yoichi Hori
Professor Hiroshi Fujimoto

Department of Electrical Engineering
The University of Tokyo
June 2011

Abstract

The objective of this work is to design new control strategies to improve safety, robustness, smoothness in human-robot interaction and performances such as speed response, maximum and precision end effector force production for power assist robots.

Power assist robots are rising in interest for three main reasons. Power assist devices increase performances such as muscle strength and endurance for workers, wild land firefighters, and soldiers. Power assist devices support elderly and disabled people. Rehabilitation process and physical training carried out with the use of power assist devices have been shown to be faster, more intense, more motivational via audiovisual feedback and game mode, and easier reproducible do to quantitative outcome measurements.

Although big progresses have been done in recent years, there are still three main challenging aspects where more investigation and innovative solutions are needed: safety for the user and the surrounding environment, a more comfortable interaction in a human-friendly way, increase in performances such as response, force production and energy efficiency.

Most of the ongoing researches focus on mechanical and control design with a pure engineering approach, neglecting the inspiration from nature. Biologically inspired robotics is a process that goes beyond merely copying what nature shows at first sight. It involves three phases: observation and understanding nature, design robots embedding the desired nature functionalities, and finally implementation and development. Understanding humans and animal functionalities and the consequent implementation on robot applications has shown to improve robot performances such as robustness, safety, and flexibility in a variety of complex dynamic tasks. In order to improve performances of power assist robots, in this work biological motion control and actuation mechanism of humans and animals play the inspirational roles.

Regarding the biological inspiration for motion control, humans and animals high vary impedance of their body to stabilize unstable dynamics. On the basis of this a new approach to force control for power assist devices — Force Sensor-less Power Assist Control (FSPAC) with Variable Impedance —

is proposed. The proposed FSPAC with Variable Impedance is successfully implementation on an experimental door actuated by either a linear motor (low friction stem) or by a rotational motor and a balls-crew (high friction system). Comparison with traditional FSPAC is carried out. The superiority of the proposed FSPAC with Variable Impedance in respect to the traditional FPAC with Constant Impedance, in terms of safety, robustness and smooth assistance are experimentally shown.

As for the biological inspiration for actuation mechanism design, humans and animals presents bi-articular muscles — muscles that span joints — which play a fundamental role for mechanical energy transfer, impedance modulation and stabilization of human and animal dynamics. In the design of bi-articularly actuated robots, our focus is on the resolution of the redundancy actuation. Two new approaches — the Infinity Norm and the Non Linear Phase Different Control (NLPDC) — are proposed. A human-like actuated robot named BiWi — Bi-articularly actuated Wi-re driven robot arm — is developed and used as an experimental apparatus to compare the two proposed redundancy resolution approach with the three traditional approaches — Phase Different Control (PDC), Pseudo inverse matrix, and Linear Programming.

The proposed infinity norm approach allows the arm to produce greater end effector force compared the traditional pseudo-inverse matrix approach. The proposed infinity norm approach is suitable to increase the performances of any system with three inputs and two outputs. The NLPDC approach increases the output force precision compared to the PDC approach, and requires less computation compared with the Linear Programming approach. Moreover, the NLPDC allows the independent design of common and different modes for robot arms actuated by three pairs of antagonistic actuators, consisting of four mono- and two bi-articular actuators couple in antagonistic pairs. In addition, the NLPDC approach is the only method capable of calculating in a precise way at the maximum output force that can be produce at the end effector of a bi-articularly actuated robot arm given the desired output force direction, with a closed form equation.

Acknowledgements

Valerio Salvucci (バレ)

"Look deep into nature,
then you will understand everything better"
– Albert Einstein –

Hori-Fujimoto lab 2009/2010

Contents

List of Figures

List of Tables

Chapter 1

Introduction

1.1 Background in Power Assist Robots

Power assist robots are devices which provide assistance to humans in order to accomplish a certain task. There are three main reasons why power assist robots are developed:

1. Increasing performances such as muscle strength and endurance for workers in health-care centers and hospitals, wild land firefighters, disaster relief workers, soldiers, heavy labour factories, and in any other emergency situation

2. Supporting elderly and disabled people

3. Providing support in rehabilitation processes and physical training

Examples of power assist robots designed to increase human performances are shown in Fig. 1.1.

On of the first power assist robots designed to help the user in carrying heavy loads is the Berkeley Lower Extremity Exoskeleton (BLEEX), developed at U.C. Berkeley (Fig. 1.1(a)). BLEEX is designed to increase the wearer strength and endurance. It is composed of two actuated robotic legs, on which a backpack is attached. The power unit consist of a hybrid power source that supply the hydraulics of the robotic legs and an electric power that supply the exoskeleton computer [133].

The HULC (Fig. 1.1(b)), Human Universal Load Carrier, is a hydraulic-powered anthropomorphic exoskeleton realized by Lockheed Martin Corporation. As its name suggest, it is used to assist the user in carrying heavy loads (up to 90 Kg) for extended periods of time and over all terrains. It is designed so to provide load-carrying ability, and works even when power is

(a) BLEEX   (b) HULC   (c) XOS 2

(d) PLL   (e) KAIT   (f) Salford University

Figure 1.1: Power assist robots designed to increase humans performances such as muscle strength and endurance

not available. By using HULC, the stress caused by heavy loads on on the body leading to potential injuries is reduced.

The XOS 2 exoskeleton (Fig. 1.1(c)) is wearable suit powered by high pressure hydraulics realized by Raytheon. It allows the user therein to lift upwards of 98 Kg, several hundred times without growing tired pressure hydraulics.

The Power Loader Light (Fig. 1.1(d)) is a power amplifying robotic suit to augment human strength developed by Panasonic Activelink. Differently from the BLEEX, HULC and XOS, it is powered by motors that respond to the movements of the operator via six-axis force sensors.

The stand-alone wearable power assist suit developed at Kanagawa Institute of Technology (KAIT, Fig. 1.1(e)) is powered by pneumatic actuators, and is meant to help workers in hospital and clinics to support and transfer

patients [48].

The ten-degree-of-freedom active lower limb robot (Fig. 1.1(f)) developed at Salford University is powered by pneumatic actuators. It is designed for force augmentation and active assisting walking training [15].

Examples of power assist robots designed for elderly or disabled support are shown in Fig. 1.2.

(a) Honda exoskeleton legs   (b) MIT   (c) Rex

Figure 1.2: Power assist robots designed for elderly/disable support

Honda's exoskeleton legs are designed to assist the users in supporting the body and reducing the load on the legs. The device is actuated by motors and powered by a lithium ion battery (Fig. 1.2(a)).

The MIT exoskeleton (Fig. 1.2(b)) is designed to be lighter and require less power than similar walking assist devices. It weights 11.7 kilograms and requires 2 watts of electrical power during loaded walking. The key aspect of its design is the attempt to exploit human-like passive dynamics for energy efficiency.

Rex, the Robotic Exoskeleton (Fig. 1.2(c)), is a pair of robotic legs developed by Rex Bionics. Rex is designed to allow the user to stand up and walk with the arms free, move sideways, turn around, go up and down steps.

Power assist robots designed to help people affected by orthoses are shown in Fig. 1.3. Devices to assist the knee joint are for example RoboKnee [89] developed by Yobotics (Fig. 1.3(a)), the robot developed at At Ecole Polytechnique Federale de Lausanne (EPFL)[105], or the smart portable rehabilitation device [20] (Fig. 1.3(b)). Other researches in which power assist

(a) RoboKnee   (b) Portable device
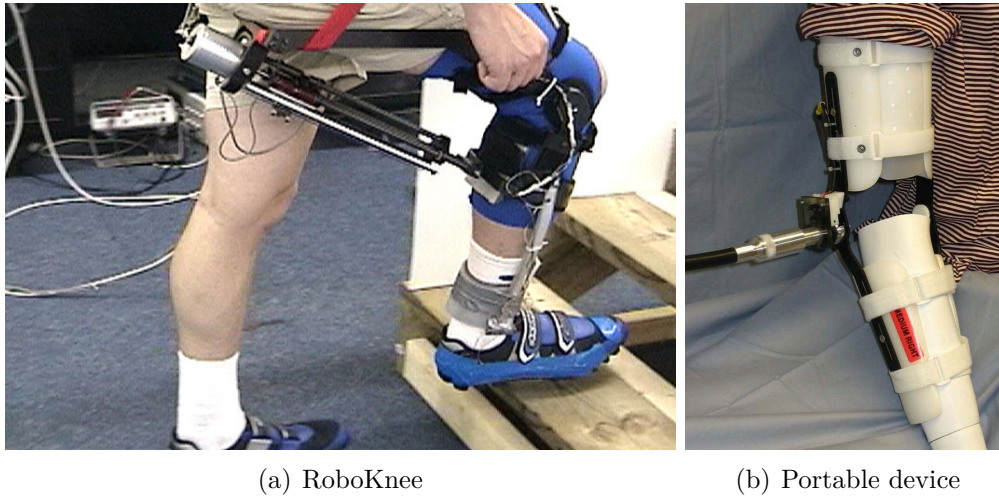
Figure 1.3: Power assist robots designed for orthosis

robots are developed to help people affected by orthoses are [7] [85] [94].

Power assist robots designed with rehabilitation and training purpose for upper and lower limb are shown in Fig. 1.4 and Fig. 1.5, respectively. Power assist robots to help in rehabilitation process of the whole forearm are the 3 DOFs robot developed at Saga University ([53]) for the shoulder and elbow, the Wilmington Robotic EXoskeleton, WREX (Fig. 1.4(a)) that is a light weight exoskeleton with two links and 4 DOFs that approximates normal human anatomy, Armin III [9] (Fig. 1.4(b)), MGA Exoskeleton [12] (Fig. 1.4(c)), and SUEFUL-6 [33], all with 6 active DOFs to assist the patient with shoulder, elbow, and wrist movements, and the KIST [51] and the upper limb multipurpose device developed at Salford University [119] both of which have 7 DOFs and pneumatic actuators. Power assist robots designed for only a part of the forearm are for example HEXORR, Hand EXOskeleton Rehabilitation Robot, HandSOME: Hand Spring Operated Movement Enhancer, and NEUROExos for the elbow [63], and the Smart portable elbow device [65].

Examples of power assist robots for low limb rehabilitation are the Lokomat (Fig. 1.5(a)) produced by Hocoma, and the KineAssist (Fig. 1.5(b)) developed by Kinea Design which are two therapeutic robotic partial body weight supporting treadmill based systems being used to improve patient walking abilities.

The Actively driven Leg EXoskeleton (ALEX) is a exoskeleton designed to help patients in walking rehabilitation [5].

(a) WREX
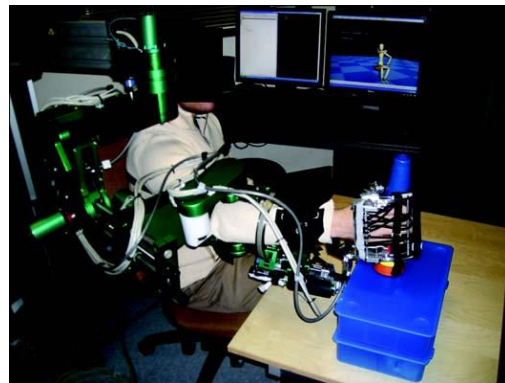
(b) Armin III

(c) MGA Exoskeleton

Figure 1.4: Power assist robots designed for rehabilitation for upper limb

(a) Lokomat

(b) KineAssist

(c) HAL

Figure 1.5: Power assist robots designed for rehabilitation for lower limb

The Robot Suit HAL (Fig. 1.5(c)) developed by Cyberdyne on the basis of The Hybrid Assistive Limb (HAL) is robot that can expand and improve physical capability. It is one of the most versatile power assist robot device as is expected to be applied in most of the field where power assistance is needed, such as rehabilitation support and physical training support in medical field, support for disabled people, heavy labour support at factories, and rescue support at disaster sites, as well as in the entertainment field.

1.2 Motivation

There are three main challenges in power assist robots:

- **Safety**: guarantee safety for the user and for the surrounding environment is probably the most challenging aspect in robot and human interaction. Under no circumstances a robot should cause harm to people in its surroundings, directly or indirectly, in regular operation or in failures [6]. From a robot control design point of view, the concept of safety is strongly related with robustness. In fact, if the robot behaviour becomes instable, then dangerous situations can occur.

- **Comfortable interaction**: humans being interacting with robots do not have to feel constrained. Power assist robots have to follow the used input in the most smooth and comfortable way.

- **Performances**: researches are moving towards the realization of always more compact and powerful devices, with a faster response as well energy efficiency.

The design of the power assist robots shown in Section 1.1 are based on mechanical and control design approaches mainly from an engineering point of view, and neglect the inspiration from nature.

Robots are fast and precise in known environment, but are not compliant nor flexible. In unknown environment robots are not robust nor safe. On the other hand, humans and animals are not as good as robots in position control and slow in computational capability, but are compliant, flexible and robust to external disturbances, even in complex dynamic tasks and unknown environments, as summarized in Tab. 1.2.

Understanding and implementing humans and animal functionalities into robot applications has shown to improve robot performances in terms of robustness, safety, and task flexibility in complex dynamic tasks such as walking [37] [75] running [77] walking over highly broken and irregular terrain

Table 1.1: Humans and robots characteristics

	Humans	Robots
Actuation	Complex (Redundancy)	Simple (1 actuator=1 joint)
Control strategy	Variable impedance	Position (mainly)
Flexibility	High	Low
Robustness	High	Low

[104] pronking [10] stair climbing [70] [69] flipping [103] vertical climbing [54] [102] and running on water [23] [24].

Our solutions to the challenges in control and hardware design for power assist robots is strongly inspired by human motion control strategy and musculo-skeletal structure:

1. **Variable impedance control strategy**: humans and animals highly vary impedance of their body to stabilize unstable dynamics, as is explained in details in Section 2.1. On the basis of such concept a new control design — Force Sensor-Less Power Assist Control (FSPAC) with Variable Impedance — is proposed and its validity is experimentally validated. FSPAC with Variable Impedance is designed in order to increase safety, provide a smoother assistance, and increase performances such as speed response of power assist robots, in particular the ones with the same (or lower, i.e. under-actuated) number of actuators and degree of freedom.

2. **Bi-articular muscles**: the role of bi-articular muscles — muscles that span two joints — is fundamental for mechanical energy transfer, impedance modulation and stabilization of human and animal dynamics, as is explained in details in Section 2.2. Due to these properties, bi-articular actuators increase safety and performances such as energy efficiency and actuator compactness in power assist robots. The presence of bi-articular actuators generally results in actuator redundancy. The resolution of the redundancy actuation is the first step in the control design of such devices, and therefore represent a crucial factor in achieving high performances. In this work we focus on the resolution of the actuator redundancy, proposing two new approaches — the Infinity Norm and the Non Linear Phase Different Control (NLPDC) — and compare them from a theoretical and experimental point of view with the three traditional approaches — Phase Different Control (PDC), Pseudo inverse matrix, and Linear Programming.

1.3 Flow Chart

The structure of this work is shown in Fig. 1.6. There are three main steps:
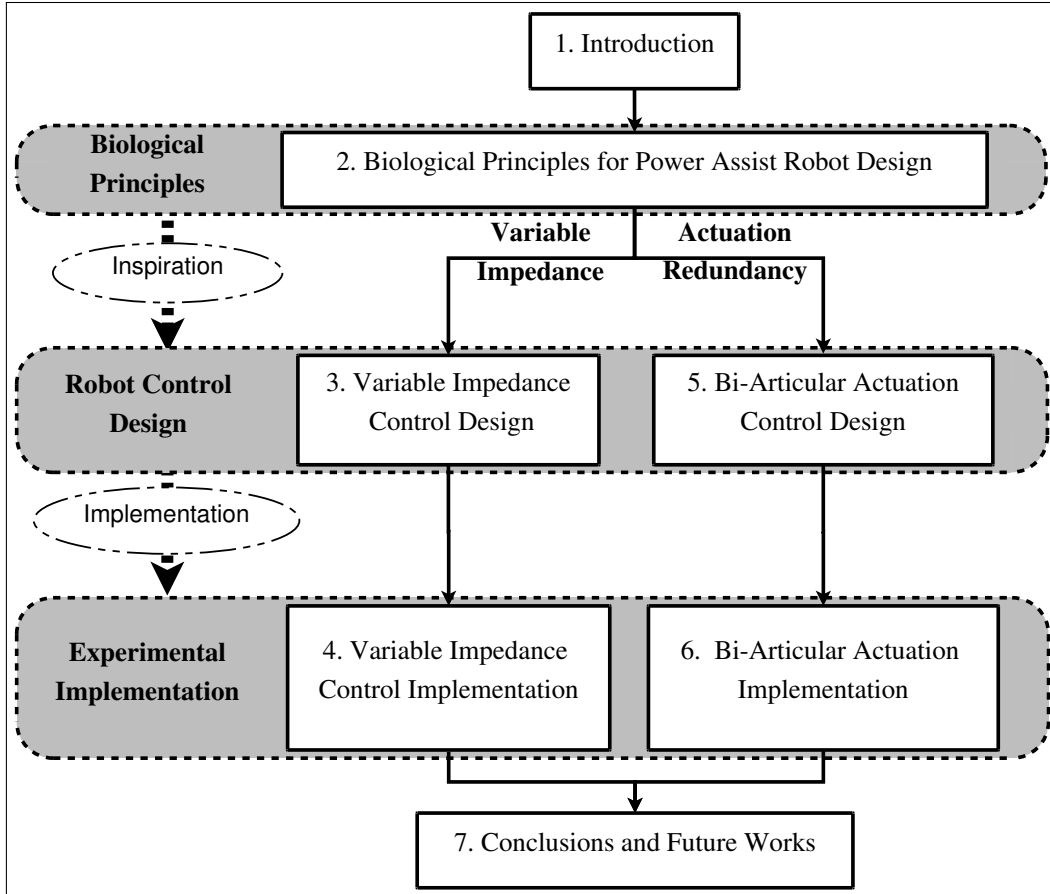
Figure 1.6: Thesis Flow Chart

1. **Biological inspiration**: the two biological principles inspiring the control and hardware design of power assist robots in this work are described in Chapter 2.

    The first principle is the variable impedance control strategy that humans and animals use to stabilize unstable dynamics illustrated in Section 2.1.

    The second principle is the redundancy in actuation of humans and animals, in particular the bi-articualr muscles — muscles that span two joints. The role of the bi-articular muscle is fundamental for mechanical energy transfer, impedance modulation and stabilization of human and animal dynamics, as explained in details in Section 2.2.

2. **Robot Control Design**: the robot design resulting from the two biological principles described in Chapter 2 represents the theoretical step at the basis of this work.

   On the basis of the variable impedance control strategy that humans use, a new approach to force control for power assist robots is proposed in Chapter 3. The proposed approach is referred as Force Sensor-less Power Assist Control (FSPAC) with Variable Impedance.

   The control design of bi-articular actuation for power assist robots is analyzed in Chapter 5. Bi-articularly actuated robots generally present more actuators that joints, resulting in actuator redundancy. The resolution of the redundancy actuation is the first step in the control design of such devices, and therefore represent a crucial factor in achieving high performances. In this work we focus on the resolution of the actuator redundancy, proposing two new approaches — the Infinity Norm and the Non Linear Phase Different Control (NLPDC).

3. **Experimental Implementation**: the implementation and validation of the proposed control strategies is the third step of this work.

   The proposed FSPAC with Variable Impedance is successfully implemented on an experimental door actuated by either a linear motor (low friction system) or by a rotational motor and a ballscrew (high friction system) in Chapter 4. A comparison with traditional FSPAC with constant impedance is carried out.

   The developed human-like actuated robot named **BiWi** — **Bi**-articularly actuated and **Wi**-re driven robot arm — is described in Chapter 6. BiWi is used as an experimental apparatus to compare the two proposed redundancy resolution approaches — the Infinity Norm and the Non Linear Phase Different Control (NLPDC) — with the three traditional approaches — Phase Different Control (PDC), Pseudo inverse matrix, and Linear Programming.

Finally, the improvements in safety, smooth human-robot interaction and performances such as compactness, speed response, and precision in output force brought by the proposed control approaches — FSPAC with Variable Impedance, and actuator redundancy resolution methods based on Infinity norm and NLPDC — are discussed in Chapter 7.

Regarding the variable impedance control design, the superiority of the proposed FSPAC with Variable Impedance in terms of safety, robustness, faster response and smoothness in assistance in respect to the traditional FSPAC with constant impedance is highlighted.

As for the actuator redundancy resolution approaches for bi-articular actuation control design, the proposed infinity norm approach superiority in terms of maximum force production in respect to the pseudo-inverse matrix approach is discussed. The Non Linear Phase Different Control increases the output force precision in respect to the Phase Different Control approach, and needs less computation in respect to the Linear Programming approach. Moreover, the NLPDC allows the independent design of common and different modes for robot arms actuated by three pairs of antagonistic actuators, that is four mono- and two bi-articular actuators couple in antagonistic pairs.

Chapter 2

Biological Principles for Power Assist Robot Design

The biological pronciples that inspired this work are described in the following. The fundamental roles playd by impedance control and by bi-articular muscles in human motion are analyzed in Secrtion 2.1 and 2.2, respectively.

2.1 The Role of Impedance Control in Human Motion

Humans are capable of performing complex task in a stable way, despite the fact that many of these, particularly those involving tool use, are inherently unstable [91]. The mechanical impedance, which depends on inertia, viscosity and stiffness, of the human musculo-skeletal system plays a fundamental role in stabilizing unstable dynamics.

The stiffness characteristics of a human hand were analyzed for the first time by Mussa-Ivaldi et al. in 1985 [72]. The human arm impedance depends on posture and muscle activation level [32] [43] [61] [117] [121]. As a consequence the co-contraction of antagonistic muscles allows the control of joint stiffness and therefore of the end effector stiffness geometry [40] [74].

Humans and animals highly vary their impedance and stiffness to stabilize unstable walking and running dynamics. For example, when humans encounter changes in terrain height, the adjustment of leg stiffness plays and important role to keep the body within the dynamically stable range [35]. For surfaces of lower stiffness, runners decrease leg spring compression by increasing leg stiffness [21] [22]. Other researches point out that leg stiffness increases with speed for an efficient running [2] [67], to accommodate higher stride frequencies [19], and to modulate gait frequency and propulsion energy

[55]. Moreover, adjustability of leg stiffness may be important in allowing the body's spring system to operate on the variety of terrain encountered in the natural world [55]. Researches on leg stiffness in hopping task conclude that active muscle stiffness contributes to the biomechanical stability and may contribute to the prevention of musculo-skeletal injury [34]. In addition, increase in stiffness relative to the increase in motor noise can be sufficient to reduce kinematic variability, allowing stiffness control to improve stability in natural tasks [106]. Human increases their impedance also to maintain limb stability in the presence of applied external forces [66] or in preparation of specific tasks as ball-catching [118].

Another key aspect in human and animal motion control is the fact that the central nervous system is not always involved in stabilizing unstable dynamics. When humans encounter changes in terrain height, the rapid adjustment of leg angle and stiffness keeps the body within the dynamically stable range [35]. This means that, even without further intervention by the brain, the runner would not fall [17]. Moreover, humans exhibit changes in leg stiffness before changes in muscle activity when they are surprised by a surface of different stiffness during hopping. Such a stiffness variation may be critical for adjustments to variable terrain encountered during locomotion in the natural world [71].

In summary, the following four points are highlighted as they represents the biological inspiration at the basis of the design of the proposed Force Sensor-less Power Assist Control with variable impedance (Section 3.2).

- Humans strongly vary their impedance and stiffness for stabilizing unstable dynamics

- Human increase their stiffness when tasks speed increase

- High impedance is used to stabilize posture

- Brain feedback is not always involved in motion control. As a consequence fast response to unexpected disturbances or unknown environmental conditions is crucial.

2.2 The Role of Bi-Articular Muscle in Human Motion

Animal and human limbs present a complex musculo-skeletal structure based on mono- and multi- articular muscles:

1. Mono-articular muscles produce torque about one joint.

2. Multi-articular muscles span more than one joint.

Examples of bi-articular muscles — muscles which span two consecutive joints — in the human body are the Gastrocnemius in leg (Fig. 2.1(a)) and the Biceps brachii in the arm (Fig. 2.1(b)).

(a) Gastrocnemius muscle   (b) Biceps brachii muscle
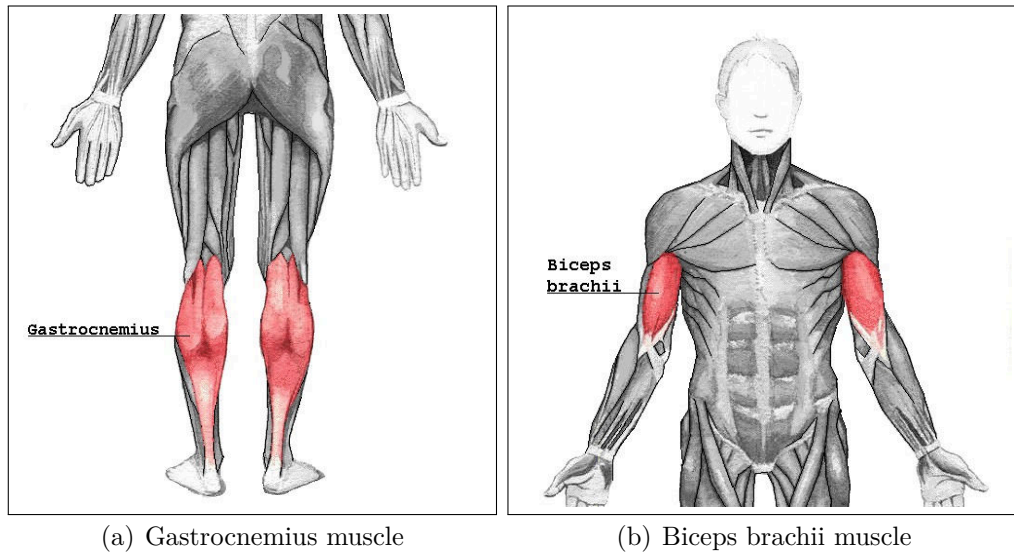
Figure 2.1: Bi-articular muscles examples in human limbs

An important role of the bi-articular muscles is the mechanical power transfer from proximal to distal joints.

The active muscles in four sequent positions during the push off in jumping are shown in Fig. 2.2(a). The acceleration of the body center of gravity in an upwards direction is initiated by the rotation of the trunk in the first two position (-330 ms and -190 ms), then antagonistic co-activation of the mono-articular hip extensor and the bi-articular Rectus femoris realize the transfer of mechanical power towards the distal joints. The coupling action of the bi-articular muscles as the Gastrocnemius can be demonstrated using a mechanical device as Jumping Jack (Fig. 2.2(b)). Jumping Jack can only move his body in the vertical direction. It has a spring as mono-articular knee extensor, which can be loaded with potential energy by pushing the trunk downwards. The Gastrocnemius is realized with wire. The length of the wire determines the knee angle at which the further knee extension is coupled to plantar flexion. Using the model it can be shown that timing of the bi-articular link activation and stiffness of the bi-articular link [3] considerably influence the height of the human jump. With an optimal length

(a) Active muscles in jumping   (b) Jumping Jack
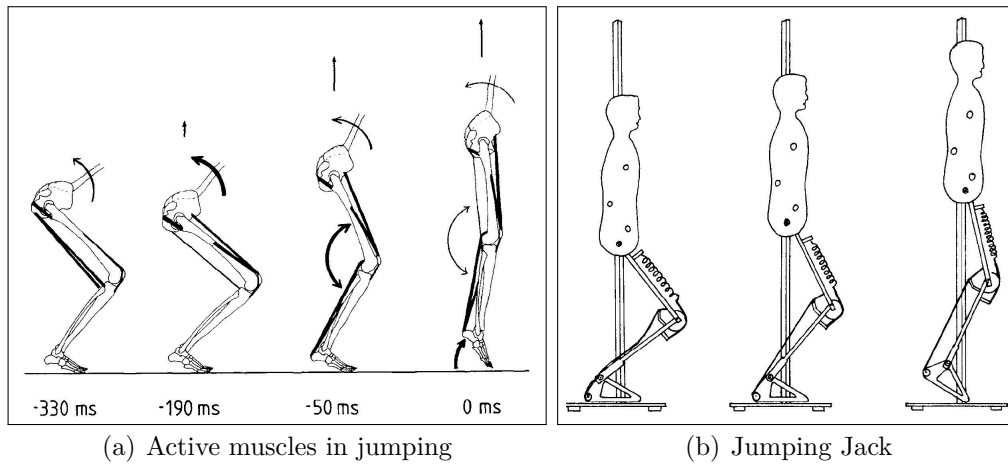
Figure 2.2: Bi-articular muscles mechanical transfer from proximal to distal joints [125]

of the bi-articular wire Jumping Jack can jump 26 cm, while only 14 cm without the bi-articular wire. The important role of bi-articular muscles in mechanical energy transfer between joints is also described in [50] [90] [127].

As second important role of the bi-articular muscles is the stiffness regulation without brain feedback. It has be shown that the pre-programmed activity for controlling the stiffness regulation by the bi-articular muscles increases the performance in drop jumps [41]. Moreover, bi-articular muscles dramatically increase the capabilities to realize impedance control without feedback at the end effector [40], which is critical for movement stability such as running over rough terrain [18] or to increase accuracy of movements [113].

Another key aspect of bi-articular muscles is the output force direction at the end effector. Mono-articular muscles produce a force directed in the direction of one of the segments (lengthwise direction). On the other hand bi-articular muscles can have a marked transverse component in the output force. Such a transverse component is also the movement direction of the endpoint which is the most favorable for the muscle to do work [38]. Moreover, bi-articular muscles appear primarily responsible for the control of the direction of the external force on the ground for humans [8] [49], as well for quadrupeds [126]. It has been also shown that the relative activation levels of the bi-articular Rectus femoris and hamstring muscles during the push-off phase of a jump play a key role in jump direction [30]. Another important consequence of the transverse component in the output force of bi-articular muscles is that the resulting maximum force at the end effector

is more homogeneously distributed in respect to the output force direction [25].

In summary, bi-articular muscles play critical role in human motion control:

- Transferring mechanical energy from proximal to distal joints

- Varying joint impedance in a feedforward way for disturbance rejection and movement stability

- Producing an end effector output force that is homogeneously distributed in respect to the direction and favorable for the muscle to do work

- Controlling the direction of ground force reaction for walking, running and jumping actions

Chapter 3

Variable Impedance Control Design

A key aspect in power assist robot control is the knowledge of the forces that the user and the environment apply on the device. Force sensors are often used to measure such forces despite their disadvantages such as cost, weight, and measurement time delay. Moreover, the force is sensed only if applied on the sensor itself, or on arigid body connected to it. These aspects can have significant impact on power assist devices performances and safety.

To overcome the disadvantages of force sensors, there are researches [14] [84] [98], in which the force to assist is estimated by using only encoders. The force is estimated by using force observer design, which is based on disturbances observer. Disturbance observer has been widely used as a robust control methodology [59] [62] [124]. Using this control design the devices are lighter, the force can be applied on any point of the device, there is no measurement delay. However the main problem of force sensor-less control is the robustness against plant uncertainties and inevitable modelling errors. To increase force sensor-less robustness approaches as learning process [1] or model independent force observer [68] have been proposed.

In this work, Force Sensor-less Power Assist Control (FSPAC) with a Variable Impedance is proposed to increase robustness and safety of power assist devices. The variable impedance is realized desiging the feedback gain with a triangular shape in respect to the measured velocity. The feedback gain is therefore referred in the following as Velocity-Dependant Triangular Gain (VD-TG). The design of the FSPAC with Variable Impedance is inspired by the concept of variable impedance higly used by humans and animals to accomplish task such as walking and running in a stable, smooth and robust way as pointed out in Section 2.1.

In Section 3.1 the general structure of FSPAC is illustrated. After that,

the proposed FSPAC with Variable Impedance is described in Section 3.2.

The proposed control design was successfully implemented on a door experimental apparatus actuated either by a high friction system such as a ballscrew [101] or by a low friction systems such as a linear motor [99], as described in Chapter 4.

3.1   General Structure of Force Sensor-Less Power Assist Control

The general structure of FSPAC is shown in Fig. 3.1 ([80]).
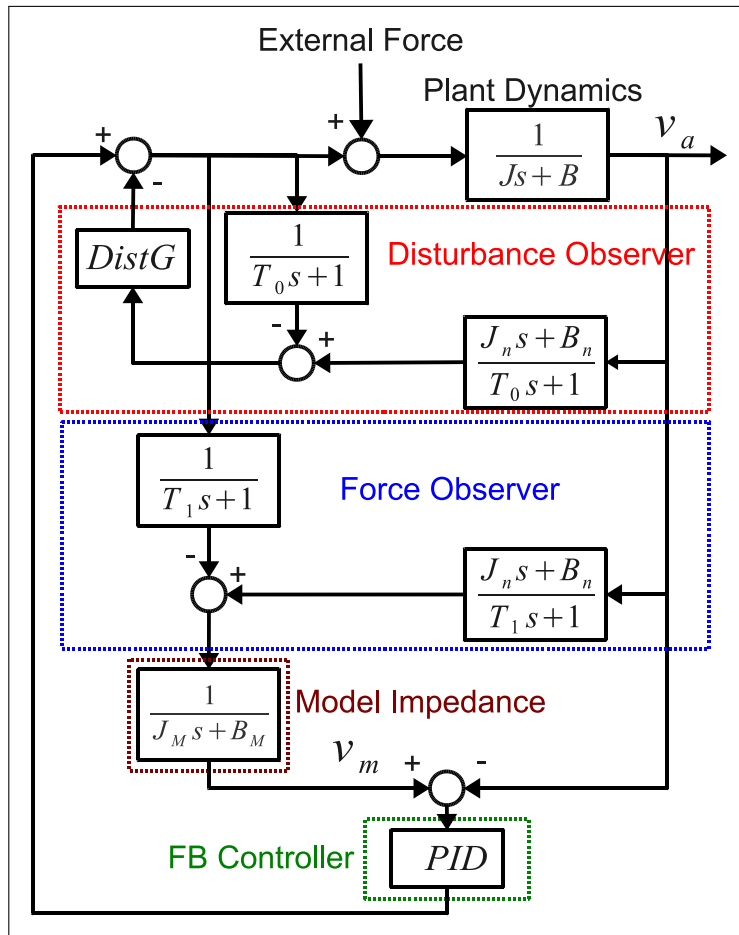
Figure 3.1: General Structure of FSPAC [80]

The real plant dynamics are represented by $\frac{1}{Js+B}$ where J is the inertia and B the damping factor. The system output is the actual velocity (v_a). This

aspect shows how FSPAC is different from typical force control. In force control implementation, the force value is controlled. On the other hand, in FSPAC states such as position or velocity are to be controlled. The controller is made of four main parts highlighted in Fig. 3.1 — the disturbance observer, the force observer, the model impedance, and the feedback gain — described in the following:

- The disturbance observer includes the inverted plant dynamics model, $\left(\frac{J_n s + B_n}{T_0 s + 1}\right)$ where J_n and B_n are respectively the nominal inertia and nominal damping factor, a low pass filter $\left(\frac{1}{T_0 + 1}\right)$, and a feedback gain (**DistG**). It is used to reject all the disturbances so that the real plant dynamics are as close as possible to the nominal model ones.

- The force observer includes the inverted plant dynamics model, $\left(\frac{J_n s + B_n}{T_1 s + 1}\right)$ and a low pass filter $\left(\frac{1}{T_1 + 1}\right)$. It is actually a disturbance observer, its name derives from its function that is to estimate the force to assist. It can also be integrated within the disturbance observer. That's the case in which T_0 is set to be the same as T_1.

- The model impedance $\left(\frac{1}{J_M s + B_M}\right)$ represents desired mechanical impedance of the controlled system. It is used to determine the model velocity (v_m), that is the desired velocity response of the controlled system. In order to assist (instead to reject) the disturbance estimated from the force observer, the impedance model is designed so that $B_M < B_n$ and $J_M < J_n$.

- The feedback gain is designed so that the actual velocity v_a tracks the model velocity v_m. A PID controller is generally used.

There are three signal paths through the real plant:

1. The external forces, from the user or the environment, which act directly on the plant.

2. The positive feedback loop through the model impedance and the feedback gain which aims to assist the user.

3. The negative feedback loop through the disturbance observer and its gain (**DistG**) used to reject disturbances.

Figure 3.2: Proposed FSPAC with VD-TG

The force/toque reference ($Ref_{F/T}$) sent to the plant from the controller is given by the last two paths:

$$Ref_{F/T} = (v_m - v_a)PID - (disturbance)DistG \qquad (3.1)$$

where the term *disturbance* includes the external forces and all the other disturbances, as for example modeling errors.

3.2 Proposed FSPAC with Variable Impedance

The structure of the proposed FSPAC with VD-TG is shown in Fig. 3.2.

In the proposed structure the same disturbance observer is used both to reject the disturbances and to determine the force to assist. The main difference in respect to FSPAC with constant impedance (Fig. 3.1) is the design of the feedback gain. Instead of the traditional PID controller, the feedback gain value in the proposed control varies in respect to the magnitude of the actual velocity ($|v_a|$).

Figure 3.3: Velocity-Dependant Triangular Gain Design

Table 3.1: Biological inspiration for the VD-TG

$|v_a|$	$|v_a| < |v_1|$	$|v_a| \approx |v_2|$	$|v_a| \to |v_3|$
VD-TG	0	high	decrease
System impedance	very high	low	increases
Biological motion control	high impedance for stability in unknown environment	low impedance in known environment and low velocity	stiffness increases with task speed

Before describing in detail the design of the VD-TG, it is opportune to consider how the reference torque ($Ref_{F/T}$) is given to the motor by the controller. From the block diagram in Fig. 3.2:

$$Ref_{F/T} = (v_m - v_a)VDTG - (disturbance)DistG \qquad (3.2)$$

Where VD-TG is the triangular gain value which depends on the magnitude of the actual velocity ($|v_a|$) in the way illustrated in Fig. 3.3. The biological principles inspiring the design of the VD-TG are summarized in Tab. 3.1 In the x-axis there is the magnitude of the actual velocity while on the y-axis there is the value of the VD-TG. A high value of the VD-TG means low impedance of the assisting system, and viceversa.

The VD-TG model design is based on 4 parameters ($VD-TGmax$, v_1, v_2, and v_3). These parameters are related to disturbance rejection, to how the user feels the device, as well to factors as friction and inertia as described in the following:

- v_1: *disturbance rejection velocity.* For $0 \leq |v_A| < v_1$ the value of the VD-TG is set to 0. This creates a sort of *dead zone* in which the estimated force/torque and disturbance are not assisted. The velocity at witch the friction function in respect to the velocity becomes linear is v_1. As a consequence, all the friction non linearities do not need to be modeled for the assisting control system. The low value of the VD-TG imply high impedance of the assisting system. Such a design was inspired by the fact that humans and animals increase their impedance to reject disturbances from undesired external forces [66], and in unmodeled environment as rough terrain [17] or in uncertain situations as the preparation of ball-catching [118].

- v_2: *velocity of maximum assistance.* v_2 is the velocity in witch the robot assisting system has a low kinetic energy and is accelerating to provide assistance or decelerating to stop. As a consequence, around v_2 a high assistance is needed to assist the user in accelerating the robot, or to avoid a too high deceleration of the system. On the basis of the experimental analysis the value of v_2 is about 8 to 10 times v_1.

- $VD-TGmax$: *maximum assistance.* This parameter is to be chosen as large as possible in order to highly assist the user around the velocity v_2 when system acceleration or smooth deceleration are needed, but not to large to avoid system instability. On the basis of the experimental analysis the value of $VD-TGmax$ is 1.4 to 2.4 times the value of the feedback P gain in the case of FSPAC with constant gain. At velocity close to v_2 the system has a low kinetic energy and the model of the plant is quite similar to the real plant. This resemble the fact that humans and animals, in contraposition to the high impedance shown in uncertain environment/situation, reduce their impedance in well known situations.

- v_3: *maximum allowed velocity.* The velocity after which the system does not provide anymore assistance is v_3. It is considered a dangerous velocity, at which the device does not have to operate. As the robotic assistance is less and less provided ad the system increases its velocity towards v_3, the safety for the user and for the environment is increased, as well system stability and robustness. The low value of the VD-TG, which correspond to an high impedance of the assisting system, is inspired by the fact that humans and animals show an increase of leg stiffness in running tasks to increase efficiency when speed increases [2] [67], and to stabilize unstable dynamics [17].

It is opportune to underline that, as the proposed FSPAC does not use force sensors, the system speed response is increased. This resembles the fundamental aspect of motion control in humans that is the absence of brain feedback when fast response to unexpected disturbances or unknown environmental conditions is needed [71].

Chapter 4

Variable Impedance Control Implementation

The proposed FSPAC with Variable Impedance control method is implemented on an experimental door actuated by either a linear motor (low friction system) or by a rotational motor and a ballscrew (high friction system).

In Section 4.1, the low friction (Section 4.1.1) and the high friction (Section 4.1.2) experimental apparatus systems are described together with the experimental methods (Section 4.1.3).

In Section 4.2 the experimental results are shown, and in Section 4.3 the improvements of the proposed FSPAC with Variable Impedance in terms of robustness, smothness in assistance and input tracking performances are discussed.

4.1 Experimental Setup

4.1.1 Low Friction Experimental Apparatus

The low friction experimental apparatus is shown in Fig. 4.1.

It represents a door, composed of a wooden and metal structure on which bricks are placed. The door is fixed to a join that rotates about an axis perpendicular to the ground (z-axis). The system has therefore one degree of freedom. The gravity is not considered due the fact that the door rotates on a plane perpendicular to the ground. The system is actuated by a linear motor through a link. The only sensor used is a linear encoder along the motor axis. Further experimental apparatus characteristics are shown in Tab. 4.1.

The system is modeled as in Fig. 4.2. The dashed (brown) lines represent the wooden bar of the door which can rotate about the z-axis. On the system

Figure 4.1: Low friction experimental apparatus

Table 4.1: Characteristic of low friction experimental apparatus

Linear Slider	SGT1F31–041AH20–0 (YASKAWA)
Linear Motor	SGLFW–35A120AP (YASKAWA)
Peak Force	220 N
Continuous Force	80 N
Wooden bar	0.75x0.1x0.027 m
Door weight	15 Kg

there are two main input forces — one is the external force applied by the user, and the other is the force applied by the linear motor on the end of link 2, F_{lm} in Fig 4.2. In order to estimate the external force, the value of the nominal inertia (J_n) in the inverted plant dynamics model $\left(\frac{J_n s + B_n}{T s + 1}\right)$ is considered constant in respect to the z-axis about which the door rotates. The torque applied about the z-axis caused by the force F is T_1 and is determined from the Jacobian of the system as follows. The Jacobian of the system is:

$$J = \begin{bmatrix} -l_1 sin(\theta_1) - l_2 sin(\theta_1 + \theta_2) & -l_2 sin(\theta_1 + \theta_2) \\ l_1 cos(\theta_1) + l_2 cos(\theta_1 + \theta_2) & l_2 cos(\theta_1 + \theta_2) \end{bmatrix} \quad (4.1)$$

As the linear motor force F_{lm} has a component only along the x-axis, $F_x = F_{lm}$
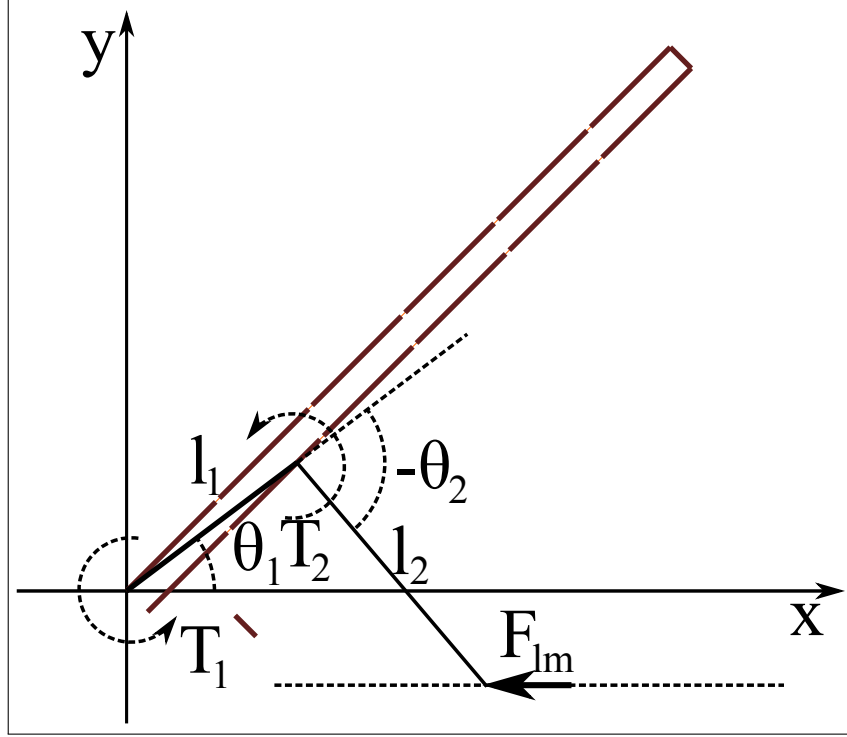
Figure 4.2: Low friction system model

and $F_y = 0$. Therefore:

$$
\begin{bmatrix} T_1 \\ T_2 \end{bmatrix} = J^T \begin{bmatrix} F_x \\ F_y \end{bmatrix}
$$

$$
= \begin{bmatrix} -l_1 S_1 - l_2 S_{12} & l_1 C_1 + l_2 C1_2 \\ -l_2 S1_2 & l_2 C_{12} \end{bmatrix} \begin{bmatrix} F_{lm} \\ 0 \end{bmatrix}
$$

$$
= \begin{bmatrix} (-l_1 S_1 - l_2 S_{12}) F_{lm} \\ (-l_2 S_{12}) F_{lm} \end{bmatrix} \tag{4.2}
$$

where $S_1 = sin(\theta_1)$, $C_1 = cos(\theta_1)$, $S_{12} = sin(\theta_1 + \theta_2)$ and $C_{12} = cos(\theta_1 + \theta_2)$.

4.1.2 High Friction Experimental Apparatus

The high friction experimental apparatus is shown in Fig. 4.3. The system is composed by the same door as for the low friction experimental apparatus, but it is actuated by an AC motor through a ballscrew system and a link. The only sensor used is the rotary encoder along the motor axis. Further experimental apparatus characteristics are shown in Tab. 4.2. The system is modeled as in Fig. 4.4. The dashed (brown) lines represent the wooden bar of
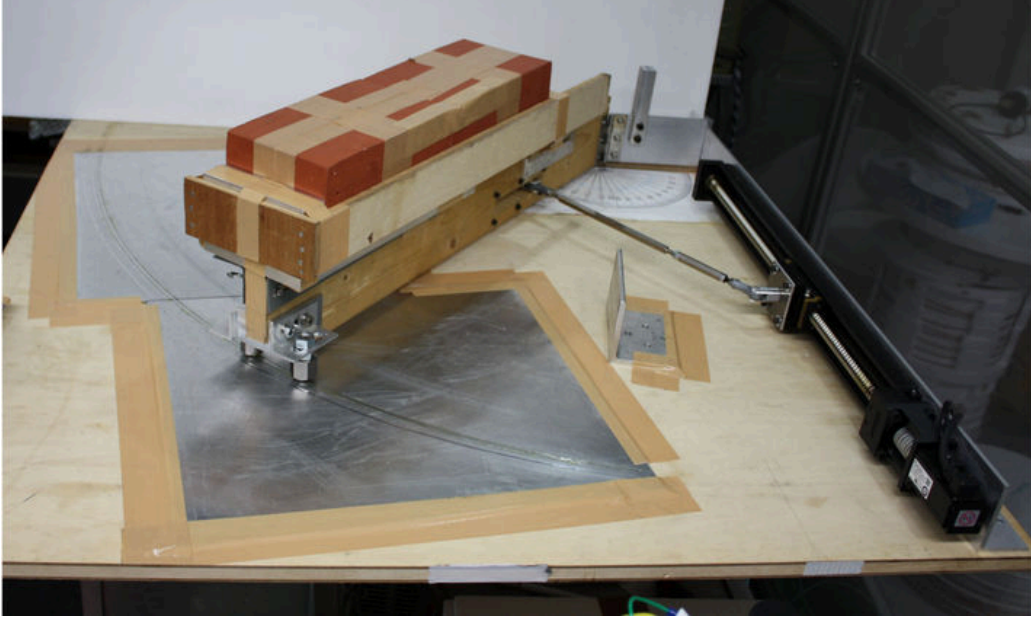
Figure 4.3: High friction experimental apparatus

Table 4.2: Characteristic of high friction experimental apparatus

AC Motor	SGMJV-A5A3A21 (YASKAWA)
Ballscrew	MCM06040H05K00 (NSK)
Ballscrew lead	5 mm
Ballscrew shaft diameter	16 mm
Ballscrew nominal stroke	400 mm
Wooden bar	0.75x0.1x0.027 m
Door weight	15 Kg

the door which can rotate about the z-axis. On the system there are two main input forces — one is the external force applied by the user, and the other is the force applied by the ballscrew system on the end of link 2, F_{bs} in Fig 4.4. In order to estimate the external force, the value of the nominal inertia (J_n) in the inverted plant dynamics model $\left(\frac{J_n s + B_n}{T s + 1}\right)$ is considered constant in respect to the z-axis about which the door rotates. The torque applied about the z-axis caused by the force F is T_1 and is determined from the Jacobian of the system. As the ballscrew force F_{bs} has a component only along the y-axis,
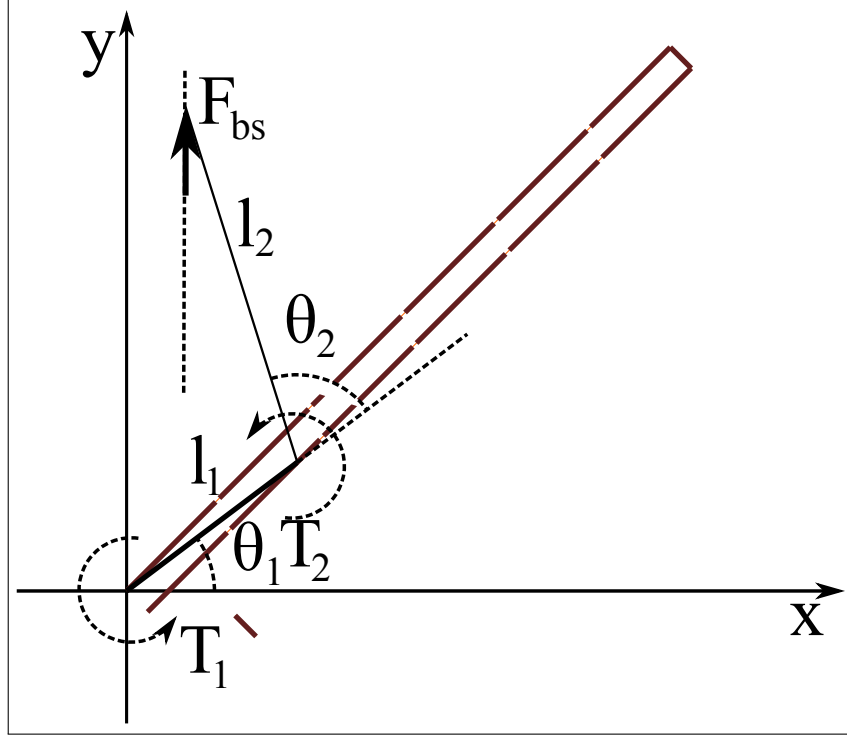
Figure 4.4: High friction system model

$F_x = 0$ and $F_y = F_{bs}$. Therefore:

$$
\begin{bmatrix} T_1 \\ T_2 \end{bmatrix} = J^T \begin{bmatrix} F_x \\ F_y \end{bmatrix}
$$

$$
= \begin{bmatrix} -l_1 S_1 - l_2 S_{12} & l_1 C_1 + l_2 C_{12} \\ -l_2 S1_2 & l_2 C_{12} \end{bmatrix} \begin{bmatrix} 0 \\ F_{bs} \end{bmatrix}
$$

$$
= \begin{bmatrix} (l_1 C_1 + l_2 C_{12}) F_{bs} \\ (l_2 C_{12}) F_{bs} \end{bmatrix} \tag{4.3}
$$

where $S_1 = sin(\theta_1)$, $C_1 = cos(\theta_1)$, $S_{12} = sin(\theta_1 + \theta_2)$ and $C_{12} = cos(\theta_1 + \theta_2)$.

4.1.3 Methods

In order to show the validity of the proposed control method the response of both the low and high friction systems using FSPAC with Constant Imped-ance (Fig. 3.1) and the proposed FSPAC with Variable Impedance (Fig. 3.2) are compared. In the experiments two types of inputs are used:

1. **User input**: the user pushes or pulls on a side of the door. The door is considered to be opening when the user pushes and closing when

pulls. This is to show what is the typical response of the system during opening and closing cycles under a user input force.

2. **Constant-magnitude-force input**: a weight of 1.5 kg and 2.0 Kg, respectively for the low and the high friction systems, is connected to the tip of the door by a wire and a pulley system as shown in figure 4.5. The door is hold in the initial position where $\theta_1 = 67°$, then it is left free to move under the weight force. The weight reaches its home limit when $\theta_1 = 52°$. Therefore the force applied by the weight on the door can be considered constant in magnitude, but not in direction respect to the door tip. The purpose of this experiment is to compare FSPAC with Constant Impedance and FSPAC with Variable Impedance to the same input. In this way any possible influence of the user is avoided.

(a) Low friction system   (b) High friction system
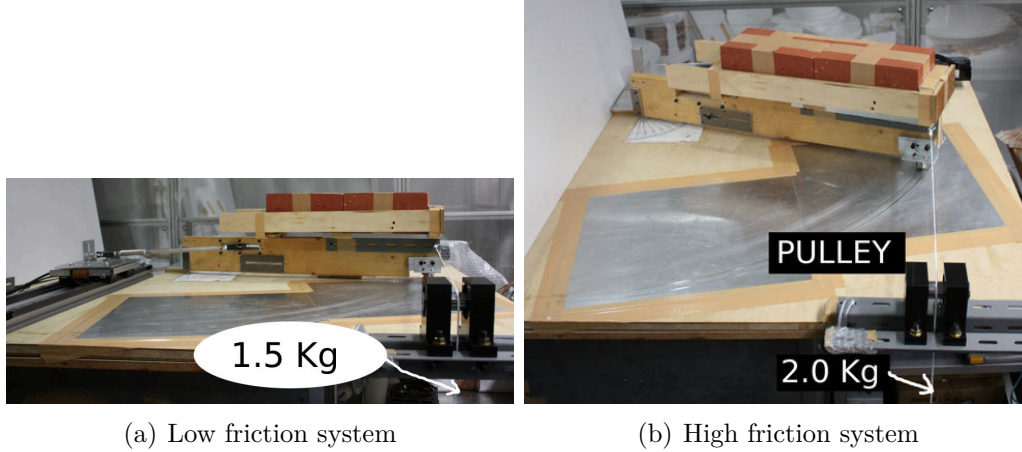
Figure 4.5: Door-pulley-weight connection system for low and high friction system

4.2   Results

4.2.1   Low Friction System

The values of the parameters used in the controller design for the low friction experimental apparatus are shown in Tab. 4.3.

The value of the constant feedback gain for the FSPAC with Constant Impedance is set to 0.6. For the FSPAC with Variable Impedance the values of the parameters of the VD-TG are shown in Tab 4.4. Graphically both the constant gain and the VD-TG are represented in Fig. 4.7.
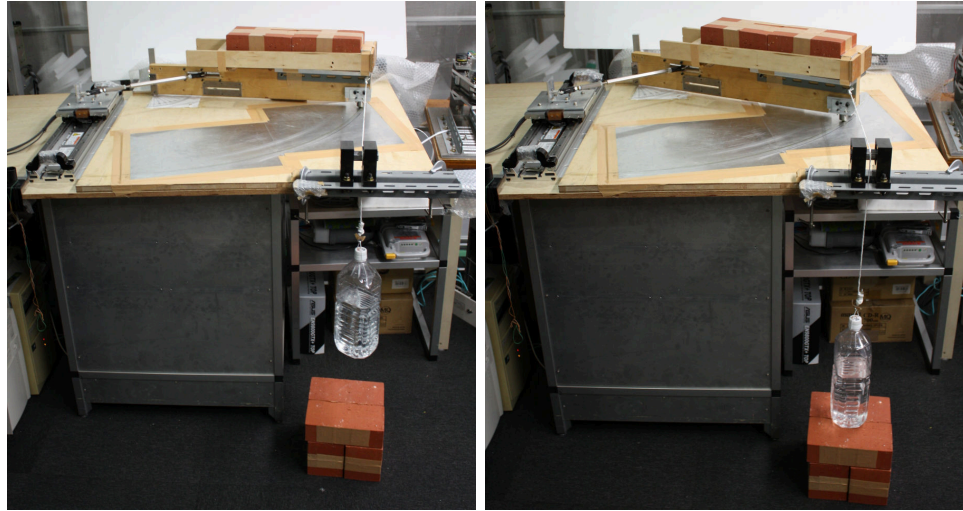
(a) Starting point   (b) Ending point

Figure 4.6: Constant-magnitude-force input: starting point (left) and ending point (right)

User input

In Fig. 4.8 the results for FSPAC with both constant impedance (Fig 4.8(a)) and Variable Impedance (Fig. 4.8(b)) are shown for a direct comparison.

In both cases the user pushes (opens) three times and pulls (close) two times the door. The data shown in Fig. 4.8 are the angular velocity of the door (v_a) about the z axis, the input torque about the z axis (T_1) calculated from the reference input to the linear motor as if the transmission system efficiency is 100%, the estimated disturbance from the disturbance observer about the z-axis, the model velocity (v_m), and the value of the VD-TG is shown in respect to the right y-axis in the figure.

Table 4.3: Values of controller parameter for the low friction experimental apparatus

Parameter	*Value*	Unit
J_n	5.6	kgm^2
B_n	4.4	Nms
J_M	0.56	kgm^2
B_M	2.86	Nms
T	0.15	s
$DistG$	0.05	

Table 4.4: Values of VD-TG parameters for the low friction experimental apparatus

Parameter	*Value*	Unit
VGmax	0.85	
v_1	0.005	*rad/s*
v_2	0.05	*rad/s*
v_3	1.2	*rad/s*
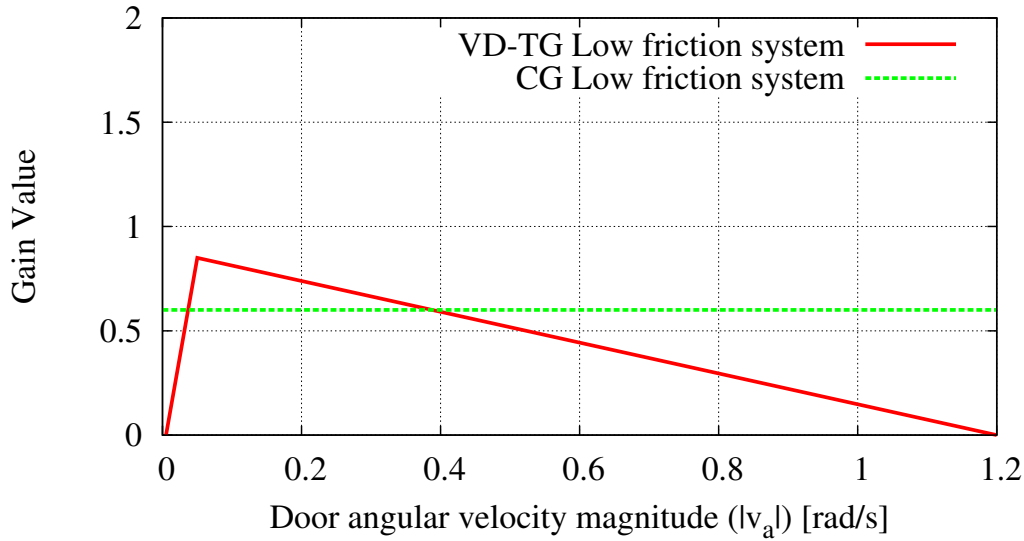
Figure 4.7: Constant gain and VD-TG for low friction system

For the FSPAC with Constant Impedance, and taking into account only the first pushing and pulling phase, the experiment is carried on as in the following:

1. Seconds 0.3–2.0: the user is pushing the door

2. Seconds 2.0–2.7: the user does not touch the door

3. Seconds 2.7–4.0: the user is pulling the door

There are two main problems in the case of FSPAC with Constant Impedance:

1. When the door is accelerating, as for example around second 1 in Fig. 4.8(a), the generated torque is too high therefore the door is opening too fast and, consequently, the user loses contact with the door.
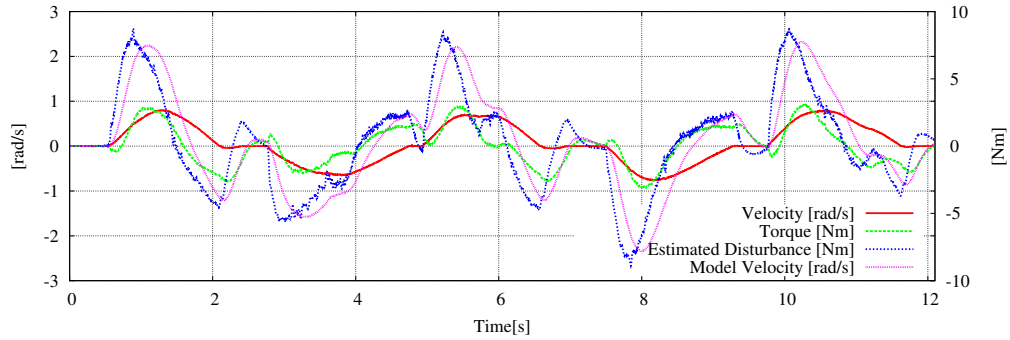
(a) FSPAC with Constant Impedance
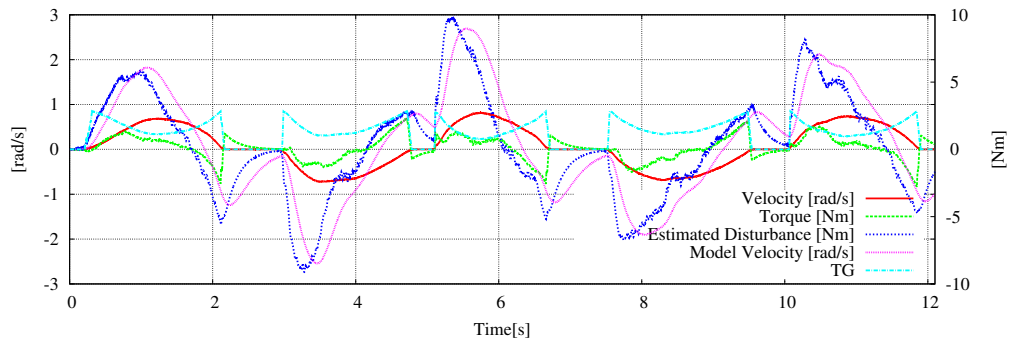
(b) FSPAC with Variable Impedance

Figure 4.8: FSPAC with constant and FSPAC with Variable Impedance for low friction system and user input

2. When on the door is coming to stop, as for example between seconds 2.1 and 2.7 in Fig. 4.8(a), friction non linearities cause an oscillatory reference disturbance, followed by oscillatory torque which can lead to oscillatory velocity.

A lower constant impedance could attenuate the two problems described above, but the assistance would be too small, especially at low velocity.

As shown by the results in Fig. 4.8(b) the previous two problems are overcome by the proposed FSPAC with Variable Impedance. When the user start pushing (or pulling) the door the VD-TG rapidly increases so to help the use to win the door inertia, then the assisting torque gradually decrease, so that the user does not lose contact with the door. Therefore the assistance is provided in a smooth way. When the door is coming to stop the VD-TG goes rapidly to 0, avoiding oscillatory torque reference, and so oscillatory velocities, which can cause system instabilities and dangerous situations.

Constant-Magnitude-Force Input

The experimental results obtained applying a constant-magnitude-force input for FSPAC with Constant Impedance and FSPAC with Variable Impedance are shown in Fig. 4.9(a) and Fig. 4.9(b), respectively.

(a) FSPAC with Constant Impedance   (b) FSPAC with Variable Impedance
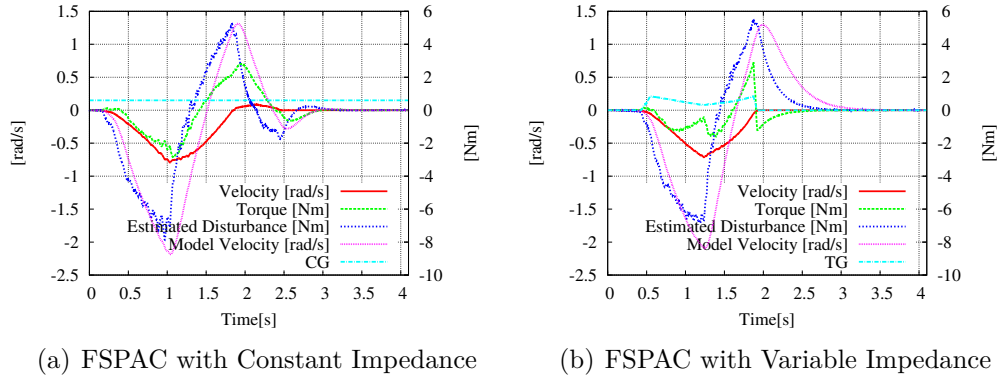
Figure 4.9: Results for FSPAC with Constant Impedance and FSPAC with Variable Impedance for constant-magnitude-force input for low friction experimental apparatus

These results confirm the one obtained with the user input (Section 4.2.1): by using the VD-TG the torque reference rises faster and is not oscillatory when the door is coming to stop (Fig. 4.9(b)). Moreover high torque reference, leading to possible dangerous velocity, is avoided.

4.2.2 High Friction System

The values of the parameters used in the controller design for the high friction experimental apparatus are shown in Tab. 4.5.

The value of the constant feedback gain for the FSPAC with Constant Impedance is set to 1.7. For the FSPAC with Variable Impedance the values of the parameters of the VD-TG are shown in Tab. 4.6. Graphically, both the constant gain and the VD-TG are represented in Fig. 4.10.

For the low friction system $v_1 = 0.005$, while for the high friction system $v_1 = 0.01$. The bigger value of v_1 for the high friction system is due to the fact that the non linear region of the friction in respect to the velocity is greater for the high friction system.

Table 4.5: Values of controller parameters for the high friction experimental apparatus

Parameter	*Value*	Unit
J_n	5.3	kgm^2
B_n	29.15	Nms
J_M	1.59	kgm^2
B_M	7.3	Nms
T	0.15	s
$DistG$	0.05	

Table 4.6: Values of VD-TG parameters for the high friction experimental apparatus

Parameter	*Value*	Unit
$VGmax$	4.1	
v_1	0.01	rad/s
v_2	0.08	rad/s
v_3	0.7	rad/s

User Input

In Fig. 4.11 the results for both FSPAC with both constant impedance (Fig. 4.11(a)) and Variable Impedance (Fig. 4.11(b)) under a user input are shown for a direct comparison. In both cases the user at first pushes (opens) and then pulls (close) the door for a total of two times. The data shown in Fig. 4.11 are the angular velocity of the door (v_a) about the z axis, the input torque about the z axis (T_1) calculated from the reference input to the linear motor as if the transmission system efficiency is 100%, the estimated disturbance from the disturbance observer about the z-axis, the model velocity (v_m), and the value of the VD-TG is shown in respect to the right y-axis in the figure.

Considering the case of FSPAC with Constant Impedance (Fig. 4.11(a)), the distribution of the torque about z-axis (T_1) shows the following two problems:

1. At low velocities: T_1 is low, as a consequence the assistance is too small. This means that the user feel the door quite stiff and heavy when starts pushing or pulling due to the high friction of the ballscrew and door inertia.

2. At high velocities: the assistance torque is to big. The data show that the torque is generally big when the velocity is high. This can easily
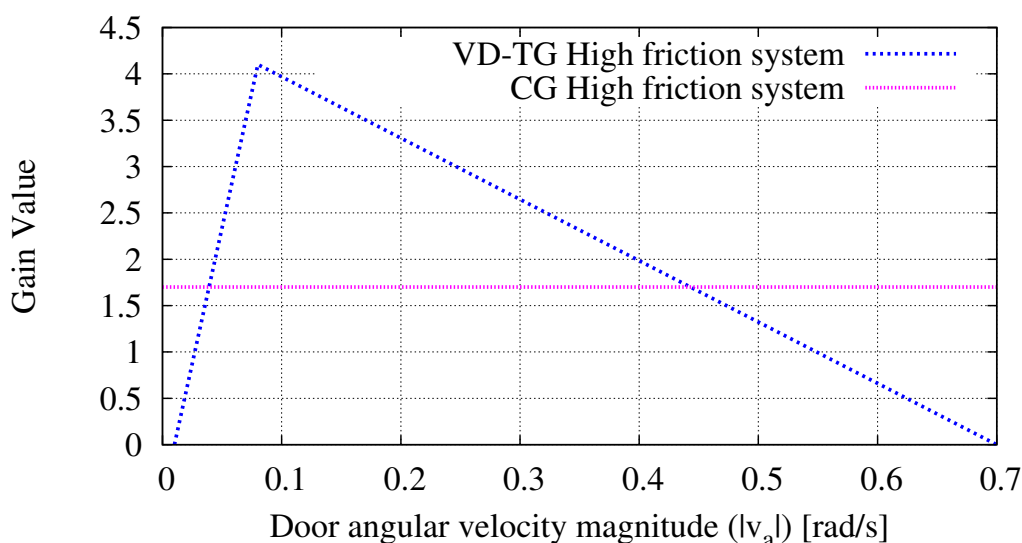
Figure 4.10: Constant gain and VD-TG for high friction system

lead to situations in which the user loses contacts with the door. This phenomenon happens for example around second 5.5 in Fig. 4.11(a).

An higher value of the feedback gain increases the assistance at low velocity solving therefore the first problem, but at the same time rises the already too high assistance at high velocities increasing therefore situations in which the user loses contacts with the door. Moreover, a higher constant feedback gain can lead the system to instability. When the door stops after the opening (closing) phase there is always a small positive (negative) torque due to unmodeled non-linear friction. This torque however does not cause significant oscillatory velocity, which is the other hand present for high friction systems with lower inertia [98]. The oscillatory velocity when the door comes to a stop is not present due to high system stiction and inertia, the generated oscillatory torque is not big enough to move the door.

As shown by the results in Fig. 4.11(b) the two mentioned problems are overcome by using FSPAC with Variable Impedance:

1. At low velocities: when the user start pushing (or pulling) the door the VD-TG rapidly increases so to generate a high torque and help the use to easily win the high ballscrew friction and door inertia.

2. At high velocities: as the velocity increases the assisting torque gradually decreases so that the user does not lose contact with the door. Therefore the assistance is provided in a smooth way.
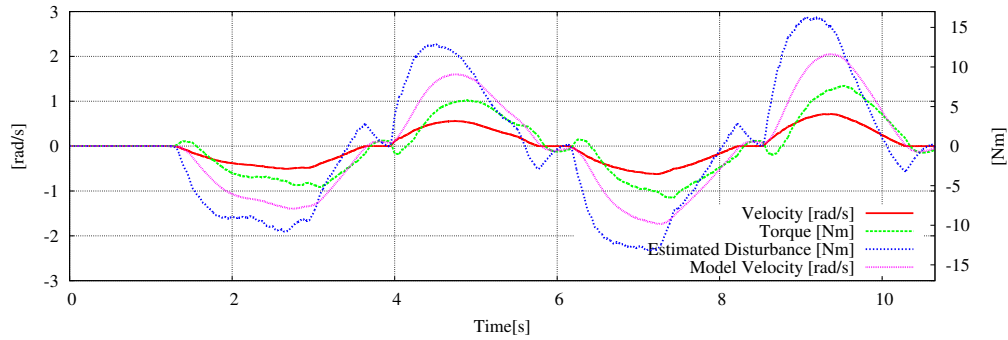
(a) FSPAC with Constant Impedance
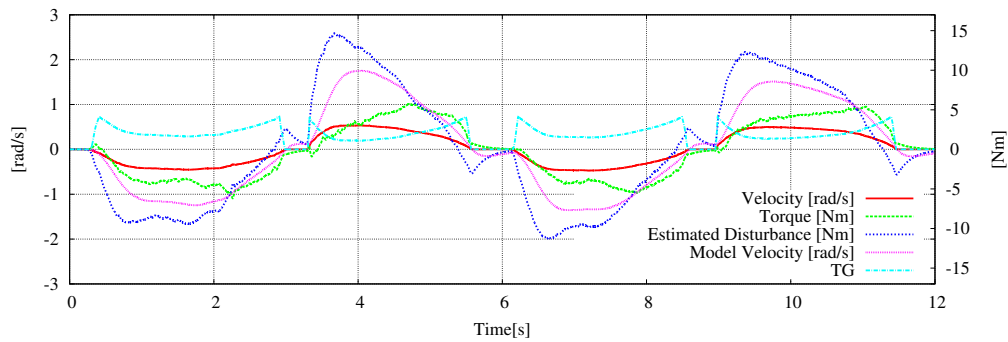
(b) FSPAC with Variable Impedance

Figure 4.11: FSPAC with Constant Impedance and FSPAC with Variable Impedance for high friction system and user input

It is opportune to underline that the positive torque that happen to be when the user start pushing the door — or the negative one when the user start pulling — is due to the negative feedback of the disturbance observer.

Constant-Magnitude-Force Input

The experimental results obtained applying a constant-magnitude-force input for FSPAC with Constant Impedance and FSPAC with Variable Impedance are shown in Fig. 4.12(a) and Fig. 4.12(b), respectively.

These results show what is the system response to the same input:

- The assistance torque rises faster in the case of FSPAC with Variable Impedance. For example, at seconds 0.5 the value of the assisting torque (T_1) for FSPAC with Constant Impedance is about 0 (Fig. 4.12(a)), while for FSPAC with Variable Impedance it is about 0.7 Nm (Fig. 4.12(b)).

(a) FSPAC with Constant Impedance   (b) FSPAC with Variable Impedance
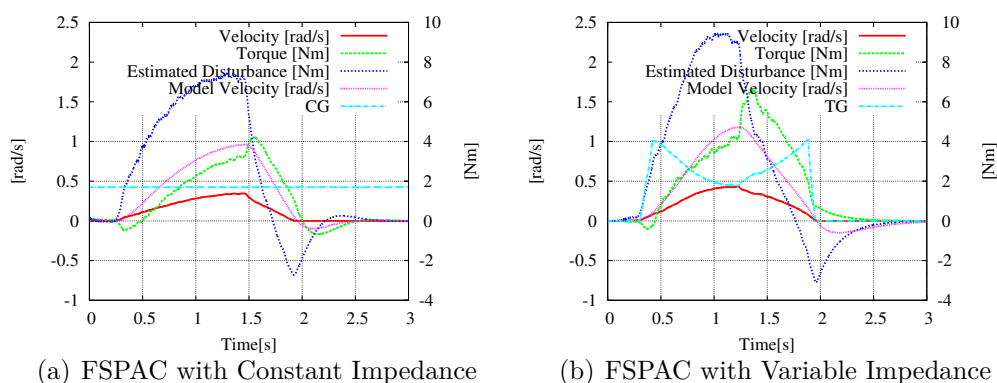
Figure 4.12: Results for FSPAC with Constant Impedance and FSPAC with Variable Impedance for constant-magnitude-force input for high friction experimental apparatus

- In Fig. 4.12(a) and in Fig. 4.12(b) the drop of disturbance that happens respectively around seconds 1.5 and 1.3 is due to the fact that the weight reaches its home limit, therefore the input force it applies on the door become zero. The torque rises just after the disturbance drops because the disturbance observer negative feedback decreases. This phenomenon is desired, otherwise the door would stop suddenly due to high friction of ballscrew. This shows that the system response is smoother for FSPAC with Variable Impedance.

These results shows that FSPAC with Variable Impedance allows the system to better track the input, so to be more reactive, and at the same time to be smoother than FSPAC with Constant Impedance.

4.3 Discussion on FSPAC with Variable Impedance

The knowledge of the force applied by the user and the environment on a power assist robot is a key aspect in the design of the controller of these devices. Generally force sensors are used to measure the force applied by the user on the device. To overcome the disadvantages of force sensors such as high cost, weight and measurement delay, Force Sensor-Less Power Assist Control (FSPAC) have been proposed in many researches. The user force is estimated using disturbance observer technology. Therefore encoders are the

only needed sensors. However, the main problem of FSPAC is its robustness against real plant uncertainties.

Inspired by the variable impedance humans use in their motion control, FSPAC with Variable Impedance is proposed to increase robustness, provide a smoother assistance to the user, and increase safety. The FSPAC with Variable Impedance is realized using a feedback Velocity Dependant Triangular Gain (VD-TG). To experimentally proof its validity, the proposed controller was successfully implemented on an experimental apparatus representing a door actuated either by a linear motor (low friction system) or by a rotational motor and a ballscrew (high friction system), and compared to the traditional FSPAC with Constant Impedance. The value of the VD-TG depends on the magnitude of the angular velocity about the door vertical axis of rotation ($|v_a|$). Its design is based on parameters related to system friction and inertia, as well as to desired disturbance rejection.

4.3.1 FSPAC with Variable Impedance: Stability Issue

In Fig. 4.13 the constant gain and VD-TG are shown for both the low and high friction systems.
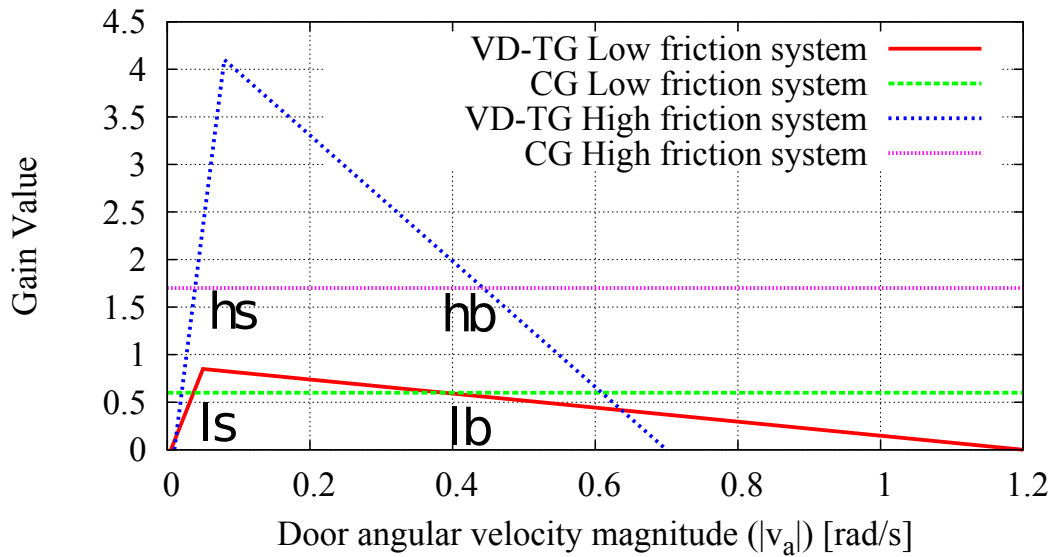
Figure 4.13: Constant gain and VD-TG for both low and high friction systems

The values of the constant gains for low and high friction systems are 0.6 and 1.7, respectively. These values were experimentally determined. For each system there is a zone in which the value of the VD-TG is above the

constant gain. Therefore the FSPAC with Variable Impedance has a velocity range where the stability can not be proof using the gain margin approach. However, FSPAC with Variable Impedance is a non linear system, and has shown to be globally stable from an experimental point of view. The theoretical proof of the system stability goes beyond the scope of this work, however on the basis of the experimental results the following issue can be addressed. The velocity ranges in which the value of the VD-TG is above the constant gain are defined by the values *ls* and *lb* for the low friction system, while *hs* and *hb* for the high friction system. For the high friction system $v_{hs} = 0.039$ and $v_{hb} = 0.39$, while for the low friction system $v_{ls} = 0.037$ and $v_{lb} = 0.44$. Therefore, these velocity ranges are almost identical as $v_{hs} \approx v_{ls}$ and $v_{hb} \approx v_{lb}$, and have relatively low values. This represent situations in which also the kinetic energy of the whole system is low. Therefore, the greater assistance provided by the FSPAC with Variable Impedance, which can be thought as greater energy input to the system of kinetic energy, is realized only when the system has a low kinetic energy.

4.3.2 FSPAC with Variable Gain: Improvements

The main improvement obtained by using FSPAC with Variable Impedance are:

- **Higher robustness**: experiments using the same plant model and controller parameters were carried over under slightly different humidity and room temperature conditions. The FSPAC with Variable Impedance has shown to be always stable, while the FSPAC with Constant Impedance required a modification of the nominal plant model parameters to better match the plant model in order to avoid system instability. This is an evident factor of the higher robustness to inevitable modeling error of the proposed FSPAC with Variable Impedance.

- **Smoother assistance**: provides higher power assistance to the user at low velocities, especially for high friction systems. Moreover, the user does never lose contact with the robot door. As direct consequence the robot better tracks the user inputs, and therefore the user feels the assisting device less stiff, and more comfortable.

- **Higher safety**: avoids oscillatory torque references and velocities that can cause system instability and dangerous situations when the door is coming to a stop.

Chapter 5

Bi-Articular Actuation Control Design

Robots presenting animal musculo-skeletal characteristics such as bi-articular actuators — actuators that span two consecutive joints — have been proposed for more than two decades [39]. In recent years there has been raising interest in such biologically inspired robos, both in control and hardware design aspects.

The characteristics and modeling of bi-articular actuators in robot arms are illustrated in Section 5.1. The advantages related to the use of bi-articular actuators are described in Section 5.2.

From a control point of view, bi-articularly actuated robots generally present more actuators than joints, resulting in actuator redundancy. The resolution of actuator redundancy is the firts step in in the control design for such robots, therefore represent a key factor for the overall performances. The actuator redundandy problem resulting from the use of bi-articular actuators is illustrated in Section 5.3. The three traditional actuator redundancy resolution approaches — Phase Different Control (PDC), Pseudo inverse matrix ($2 - norm$), and Linear Programming — as well as the two proposed approaches — Infinity norm ($\infty - norm$) and Non Linear Phase Different Control (NLPDC) — are described in Section 5.4.

The state-of-the-art in bi-articular actuation hardware design, the proposed biologically inspired robot — **BiWi**, **Bi**-articularly actuated and **Wi**re driven robot arm —, the experimental setup and analysis methods, and the theoretical and experimental comparison of the five redudnancy resolution approaches are provided in Chapter 6.

5.1 Modeling of Bi-Articularly Actuated Robot Arms

In conventional manipulators each joint is driven by one actuator. On the other hand, animal and human limbs present a complex musculo-skeletal structure based on mono- and multi- articular muscles:

1. Mono-articular muscles produce a torque on one joint.

2. Multi-articular muscles span more than one joint. Gastrocnemius is an example of bi-articular muscle in the human leg.

A widely used simplified model of the complex animal musculo-skeletal system [31] [60] [79] [83] [96] [120] is shown in Fig. 5.1(a).

(a) Model   (b) Resulting forces at end effector
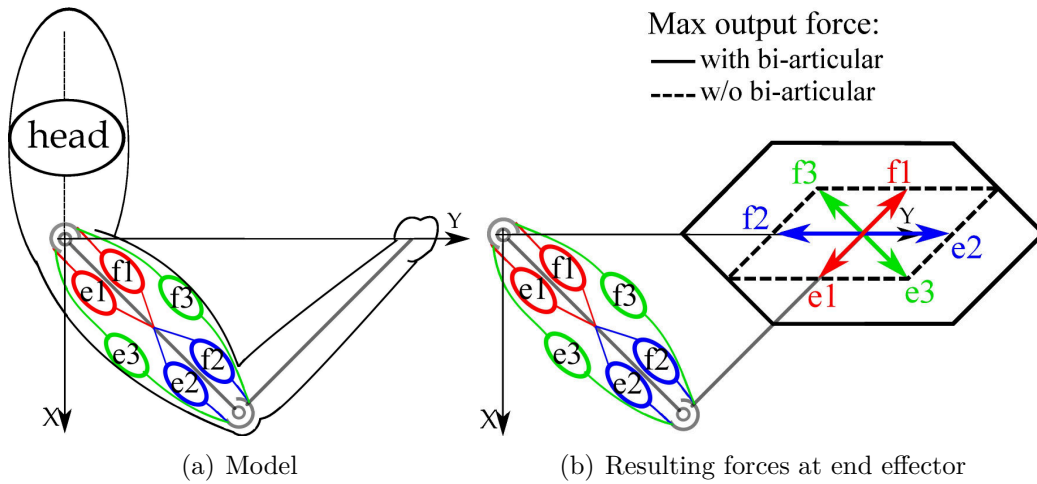
Figure 5.1: Two-link arm with four mono- and two bi-articular actuators: model and resulting forces at end effector

The muscles' name, type and relative symbol are illustrated in Tab. 5.1

This model is based on six contractile actuators — three extensors (e1, e2, and e3) and three flexors (f1, f2, and f3) — coupled in three antagonistic pairs:

- e1–f1 and e2–f2: couples of mono-articular actuators that produce torques at joint 1 and 2, respectively.

- e3–f3: couple of bi-articular actuators that produce torque at joint 1 and 2 contemporaneously.

Table 5.1: Muscles' name, type and symbol

Name	Type	Symbol
Deltoid, posterior part	mono	e1
Deltoid, anterior part	mono	f1
Triceps, lateral head	mono	e2
Brachialis	mono	f2
Triceps, long head	bi	e3
Biceps brachii	bi	f3

The resulting forces at the end effector are shown in Fig. 5.1(b). If only mono-articular muscles are considered, there are four resulting forces at the end effector and the maximum output force space is a quadrilateral. On the other hand, if bi-articular actuators are added, there are six forces at the end effector, hence the maximum output force space becomes an hexagon.

5.2 Advantages of Bi-Articular Actuation

Bi-articular actuators bring numerous advantages in robot applications.

1. **Homogeneously distributed output force**
   Another advantage of bi-articularly actuated manipulators is the ability to produce a maximum output force at the end effector in a more homogeneously distributed way [25]. The maximum output force at the end effector for a two-link conventional manipulator and for a bi-articularly actuated robot arm is shown in Fig. 5.2 for comparison. The conventional manipulator has two actuators with maximum joint torques $T_1 = T_2 = 10$ Nm, and the bi-articularly actuated robot arm has three actuators with maximum joint torques $\tau_1 = \tau_2 = \tau_3 = 6.66$ Nm. All the gear ratios of all the actuators are the same. Therefore, the sum of maximum actuator torques are the same (i.e. 20 Nm) in the two cases. The conventional quadrilateral shape becomes an hexagon for bi-articularly driven arms, which therefore produces a maximum force at the end effector more homogeneously distributed in respect to output force direction. The maximum output force that can be physically produced by applications which interact with humans is a key aspect in safety. There are researches in which rehabilitation robots are pneumatically actuated to increase safety for the users [16] [73] [78] [92]. Peak output forces such as the one in point M in Fig. 5.2 can not be produced by the human arm, therefore are unnecessary and
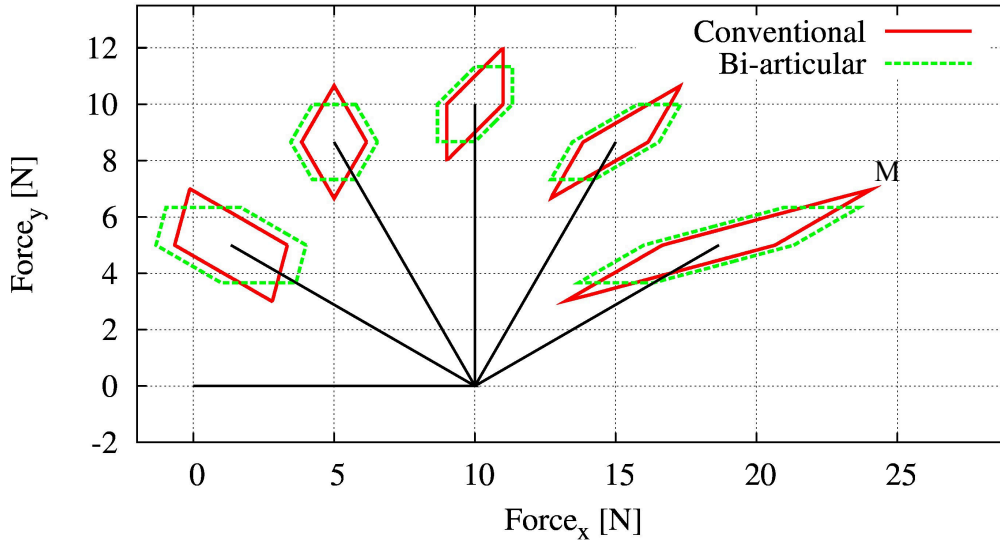
Figure 5.2: Maximum output force at the end effector for conventional and bi-articularly driven arm

dangerous in case of failure of the controller. As a consequence, the use of bi-articular actuators further increases safety for rehabilitation applications [29] [93] [109] [110] [122].

2. **Mechanical energy transfer**
   A second aspect is the mechanical energy transfer from proximal to distal joints realized by bi-articular actuators [125]. This aspect is a key aspect in legged robots for hopping [4] [42] [44] [58] [64], for jumping [76] [87], and for running [77]. This important property of bi-articular actuators is also used to design in power assist robots for lower limbs [47] [94] [108], upper limbs [52], and hands [116].

3. **Feedforward impedance control**
   An important advantage is the dramatical increase in range of end effector impedance which can be achieved without feedback [39]. Consequences are, for example, the capability of path tracking and disturbance rejection using just feedforward control [41] [130], the improvement of balance control for legged robots without force sensors [82], and the increasing walking capability for bipedal robot [46].

In addition to these advantages, multi-articular actuators, such as tri-articular actuators, increase the efficiency in output force generation, as for example in lancelet-like swimming robots [120].
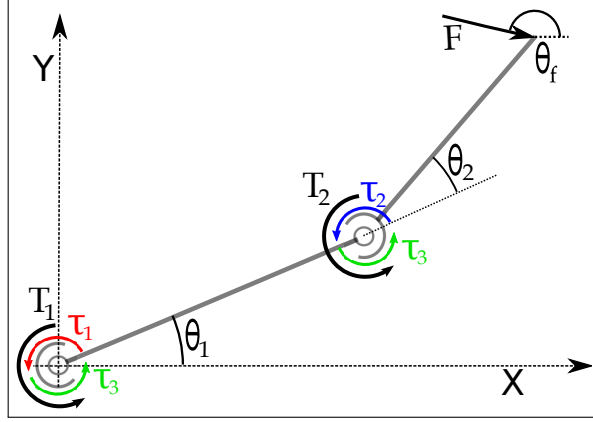
Figure 5.3: Statics of a two-link arm with four mono- and two bi-articular actuators

5.3   Actuator Redundancy Problem

A robot arm modeled as in Fig. 5.1 is redundant in actuation: has six actuators and two DOF. The resulting statics are shown in Fig. 5.3 where $\boldsymbol{F}$ is a general force at the end effector, and T_1 and T_2 are total torques at joint 1 and 2, respectively. The difference mode is the difference between the activation levels of the antagonistic muscles in a pair. The difference mode generates the joint actuator torques,

$$\tau_1 = (f_1 - e_1)r \tag{5.1}$$
$$\tau_2 = (f_2 - e_2)r \tag{5.2}$$
$$\tau_3 = (f_3 - e_3)r \tag{5.3}$$

where τ_1 and τ_2 are torques produced by mono-articular actuators about joints 1 and 2, respectively; τ_3 is the bi-articular torque produced about both joints simultaneously; r is distance between the joint and the point where the muscle force is applied, considered to be the same for all the muscles.

The sum mode is the sum of the activation levels of the antagonistic muscles in a pair. The sum mode is related to the joint stiffness as:

$$s_1 = K(f_1 + e_1)r \tag{5.4}$$
$$s_2 = K(f_2 + e_2)r \tag{5.5}$$
$$s_3 = K(f_3 + e_3)r \tag{5.6}$$

where K represent the elasticity of the muscles. In this work, the stiffness produced about the joints by the sum mode is considered to be independent

from joint angles ($\boldsymbol{\theta}$). The statics of this system are therefore expressed by:

$$T_1 = (f_1 - e_1)r + (f_3 - e_3)r \tag{5.7}$$
$$T_2 = (f_2 - e_2)r + (f_3 - e_3)r \tag{5.8}$$

Substituting (5.1), (5.2), and (5.3) in (5.7) and (5.8) follows:

$$T_1 = \tau_1 + \tau_3 \tag{5.9}$$
$$T_2 = \tau_2 + \tau_3 \tag{5.10}$$

The problem represented by (5.9) and (5.10) is referred in the following as the redundancy actuator problem. Given $\boldsymbol{\tau} = [\tau_1, \tau_2, \tau_3]^T$, it is possible to determine $\boldsymbol{T} = [T_1, T_2]^T$ by using (5.9) and (5.10), and $\boldsymbol{F} = [F_x, F_y]^T$ by:

$$\begin{bmatrix} F_x \\ F_y \end{bmatrix} = (J^T)^{-1} \begin{bmatrix} T_1 \\ T_2 \end{bmatrix} \tag{5.11}$$

where

$$J = \begin{bmatrix} -l_1\sin(\theta_1) - l_2\sin(\theta_1 + \theta_2) & -l_2\sin(\theta_1 + \theta_2) \\ l_1\cos(\theta_1) + l_2\cos(\theta_1 + \theta_2) & l_2\cos(\theta_1 + \theta_2) \end{bmatrix} = \begin{bmatrix} a & b \\ c & d \end{bmatrix} \tag{5.12}$$

and F_x and F_y are the orthogonal projection of $\boldsymbol{F}$ on the x-axis and y-axis, respectively. On the other hand, given $\boldsymbol{F}$, and therefore $\boldsymbol{T}$, it is generally not possible to determine uniquely $\boldsymbol{\tau}$ due to the presence of the bi-articular actuator (see (5.9) and (5.10)).

The three traditional actuator redundancy resolution approaches — Phase Different Control (PDC), Pseudo inverse matrix (2-norm), and Linear Programming — as well as the two proposed approaches — Infinity norm and Non Linear Phase Different Control (NLPDC) — are described in the following.

5.4 Actuator Redundancy Resolution Approaches

5.4.1 Traditional 1: Phase Different Control

The Phase Different Control (PDC) is a biologically inspired approach proposed in [60] and [86]. The muscle activation level patterns on which the PDC is based are shown in 5.4(b). These patterns are the linearization of the patterns resulting from electromyography activity observation of human arm muscles while applying forces at the end effector under isometric and

(a) Muscle activation level patterns used as input references for the PDC approach

(b) Resulting end effector maximum force
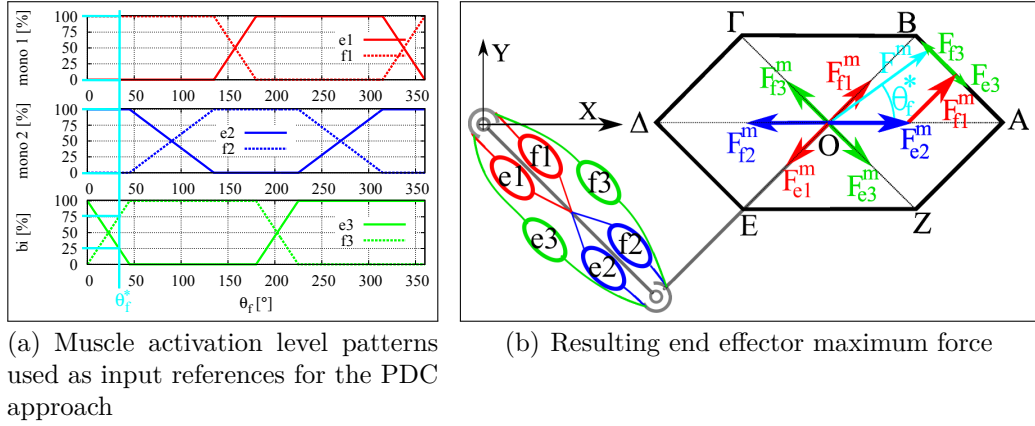
Figure 5.4: The PDC approach, muscle activation level patterns and resulting end effector maximum force [86]

maximal effort conditions [86]. The six muscle activation level patterns are expressed in respect to the force direction (θ_f). According to the PDC approach [86], the end effector maximum force $\boldsymbol{F}^m$ with angle θ_f^* in Fig. 5.4(b) can be obtained using the muscle activation level patterns in Fig. 5.4(a) as inputs. The maximum end effector force $\boldsymbol{F}^m$ in direction θ_f^* is the sum of the six forces produced by the six muscles:

$$\boldsymbol{F}^m = \boldsymbol{F}_{e1} + \boldsymbol{F}_{f1} + \boldsymbol{F}_{e2} + \boldsymbol{F}_{f2} + \boldsymbol{F}_{e3} + \boldsymbol{F}_{f3} \tag{5.13}$$

For the particular case in Fig. 5.4(b), where $l_1 = l_2 = 1$ m, $\theta_1 = -45°$, $\theta_2 = 90°$, $e_i^m r = f_i^m r = 1$ Nm for $i = (1, 2, 3)$, and $\theta_f^* = 33.75°$ results:

$$\boldsymbol{F}^m = \boldsymbol{F}_{f1}^m + \boldsymbol{F}_{e2}^m + 0.25 \boldsymbol{F}_{e3}^m + 0.75 \boldsymbol{F}_{f3}^m \tag{5.14}$$

Given a desired force angle θ_f^*, the six muscle activation levels to obtain the maximum end effector force ($\boldsymbol{F}^m$) are calculated as follows.

1. On the basis of the manipulator Jacobian (5.12), the actual configuration (θ_1 and θ_2) and the maximum muscle forces, calculate the angles α, β, γ, δ, ε, and ζ, defined as the angles between the x-axis and the line passing through the center O and points A, B, Γ, Δ, E, and Z in Fig. 5.4(b), respectively.

2. Calculate the muscle activation level — e_1, e_2, e_3, f_1, f_2, f_3 — using the graph in Fig. 5.4(a). The graphical illustration of the muscle activation levels for the PDC approach (Fig. 5.4(a)), is mathematically

Table 5.2: Muscle Activation Levels for PDC

	$\zeta \leq \theta_f^* < \alpha$	$\alpha \leq \theta_f^* < \beta$	$\beta \leq \theta_f^* < \gamma$	$\gamma \leq \theta_f^* < \delta$	$\delta \leq \theta_f^* < \varepsilon$	$\varepsilon \leq \theta_f^* < \zeta$
e_1	$e_1^m - \frac{\theta_f^*-\zeta}{\alpha-\zeta}e_1^m$	0	0	$\frac{\theta_f^*-\gamma}{\delta-\gamma}e_1^m$	e_1^m	e_1^m
f_1	$\frac{\theta_f^*-\zeta}{\alpha-\zeta}f_1^m$	f_1^m	f_1^m	$f_1^m - \frac{\theta_f^*-\gamma}{\delta-\gamma}f_1^m$	0	0
e_2	e_2^m	e_2^m	$e_2^m - \frac{\theta_f^*-\beta}{\gamma-\beta}e_2^m$	0	0	$\frac{\theta_f^*-\varepsilon}{\zeta-\varepsilon}e_2^m$
f_2	0	0	$\frac{\theta_f^*-\beta}{\gamma-\beta}f_2^m$	f_2^m	f_2^m	$f_2^m - \frac{\theta_f^*-\varepsilon}{\zeta-\varepsilon}f_2^m$
e_3	e_3^m	$e_3^m - \frac{\theta_f^*-\alpha}{\beta-\alpha}e_3^m$	0	0	$\frac{\theta_f^*-\delta}{\varepsilon-\delta}e_3^m$	e_3^m
f_3	0	$\frac{\theta_f^*-\alpha}{\beta-\alpha}f_3^m$	f_3^m	f_3^m	$f_3^m - \frac{\theta_f^*-\delta}{\varepsilon-\delta}f_3^m$	0

represented by a set of six piecewise linear functions, one for every muscle. Every piece wise function is defined on six intervals, as shown in Tab. 5.2.

The actuator joint input torques τ_1, τ_2, and τ_3 which produce the maximum end effector force $\boldsymbol{F}^m$, can be calculated using the difference modes of the six muscle activation levels as in (5.1), (5.2), and (5.3). In the case illustrated in Fig. 5.4(b):

$$\tau_1 = (f_1 - e_1)r = f_1^m r \tag{5.15}$$
$$\tau_2 = (f_2 - e_2)r = -e_2^m r \tag{5.16}$$
$$\tau_3 = (f_3 - e_3)r = \left(0.75 f_3^m - 0.25 e_3^m\right) r \tag{5.17}$$

By using the PDC approach the sum modes of the three antagonistic muscle pairs can not be designed independently from the difference modes. In the case illustrated in Fig. 5.4(b) the sum modes are:

$$s_1 = K(f_1 + e_1 + \sigma_1)r = K f_1^m r \tag{5.18}$$
$$s_2 = K(f_2 + e_2 + \sigma_2)r = K e_2^m r \tag{5.19}$$
$$s_3 = K(f_3 + e_3 + \sigma_3)r = K\left(0.75 f_3^m + 0.25 e_3^m\right) r \tag{5.20}$$

5.4.2 Traditional 2: Pseudo Inverse Matrix

Approaches based on pseudo-inverse matrices are widely used in the control design for kinematically redundant manipulator [13] [88] [128]. Pseudo-inverse matrices are also used for actuator redundancy resolution [129] [111]. Moore-Penrose is the simplest pseudo-inverse matrix, and correspond to the minimization of the euclidean norm [57].

Given the arm with the statics as in Fig. 5.3 and a force at the end effector $\boldsymbol{F}$, the joint torques $\boldsymbol{T}$ are calculated using (5.12), and the three joint actuator torques τ_1, τ_2 and τ_3 that produces $\boldsymbol{T}$ are calculated using the $2 - norm$ by resolving the following problem:

$$\begin{aligned} \min \quad & \sqrt{\frac{(\tau_1)^2}{(\tau_1^m)^2} + \frac{(\tau_2)^2}{(\tau_2^m)^2} + \frac{(\tau_3)^2}{(\tau_3^m)^2}} \\ \text{s.t.} \quad & T_1 = \tau_1 + \tau_3 \\ & T_2 = \tau_2 + \tau_3 \end{aligned} \tag{5.21}$$

where $\tau_i^m, i \in \{1,2,3\}$ is the maximum joint torque that the actuator i can produce.

The solution of the problem (5.21) is:

$$\tau_1 = \frac{(T_1 - T_2)(\tau_1^m)^2(\tau_3^m)^2 + T_1(\tau_1^m)^2(\tau_2^m)^2}{(\tau_1^m)^2(\tau_2^m)^2 + (\tau_1^m)^2(\tau_3^m)^2 + (\tau_2^m)^2(\tau_3^m)^2} \tag{5.22}$$

$$\tau_2 = \frac{T_2(\tau_1^m)^2(\tau_2^m)^2 + (T_2 - T_1)(\tau_2^m)^2(\tau_3^m)^2}{(\tau_1^m)^2(\tau_2^m)^2 + (\tau_1^m)^2(\tau_3^m)^2 + (\tau_2^m)^2(\tau_3^m)^2} \tag{5.23}$$

$$\tau_3 = \frac{T_1(\tau_2^m)^2(\tau_3^m)^2 + T_2(\tau_1^m)^2(\tau_3^m)^2}{(\tau_1^m)^2(\tau_2^m)^2 + (\tau_1^m)^2(\tau_3^m)^2 + (\tau_2^m)^2(\tau_3^m)^2} \tag{5.24}$$

Proof of (5.22), (5.23), and (5.24) is reported in Appendix A.

If $\tau_1^m = \tau_2^m = \tau_3^m$ the solution becomes:

$$\tau_1 = \frac{2}{3}T_1 - \frac{1}{3}T_2 \tag{5.25}$$

$$\tau_2 = -\frac{1}{3}T_1 + \frac{2}{3}T_2 \tag{5.26}$$

$$\tau_3 = \frac{1}{3}T_1 + \frac{1}{3}T_2 \tag{5.27}$$

5.4.3   Traditional 3: Linear Programming

Linear Programming approach to resolve actuation redundancy for robot arm is proposed in [114]. This approach is based on a recursive algorithm, and can be used to determine the actuators inputs that allow to obtain the maximum output force at the end effector of an arm with any number of actuators and joints. For the arm with the statics as in Fig. 5.3 the Linear Programming approach is shown in the following.

The relationship between the force $\boldsymbol{F}$ at the end effector of a manipulator and the joint torque is:

$$\boldsymbol{T} = \boldsymbol{J}(\boldsymbol{\theta})^T \boldsymbol{F} \tag{5.28}$$

where $\boldsymbol{J}(\boldsymbol{\theta})$ is the manipulator Jacobian.

The joint torques $\boldsymbol{T}$ depends on the joint actuator torques $\boldsymbol{\tau}$:

$$\boldsymbol{T} = \boldsymbol{A}\boldsymbol{\tau} \tag{5.29}$$

where $\boldsymbol{A}$ represents the relationship between the muscle forces and the joint actuator torques.

$$\boldsymbol{A} = \begin{bmatrix} 1 & 0 & 1 \\ 0 & 1 & 1 \end{bmatrix} \tag{5.30}$$

and $\boldsymbol{\tau}$ is:

$$\boldsymbol{\tau} = [\tau_1, \tau_2, \tau_3]^T \tag{5.31}$$

The joint actuator torque are subjected to:

$$-\boldsymbol{\tau}^m \leq \boldsymbol{\tau} \leq \boldsymbol{\tau}^m \tag{5.32}$$

which corresponds to:

$$\begin{bmatrix} -\tau_1^m \\ -\tau_2^m \\ -\tau_3^m \end{bmatrix} \leq \begin{bmatrix} \tau_1 \\ \tau_2 \\ \tau_3 \end{bmatrix} \leq \begin{bmatrix} \tau_1^m \\ \tau_2^m \\ \tau_3^m \end{bmatrix} \tag{5.33}$$

where τ_i^m for $i \in \{1, 2, 3\}$ is the magnitude of the maximum joint actuator torque the actuator i can produce.

From (5.28) and (5.29) follows:

$$\boldsymbol{T} = \boldsymbol{J}(\theta)^T \boldsymbol{F} = \boldsymbol{A}\boldsymbol{\tau} \tag{5.34}$$

The force $\boldsymbol{F}$ at the end effector can be expressed as:

$$\boldsymbol{F} = \begin{bmatrix} F_x \\ F_y \end{bmatrix} = F \begin{bmatrix} \cos \theta_f \\ \sin \theta_f \end{bmatrix} \tag{5.35}$$

where θ_f is the output force direction at the end effector.

Substituting (5.35) into (5.34):

$$F \boldsymbol{J}(\boldsymbol{\theta})^T \begin{bmatrix} \cos \theta_f \\ \sin \theta_f \end{bmatrix} = F\boldsymbol{b}(\theta_f, \boldsymbol{\theta}) = \boldsymbol{A}\boldsymbol{\tau} \tag{5.36}$$

where $\boldsymbol{b}(\theta_f, \boldsymbol{\theta}) = \boldsymbol{J}(\boldsymbol{\theta})^T [\cos \theta_f, \sin \theta_f]^T$.

From (5.36) it follows:

$$F = \boldsymbol{b}^+(\theta_f, \boldsymbol{\theta})\boldsymbol{A}\boldsymbol{\tau} \tag{5.37}$$

$$(\boldsymbol{I} - \boldsymbol{b}(\boldsymbol{\theta}_f, \boldsymbol{\theta})\boldsymbol{b}^+(\boldsymbol{\theta}_f, \boldsymbol{\theta}))\boldsymbol{A}\boldsymbol{\tau} = \boldsymbol{0} \tag{5.38}$$

where $\boldsymbol{b}(\boldsymbol{\theta}_f, \boldsymbol{\theta})^+$ is the pseudo inverse matrix of $\boldsymbol{b}(\boldsymbol{\theta}_f, \boldsymbol{\theta})$, and $\boldsymbol{I}$ is the identity matrix.

If (5.38) is satisfied, then exist $\boldsymbol{\tau}$ such that $\boldsymbol{F}$ in the direction of $\boldsymbol{\theta}_f$ exists.

If the objective is to determine the joint actuator torques $\boldsymbol{\tau}$ that maximize the output force at the end effector in direction $\boldsymbol{\theta}_f^*$, then the linear problem formulation is expressed as:

$$\begin{aligned} \max_{\boldsymbol{\tau}} \quad & F = \boldsymbol{b}^+(\boldsymbol{\theta}_f^*, \boldsymbol{\theta})\boldsymbol{A}\boldsymbol{\tau} \\ s.t. \quad & (\boldsymbol{I} - \boldsymbol{b}(\boldsymbol{\theta}_f^*, \boldsymbol{\theta})\boldsymbol{b}^+(\boldsymbol{\theta}_f^*, \boldsymbol{\theta}))\boldsymbol{A}\boldsymbol{\tau} = \boldsymbol{0} \\ & -\boldsymbol{\tau}^m \le \boldsymbol{\tau} \le \boldsymbol{\tau}^m \end{aligned} \tag{5.39}$$

The solution of this problem requires an iterative algorithm. Software tools as MATLAB can resolve such problems.

5.4.4   Proposed 1: Infinity Norm

Given the arm with the statics as in Fig. 5.3 and a force at the end effector $\boldsymbol{F}$, the joint torques $\boldsymbol{T}$ are calculated using (5.12), and the three joint actuator torques τ_1, τ_2 and τ_3 that produces $\boldsymbol{T}$ are calculated using the $\infty - norm$ by resolving the following problem:

$$\begin{aligned} \min \quad & \max\left\{ \frac{|\tau_1|}{\tau_1^m}, \frac{|\tau_2|}{\tau_2^m}, \frac{|\tau_3|}{\tau_3^m} \right\} \\ s.t. \quad & T_1 = \tau_1 + \tau_3 \\ & T_2 = \tau_2 + \tau_3 \end{aligned} \tag{5.40}$$

where τ_i^m is the maximum joint torque that the actuator i can produce. The fact that three torque values are scaled by the respective maximum torque guarantees that the solution, when exists, does not violate any of the three constraints (5.33).

Let us define:

$$c_1 = \frac{\tau_3^m - \tau_1^m}{\tau_3^m + \tau_2^m} \tag{5.41}$$

$$c_2 = \frac{\tau_3^m + \tau_2^m}{\tau_3^m + \tau_1^m} \tag{5.42}$$

$$c_3 = \frac{\tau_3^m - \tau_2^m}{\tau_3^m + \tau_1^m} \tag{5.43}$$

The three parameters c_1, c_2 and c_3 are defined for any maximum joint actuator torque, and are constant. A closed form solution of the problem (5.40)

is determined on the basis of the values of T_1 and T_2 as follows:

$$\tau_1 = \begin{cases} (T_1 - T_2)\frac{\tau_1^m}{\tau_1^m+\tau_2^m} & \text{if } case_1 \\ T_1 - T_2\frac{\tau_3^m}{\tau_2^m+\tau_3^m} & \text{if } case_2 \\ T_1\frac{\tau_1^m}{\tau_1^m+\tau_3^m} & \text{if } case_3 \end{cases} \tag{5.44}$$

$$\tau_2 = \begin{cases} (T_2 - T_1)\frac{\tau_2^m}{\tau_1^m+\tau_2^m} & \text{if } case_1 \\ T_2\frac{\tau_2^m}{\tau_2^m+\tau_3^m} & \text{if } case_2 \\ T_2 - T_1\frac{\tau_3^m}{\tau_1^m+\tau_3^m} & \text{if } case_3 \end{cases} \tag{5.45}$$

$$\tau_3 = \begin{cases} \frac{T_1\tau_2^m+T_2\tau_1^m}{\tau_1^m+\tau_2^m} & \text{if } case_1 \\ T_2\frac{\tau_3^m}{\tau_2^m+\tau_3^m} & \text{if } case_2 \\ T_1\frac{\tau_3^m}{\tau_1^m+\tau_3^m} & \text{if } case_3 \end{cases} \tag{5.46}$$

where

$$case_1 = (T_1 \le c_1 T_2 \text{ and } T_2 \ge c_3 T_1) \text{ or } (T_1 > c_1 T_2 \text{ and } T_2 < c_3 T_1) \tag{5.47}$$
$$case_2 = (T_1 \ge c_1 T_2 \text{ and } T_2 \ge c_2 T_1) \text{ or } (T_1 < c_1 T_2 \text{ and } T_2 < c_2 T_1) \tag{5.48}$$
$$case_3 = (T_2 \le c_2 T_1 \text{ and } T_2 \ge c_3 T_1) \text{ or } (T_2 > c_2 T_1 \text{ and } T_2 < c_3 T_1) \tag{5.49}$$

Proof of (5.44), (5.45), and (5.46) is reported in Appendix B.

It is trivial to verify that the three linear piecewise functions (5.44), (5.45), and (5.46) are continuous in all the domain $D = (T_1, T_2)$.

In summary, the values of τ_1, τ_2 and τ_3 that produce a given $\boldsymbol{F}$ at the end effector, are determined as follows:

1. Calculate the joint torques $\boldsymbol{T} = \boldsymbol{J}^T \boldsymbol{F}$.

2. According to calculated T_1 and T_2, the three joint actuator torques are directly determined using the three piecewise linear function (5.44), (5.45), and (5.46)

When all the actuators produce the same maximum joint torque, that is $\tau_1^m = \tau_2^m = \tau_3^m$, $c_1 = c_3 = 0$ and $c_2 = 1$. Therefore, the solution becomes as in
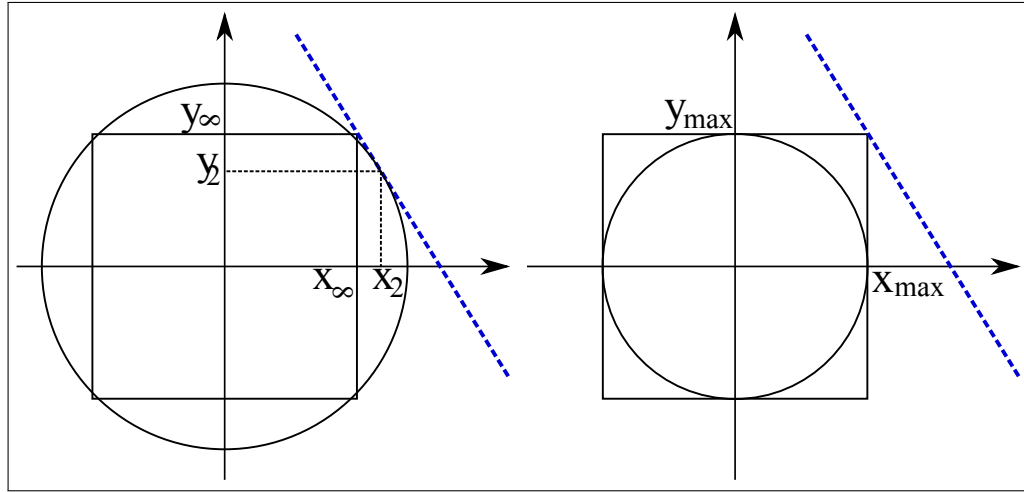
Figure 5.5: Graphical comparison between $\infty - norm$ and $2 - norm$: solution comparison (left), no solution for $2 - norm$ (right)

the following [97]:

$$\tau_1 = \begin{cases} \frac{T_1 - T_2}{2} & \text{if } T_1 T_2 \leq 0 \\ T_1 - \frac{T_2}{2} & \text{if } T_1 T_2 > 0 \text{ and } |T_1| \leq |T_2| \\ \frac{T_1}{2} & \text{if } T_1 T_2 > 0 \text{ and } |T_1| > |T_2| \end{cases} \tag{5.50}$$

$$\tau_2 = \begin{cases} \frac{T_2 - T_1}{2} & \text{if } T_1 T_2 \leq 0 \\ \frac{T_2}{2} & \text{if } T_1 T_2 > 0 \text{ and } |T_1| \leq |T_2| \\ T_2 - \frac{T_1}{2} & \text{if } T_1 T_2 > 0 \text{ and } |T_1| > |T_2| \end{cases} \tag{5.51}$$

$$\tau_3 = \begin{cases} \frac{T_1 + T_2}{2} & \text{if } T_1 T_2 \leq 0 \\ \frac{T_2}{2} & \text{if } T_1 T_2 > 0 \text{ and } |T_1| \leq |T_2| \\ \frac{T_1}{2} & \text{if } T_1 T_2 > 0 \text{ and } |T_1| > |T_2| \end{cases} \tag{5.52}$$

Infinity Norm Approach: the Reason Why

Fig. 5.5 shows the graphical comparison between $\infty - norm$ and $2 - norm$ optimization criteria in selecting the optimal solution for a problem in $\mathbb{R}^2$. The dashed line represents the infinite set of solutions (x, y) that satisfy,

$$k = \alpha x + y \tag{5.53}$$

where α represent the relationship between the desired output k and the necessary inputs x and y. The positive constants mx and my define the allowable

Table 5.3:   Muscle Activation Levels for NLPDC. $(x)^+ = \mathrm{m}(0,x)$ and $(x)^- = \mathrm{m}(-x,0)$

	$\zeta \leq \theta_f^* < \alpha$	$\alpha \leq \theta_f^* < \beta$	$\beta \leq \theta_f^* < \gamma$	$\gamma \leq \theta_f^* < \delta$	$\delta \leq \theta_f^* < \varepsilon$	$\varepsilon \leq \theta_f^* < \zeta$
e_1	$\left(m_1^{\zeta\alpha}\right)^- + \sigma_1$	0	0	$\left(m_1^{\gamma\delta}\right)^- + \sigma_1$	e_1^m	e_1^m
f_1	$\left(m_1^{\zeta\alpha}\right)^+ + \sigma_1$	f_1^m	f_1^m	$\left(m_1^{\gamma\delta}\right)^+ + \sigma_1$	0	0
e_2	e_2^m	e_2^m	$\left(m_2^{\beta\gamma}\right)^- + \sigma_2$	0	0	$\left(m_2^{\varepsilon\zeta}\right)^i -+\sigma_2$
f_2	0	0	$\left(m_2^{\beta\gamma}\right)^+ + \sigma_2$	f_2^m	f_2^m	$\left(m_2^{\varepsilon\zeta}\right)^+ + \sigma_2$
e_3	e_3^m	$\left(m_3^{\alpha\beta}\right)^- + \sigma_3$	0	0	$\left(m_3^{\delta\varepsilon}\right)^- + \sigma_3$	e_3^m
f_3	0	$\left(m_3^{\alpha\beta}\right)^+ + \sigma_3$	f_3^m	f_3^m	$\left(m_3^{\delta\varepsilon}\right)^+ + \sigma_3$	0

ranges for x and y:

$$-mx \leq x \leq mx \tag{5.54}$$

$$-my \leq y \leq my \tag{5.55}$$

The two sets (x_2, y_2) and (x_∞, y_∞) in Fig. 5.5 are the two solutions of (5.53) calculated using the $2-norm$ (the circle) and $\infty-norm$ (the square) optimization criteria, respectively. By definition, the infinity norm minimize the maximum input, therefore it holds:

$$\mathrm{m}\{|x_\infty|, |y_\infty|\} \leq \mathrm{m}\{|x_2|, |y_2|\} \tag{5.56}$$

Therefore, if x and y are bounded, that is $-mx \leq x \leq mx$ and $-my \leq y \leq my$, the $\infty-norm$ model admits solution for higher values of k than the $2-norm$, as shown in Fig. 5.5.

The greater solution space of the $\infty-norm$ model holds also for $\mathbb{R}^3$, which represents the mathematical space of the redundancy resolution problem in this work.

5.4.5   Proposed 2: Non-Linear Phase Different Control

Given a desired output force direction θ_f^*, the muscle activation levels that produce the maximum end effector force $\boldsymbol{F}^m$ using the proposed NLPDC approach are calculated using the same method as in the PDC approach, with the exception of the use of the activation levels in Tab. 5.3 instead than Tab. 5.2 The muscle activation levels m_j^{kl} in Tab. 5.3 are calculated as follows:

$$m_1^{\zeta\alpha} = \frac{(-e_2^m - e_3^m)(a + c\tan(\theta_f^*))}{d\tan(\theta_f^*) + b} + e_3^m \tag{5.57}$$

$$m_3^{\alpha\beta} = \frac{(-f_1^m - e_2^m)(a + c\tan(\theta_f^*))}{(d-c)\tan(\theta_f^*) + b - a} - f_1^m \tag{5.58}$$

$$m_2^{\beta\gamma} = \frac{(f_1^m + f_3^m)(b + d\tan(\theta_f^*))}{c\tan(\theta_f^*) + a} - f_3^m \tag{5.59}$$

$$m_1^{\gamma\delta} = \frac{(f_2^m + f_3^m)(a + c\tan(\theta_f^*))}{d\tan(\theta_f^*) + b} - f_3^m \tag{5.60}$$

$$m_3^{\delta\varepsilon} = \frac{(e_1^m + f_2^m)(a + c\tan(\theta_f^*))}{(d-c)\tan(\theta_f^*) + b - a} + e_1^m \tag{5.61}$$

$$m_2^{\varepsilon\zeta} = \frac{(-e_1^m - e_3^m)(b + d\tan(\theta_f^*))}{c\tan(\theta_f^*) + a} + e_3^m \tag{5.62}$$

where a, b, c, and d are the Jacobian matrix components as in (5.12), m_j^{kl} is the activation level of muscle m, where m is either e or f, which produce torque τ_j with $j = (1,2,3)$ such that the end effector force is maximum in direction θ_f^*. The calculated output force direction (θ_f) is equal to the desired output force direction (θ_f^*), if the two muscles that produce force in direction k and l have maximum activation level. Equations (5.57), (5.58), (5.59), (5.60), (5.61), and (5.62) are derived considering the geometry of the robot arm as reported in the proof in Appendix D.

The values σ_1, σ_2, and σ_3 represent the minimum activation level between two muscles of the every antagonistic pair, which influences the sum mode for the mono-articular muscles at joint 1, the mono-articular ones at joint 2, and the bi-articular ones, respectively. The range values of σ_1, σ_2, and σ_3 depend on the maximum muscle forces as in the following:

$$\sigma_i \in \left[0, \min\left(e_i^m - \left(m_i^{kl}\right)^-, f_i^m - \left(m_i^{kl}\right)^+\right)\right] \tag{5.63}$$

where $i = (1,2,3)$ and $(k,l) = \{(\alpha,\beta), (\beta,\gamma), (\gamma,\delta), (\delta,\varepsilon), (\varepsilon,\zeta), (\zeta,\alpha)\}$.

A graphical example of the use of NLPDC approach is illustrated in Fig. 5.6(b) for $l_1 = l_2 = 1$ m, $\theta_1 = -45°$, $\theta_2 = 90°$, $e_i^m r = f_i^m r = 1$ Nm for $i = (1,2,3)$, and $\sigma_1 = \sigma_2 = \sigma_3 = 0$. The end effector maximum force $\boldsymbol{F}^m$ for $\theta_f^* = 33.75°$ is:

$$\boldsymbol{F}^m = \boldsymbol{F}_{f1}^m + \boldsymbol{F}_{e2}^m + 0.6\boldsymbol{F}_{f3}^m \tag{5.64}$$

Using Tab. 5.3 results:

$$\tau_1 = (f_1 - e_1)r = (f_1^m - 0)r = f_1^m r \tag{5.65}$$

$$\tau_2 = (f_2 - e_2)r = (0 - e_2^m)r = -e_2^m r \tag{5.66}$$

$$\tau_3 = (f_3 - e_3)r = \left(\left(\left(m_3^{\alpha\beta}\right)^+ + \sigma_3\right) - \left(\left(m_3^{\alpha\beta}\right)^- + \sigma_3\right)\right)r = 0.6f_3^m \tag{5.67}$$

(a) Muscle activation level patterns

(b) End effector maximum force
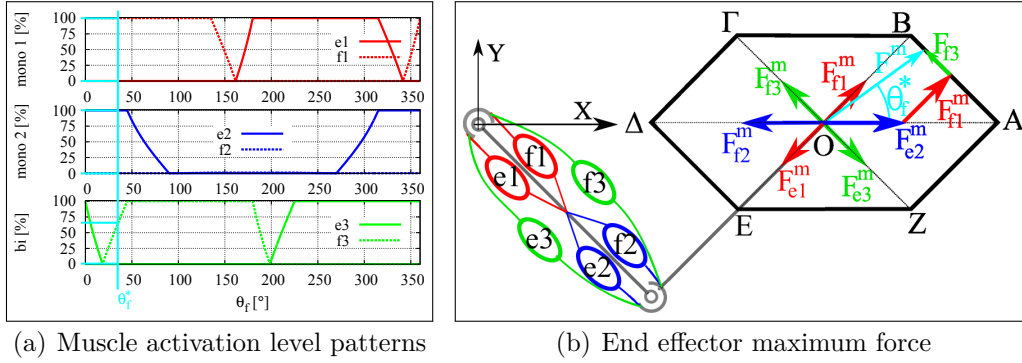
Figure 5.6: The NLPDC approach: muscle activation level patterns and end effector maximum force

By using the NPDCL approach, the sum modes of the three antagonistic pairs can be designed independently from the difference modes. In the case illustrated in Fig. 5.6(b):

$$s_1 = K(f_1 + e_1 + \sigma_1)r = K f_1^m r \tag{5.68}$$

$$s_2 = K(f_2 + e_2 + \sigma_2)r = K e_2^m r \tag{5.69}$$

$$s_3 = K(f_3 + e_3 + \sigma_3)r = K\left(0.6 f_3^m + [0, \min(e_3^m, 0.4 f_3^m)]\right)r \tag{5.70}$$

where $\sigma_1 = \sigma_2 = 0$ because $m_1^{\alpha\beta} = f_1^m$ and $m_2^{\alpha\beta} = -e_2^m$. If an end effector force lower than the maximum one is required, then also $\sigma_1 \geq 0$ and $\sigma_2 \geq 0$.

The six piecewise non linear functions represented in Tab. 5.3 are defined and continuous on the domain $\theta_f \in [0, 360°]$

5.4.6 Simplified NLPDC Approach

If the antagonistic muscles of every pair produce the same maximum joint actuator torque, that is $e_i^m r = f_i^m r = \tau_i^m$ for $i = (1, 2, 3)$, and the is no interest in controlling the sum mode, that is $\sigma_1 = \sigma_2 = \sigma_3 = 0$, then the actuator torque inputs calculation for the NLPDC approach are simply calculated by using Tab. 5.4, where:

Table 5.4: Joint actuator torque for NLPDC

	$\zeta \leq \theta_f^* < \alpha$	$\alpha \leq \theta_f^* < \beta$	$\beta \leq \theta_f^* < \gamma$	$\gamma \leq \theta_f^* < \delta$	$\delta \leq \theta_f^* < \varepsilon$	$\varepsilon \leq \theta_f^* < \zeta$
τ_1	τ_1^{inp}	τ_1^m	τ_1^m	$-\tau_1^{inp}$	$-\tau_1^m$	$-\tau_1^m$
τ_2	$-\tau_2^m$	$-\tau_2^m$	τ_2^{inp}	τ_2^m	τ_2^m	$-\tau_2^{inp}$
τ_3	$-\tau_3^m$	τ_3^{inp}	τ_3^m	τ_3^m	$-\tau_3^{inp}$	$-\tau_3^m$

$$\tau_1^{inp} = \frac{(-\tau_2^m - \tau_3^m)(a + c\tan(\theta_f^*))}{d\tan(\theta_f^*) + b} + \tau_3^m \tag{5.71}$$

$$\tau_2^{inp} = \frac{(\tau_1^m + \tau_3^m)(b + d\tan(\theta_f^*))}{c\tan(\theta_f^*) + a} - \tau_3^m \tag{5.72}$$

$$\tau_3^{inp} = \frac{(-\tau_1^m - \tau_2^m)(a + c\tan(\theta_f^*))}{(d - c)\tan(\theta_f^*) + b - a} - \tau_1^m \tag{5.73}$$

The simplified NLPDC approach is suitable for the following two cases:

1. The antagonistic muscles of every pair produce the same maximum joint actuator torque and the sum mode is desired to be minimum or not to be controlled.

2. A two-link robot arm is actuated by two mono- and one bi-articular actuators, as for example [28], [81].

Chapter 6

Bi-Articular Actuation Implementation

The state of the art in bi-articularly actuated robots is illustarted in Section 6.1, with an highligth on power assist robots equipped with bi-articular actuators (Section 6.1.1). Then, the proposed experimental apparatus, **BiWi** — **Bi**-articularly actuated and **Wi**-re driven robot arm — is described in Section 6.2. The experimental setup, together with the analisys methods are illustrated in Section 6.3. The calculation and experimental results are shown in Section 6.4 and discussed in Section 6.5

6.1 Bi-Articularly Actuated Robots

Regarding the hardware design, bi-articularly actuated robots have been realized by means of pneumatic actuators and motors. As for the transmission systems, timing belts, wires, planetary gears, and passive springs have been used. In the following the state of the art in hardware design of bi-articularly actuated robots is illustrated.

Robots with bi-articular actuators realized using pneumatic actuators are shown in Fig.6.1. The use of pneumatic actuation allows the placement of a high number of actuators on robot links without affecting the link's weight significantly. Moreover, the actuator intrinsic compliance guarantees a certain level of safety. However, pneumatic actuators are non linear and present a limited bandwidth.

Robot legs with bi-articular actuators realized using springs are shown in Fig.6.2. The presence of spring is used in these robots to resemble human muscles characteristics such as compliance, energy storage and proximal to distal joint mechanical energy transfer. In fact, the presence of bi-articular

(a) Airic by Festo

(b) Athlete robot [77]

(c) Mowgly [76]

(d) Anthropomorphic monopod [42]
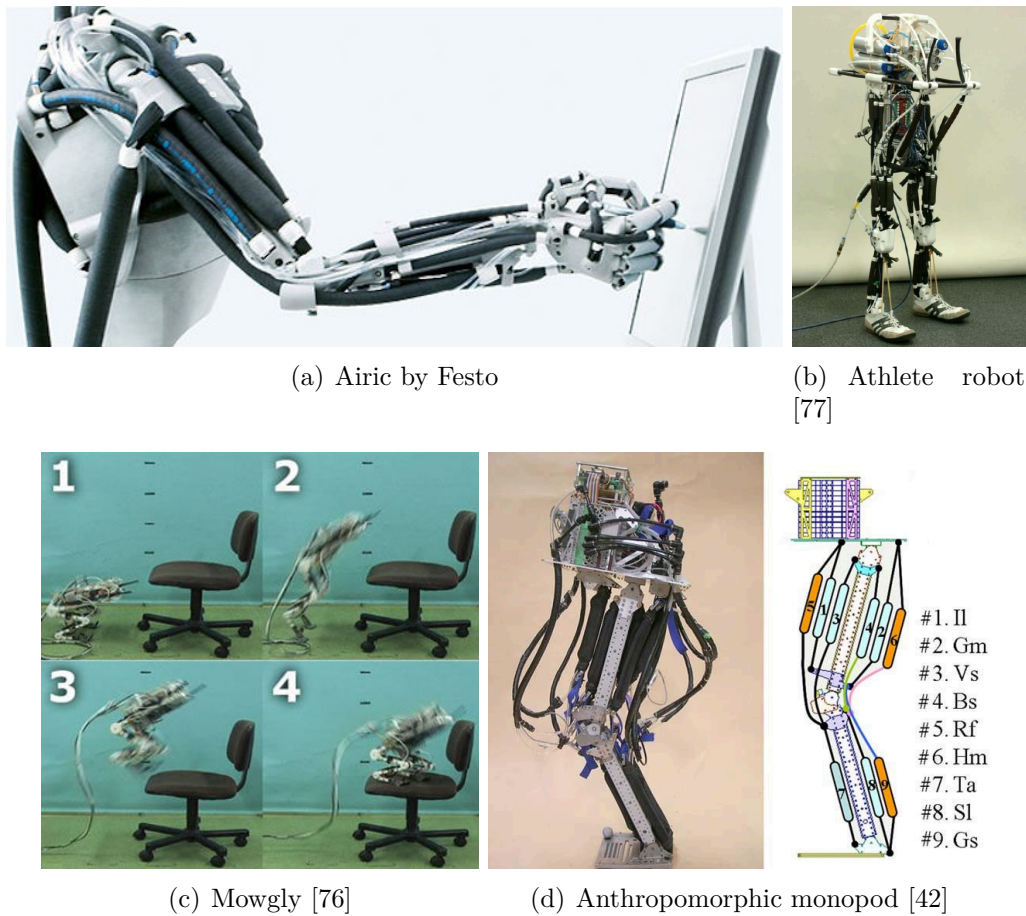
Figure 6.1: Bi-articular actuation realized using pneumatic actuators

springs allows mechanical energy storage [44], as well as increase in walking efficiency [107], in stability [36], and in jump height [4] [64].

In Fig.6.3 robots with bi-articular actuators realized using planetary gears are shown. These robots are designed using the fact that planetary gears are three inputs and two outputs systems. Such systems allows a high freedom in the design of the mono and bi- articular torque gear ratio in a compact form. However, mono- and bi- articular torques are mechanically coupled, therefore a decoupling control strategy is necessary [56]. As a consequence the torque transmission efficiency decreases.

Robots with bi-articular actuators realized using pulleys and timing belts are shown in Fig.6.4. The presence of timing belt without the use of antagonistic actuators causes mono- and bi-articular torque coupling [95]. The Lancelet robot [120] is actuated by tri-articular actuators to mimic the ac-

(a) Jena Walker 2 [107]   (b) Mabel [36]   (c) Kenken[45]
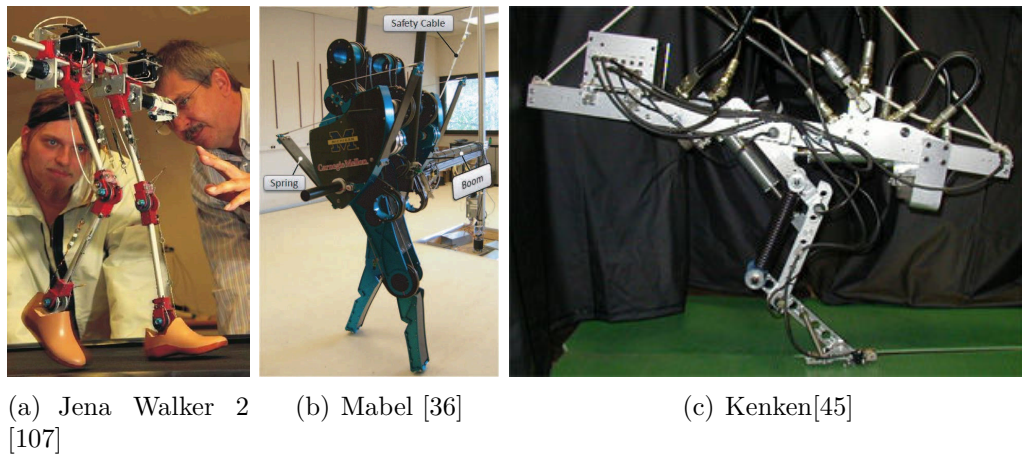
Figure 6.2: Bi-articular actuation realized using motors and springs

(a) Planetary gear based transmission arm [56]   (b) Planetary gear based transmission arm [123]
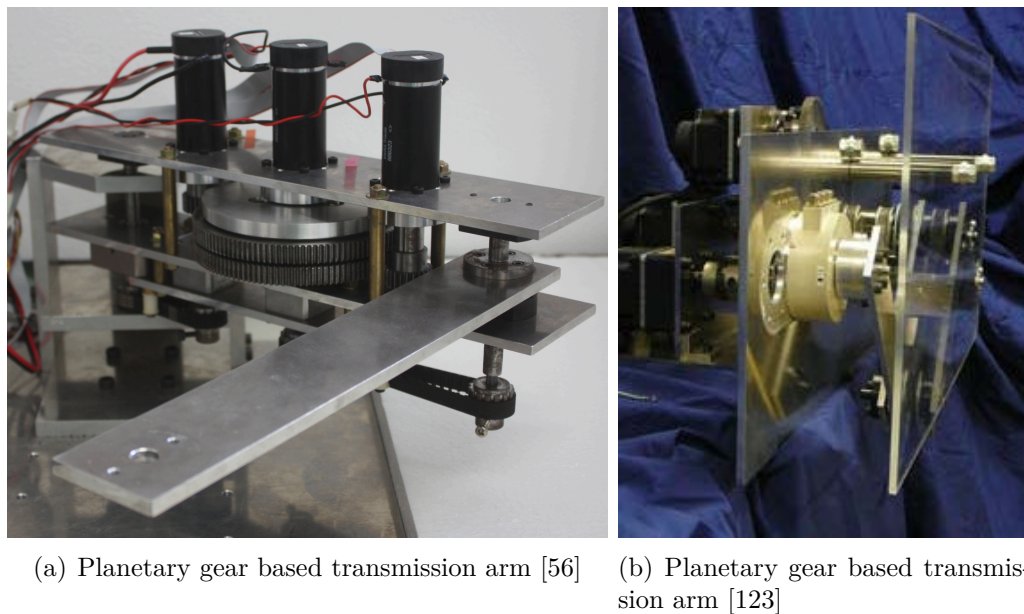
Figure 6.3: Bi-articular actuation realized by planetary gears

tuation of the Lancelet fish. The presence of tri-articular actuators increases the torque transmission efficiency at joint level and allows the Lancelet robot to swim by using a simple sinusoidal time sequence control strategy.

In Fig.6.5 robots with bi-articular actuators realized using pulleys and wires are shown. The use of wires allows the realization of antagonistic bi-

(a) Timing belt based transmission arm [129]

(b) Lancelet robot [120]
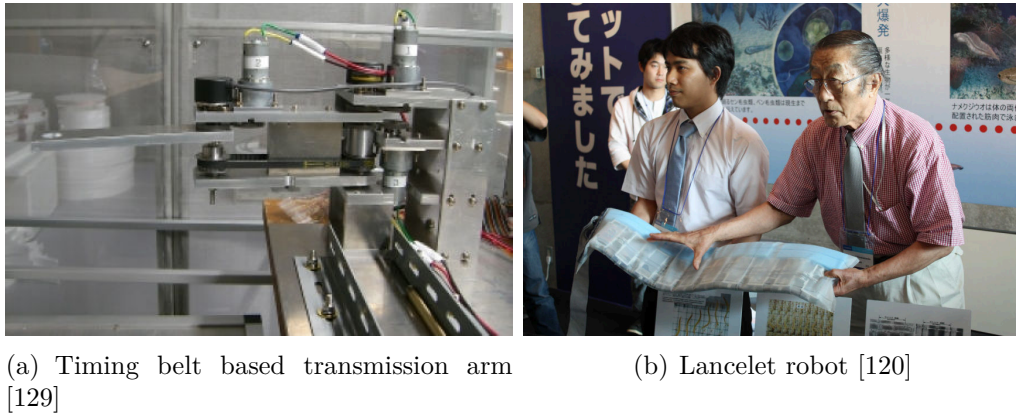
Figure 6.4: Bi-articular actuation realized using pulleys and timing belts

(a) Achille [64]

(b) BiWi [95]
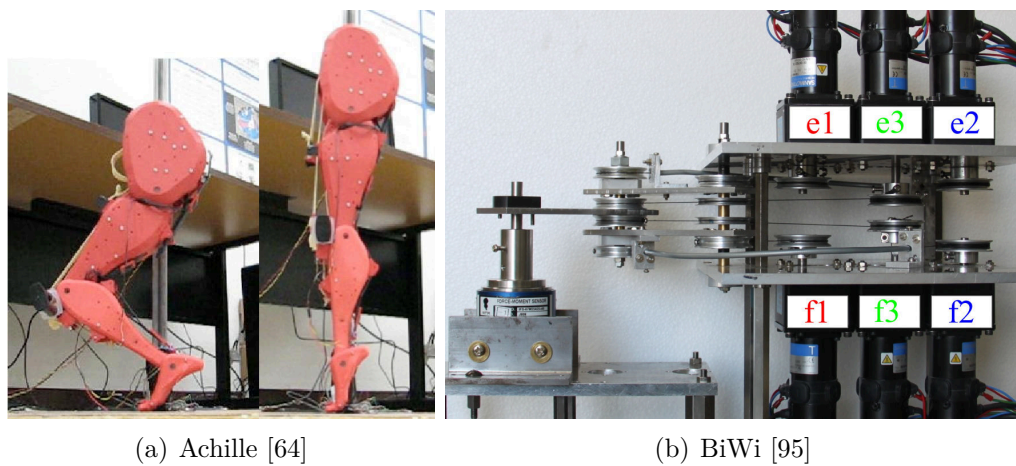
Figure 6.5: Bi-articular actuation realized using pulleys and wires

articular actuators without the necessity of placement of the actuators on the robot link, decreasing link inertia, and increasing energy efficiency and safety [95]. The presence of motors allows a high bandwidth and precise positioning. More details about the proposed experimental apparatus **BiWi** — **Bi**-articularly actuated and **Wi**-re driven robot arm — shown in Fig. 6.5(b) are provided in Section 6.2

A walking robots equipped with bi-articular actuator realized using by spiral motors is shown in Fig. 6.6. Spiral motors have the advantage of producing a great output force in respect to their size, being at the same time backdriveable [27]. These properties make the spiral motor an attractive

(a) Spiral motors   (b) Biped robot

Figure 6.6: Biped robot with bi-articular actuation realized using spiral motors [27] [112]

actuation solution for bipedal robots.

6.1.1 Bi-Articularly Actuated Power Assist Robots

Bi-articular actuation provides important advantages in power assist robots.

Robots with a human-like actuation structure based on mono- and bi-articular actuators produce a maximum output force at the end effector similar to one of the human limbs. In case of controller failure, a rehabilitation robot with a human-like actuation can not produce excessive forces. On the other hand, excessive forces can be produced if only mono-articular actuators are used, as described in detail in Section 5.2.

The upper limb rehabilitation robot developed at Saitama University (Fig. 6.7(a)) is actuated by four mono- and two bi-articular pneumatic actuators to ensure the maximum safety for the user. Other rehabilitation robots equipped with bi-articular actuators are the arm developed at Tokyo Denki University [122] (Fig. 6.7(b)) that is actuated by hydraulic bi-articular actuators, and the lower limb robot realized at Shibaura Institute of Technology [109] (Fig. 6.7(c)) that is actuated by pneumatic bi-articular actuators. Other researches on design and control of bi-articualarly actuated rehabilitation robots for lower limbs can be found in [93] [110].

Power assist devices equipped with bi-articular actuators for lower limb

(a) Saitama University

(b) Tokyo Denki University [122]

(c) Shibaura Institute of Technology [109]
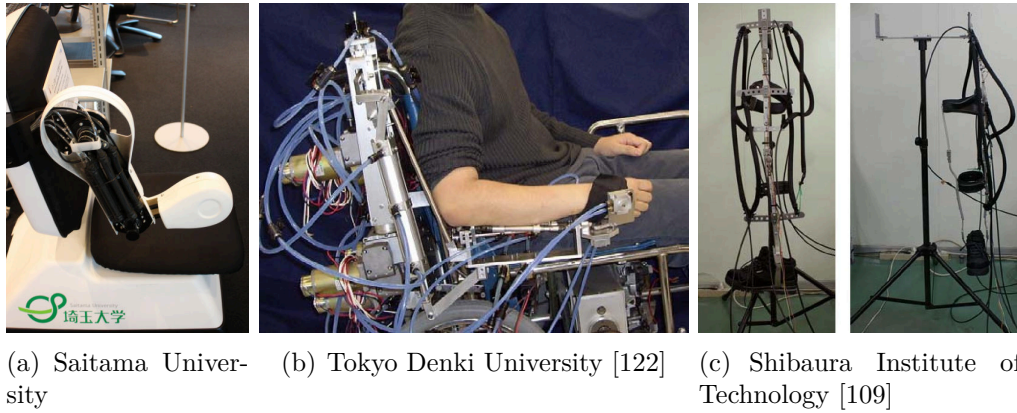
Figure 6.7: Rehabilitation robots equipped with bi-articular actuators

assistance are the device developed Tokyo Denki University [94] illustrated in Fig. 6.8(a), which is actuated by two bi-articular hydraulic actuators for every leg, and the robot realized at Okayama University [47] shown in Fig. 6.8(b).

(a) Tokyo Denki University [94]

(b) Okayama University [47]
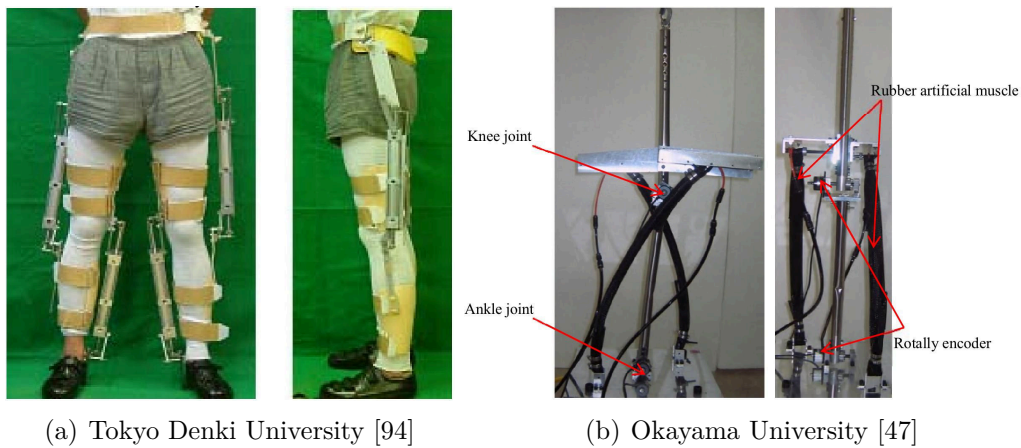
Figure 6.8: Power assist robots equipped with bi-articular actuators

Power assist devices equipped with bi-articular actuators for the upper limb assistance are the robot arm and the glove developed at Tokyo Denki University illustrated in Fig. 6.9(b) and in Fig. 6.9(c), respectively. These devices are actuated by pneumatic artificial rubber bi-articular muscles.

(a) Actuator [116]   (b) Upper limb [116]   (c) Glove [52]
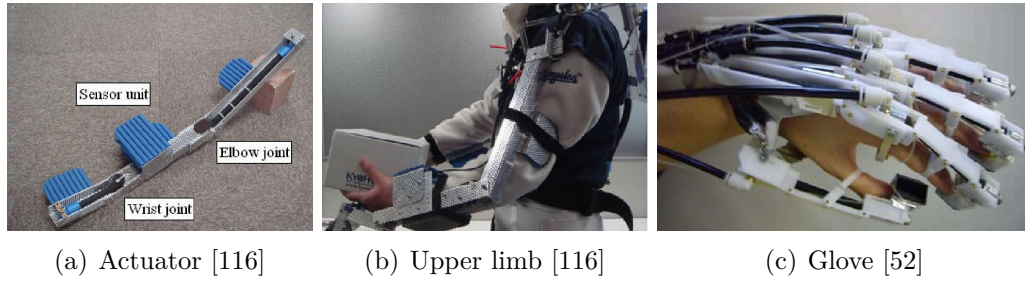
Figure 6.9: Power assist robots equipped with bi-articular actuators developed at the Tokyo Institute of Technology

6.2   BiWi: Bi-Articularly Actuated and Wire Driven Robot Arm

In order to experimentally validate the proposed redundancy resolution approaches ($\infty - norm$ and NLPDC), and compare them with the three traditional redundancy approaches (PDC, $2 - norm$, Linear Programming), **BiWi** — **Bi**-articularly actuated and **Wi**-re driven robot arm — shown in Fig. 6.10 is proposed [95].

BiWi is a two-link planar manipulator actuated by six motors, each representing one of the six muscles in Fig. 5.1(a). The power is transmitted to the joints through pulleys and polyethylene wires as shown in Fig. 6.11:

- A pair of antagonistic mono-articular motors (e_1–f_1) is connected by mean of polyethylene wires to two pulleys fixed on joint 1. This motor pair produces the torque τ_1 about joint 1 as in Fig. 5.1(a).

- A pair of antagonistic mono-articular motors (e_2–f_2) is connected by thrust wires to two pulleys fixed on joint 2. This motor pair produces the torque τ_2 about joint 2 as in Fig. 5.1(a).

- A pair of antagonistic bi-articular motors (e_3–f_3) is connected by mean of polyethylene wires to two pulleys fixed on joint 2, and to free pulleys about joint 1. This motor pair produces the torque τ_3 about joints 1 and 2 as in Fig. 5.1(a).

Further characteristics of BiWi and of the actuator and sensor systems are shown in Tab. 6.1 and Tab. 6.2, respectively.

In the following the main characteristics of the proposed robot arm are described:
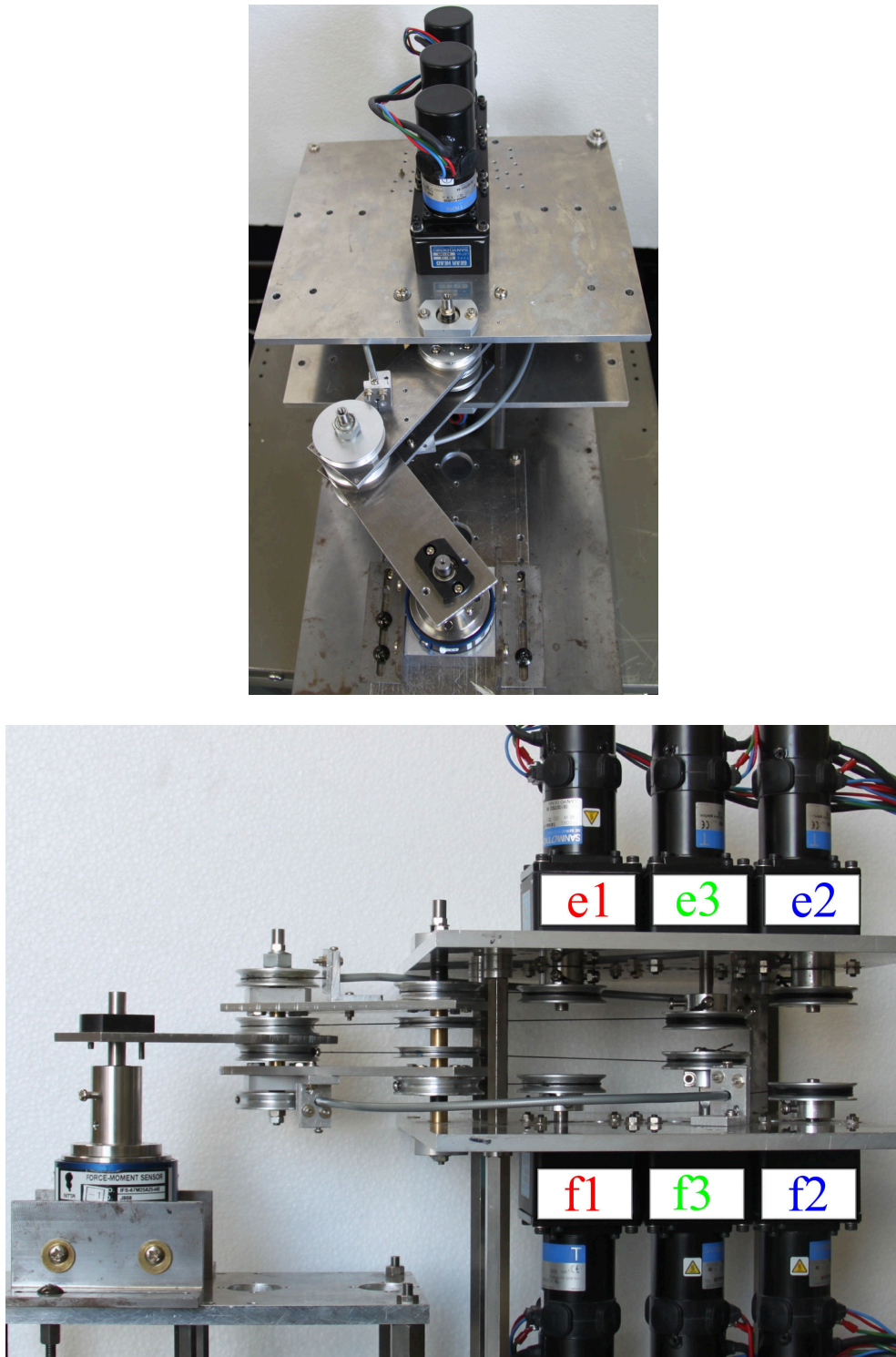
Figure 6.10: BiWi: Bi-articulated and Wire driven robot arm: top view (top), side view (bottom).
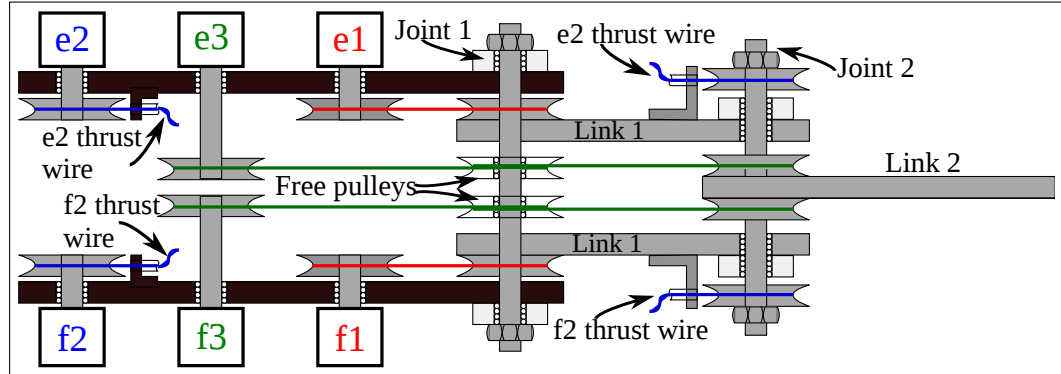
Figure 6.11: Torque transmission system of BiWi

Table 6.1: Biwi characteristics

Parameter	value
Link 1	112 [mm]
Link 2	112 [mm]
Pulleys diameter (all)	44 [mm]
Thrust wire length	30 [mm]

- **Decoupling between mono- and bi-articular actuators joint torques**: in many bi-articularly actuated manipulators, coupling between mono- and bi-articular torques at joint level represents a problem [56] [130]. In fact, if such a torque coupling is present, the maximum output force at the end effector results in a less homogeneous distribution in respect to force direction. Moreover, as input torque in necessary to decouple the actuators, efficiency decreases. On the other hand, thanks to the presence of antagonistic actuators and wire transmission, BiWi presents no coupling between mono- and bi-articular torques at joint level.

- **Low link inertia**: the use of thrust wires to transmit the torque of mono-articular actuators on joint $2 - e_2$ and f_2 – allows the placement

Table 6.2: Actuation and sensing systems

Motors	Sanyo T404-012E59
Gear head	G6-12 (ratio 12.5)
Servo system	TS1A02AA
Force sensor	Nitta IFS-67M25A25-I40

of the motors away from the links reducing their inertia.

- **Safety**: low links inertia increases important factors such as safety in case of impact with human beings [132].

6.3 Experimental Setup

6.3.1 Analysis Methods

Objective

The objective of this work is to investigate new approaches for resolution of actuator redundancy, and comparing them to the traditional methods.

Methods

The two proposed approaches to resolve actuator redundancy for robot arms driven by bi-articular actuators — $\infty-norm$ and NLPDC — are compared with three traditional approaches — PDC, $2-norm$, and Linear Programming — by theoretical and experimental analysis. **BiWi**— **Bi**-articularly actuated and **Wi**-re driven robot arm — is used as an apparatus for the experimental analysis.

Taking into account the arm model in Fig. 5.1(a), the PDC, Linear Programming, and NLPDC approaches determine the six input muscle forces that allow the production of the maximum end effector output force given a desired force direction (θ_f^*). As this work focuses on the resolution of the actuator redundancy problem, the muscle common modes are not taken into account. Therefore, the six input muscle forces determined using these approaches are used together with (5.1), (5.2), and (5.3) to calculate the three actuator joint input torques τ_1, τ_2, and τ_3. This calculation process is illustrated in Fig. 6.12.

On the other hand the $2-norm$ and $\infty-norm$ approaches determine the three actuator joint torque that produce an end effector output force $\boldsymbol{F}$. The iterative algorithm illustrated Fig. 6.13 is used to determine the three actuator joint input torques τ_1, τ_2, and τ_3 that produce the maximum end effector output force given a force direction (θ_f). The algorithm is described in details in Appendix C.

Analyzed Aspects

Given a desired force direction (θ_f^*), the Linear Programming, NLPDC, and $\infty-norm$ approaches determine the same joint actuator torques, τ_1, τ_2, and
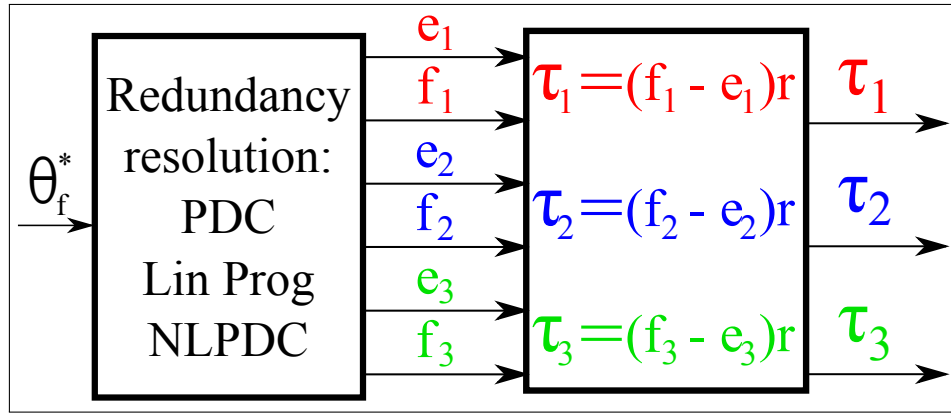
Figure 6.12: Calculation of actuator joint input torques for the PDC, Linear Programming, and NLPDC approaches

τ_3 that produce the maximum output force $\boldsymbol{F}^m$. As a consequence these three three methods are not compared among each other from a maximum output force $\boldsymbol{F}^m$ to joint actuator torques τ_1, τ_2, and τ_3.

The proposed $\infty - norm$ is compared with the $2 - norm$ in in Section 6.4.1, while the NLPDC is compared to PDC in 6.4.2. The comparison in both cases is realized showing what are the calculated joint actuator input torques, and the calculated and experimentally measured end effector maximum output force at BiWi.

Other criteria of comparisons among the five actuator redundancy methods, as for example the possibility to be extended to manipulator with more than two joints, are discussed in Section 6.5.

6.3.2 Feedforward Control Strategy

The feedforward control strategy used to collect the experimental data is shown in Fig. 6.14.

Given the desired end effector output force direction ($\boldsymbol{\theta}_f^*$), one of the five approaches to resolve actuator redundancy is used to calculate the joint actuator torques, τ_1, τ_2, and τ_3 as shown in Sections 6.3.1.

The six motor reference torques that correspond to the six muscles of
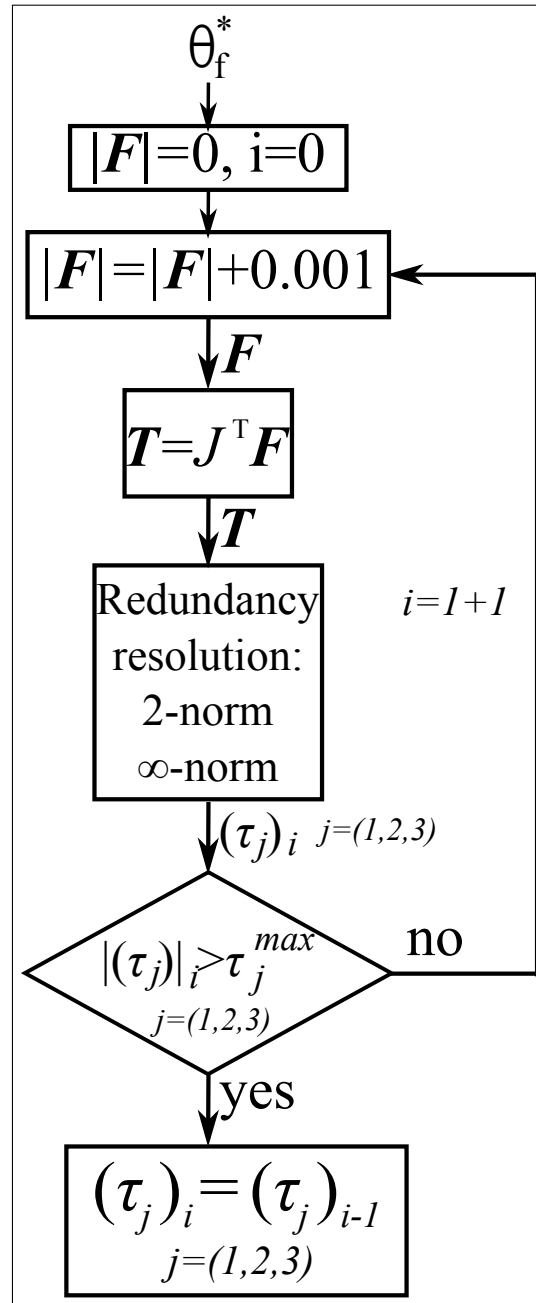
Figure 6.13: Calculation of actuator joint input torques for the $2-norm$ and $\infty-norm$ approaches
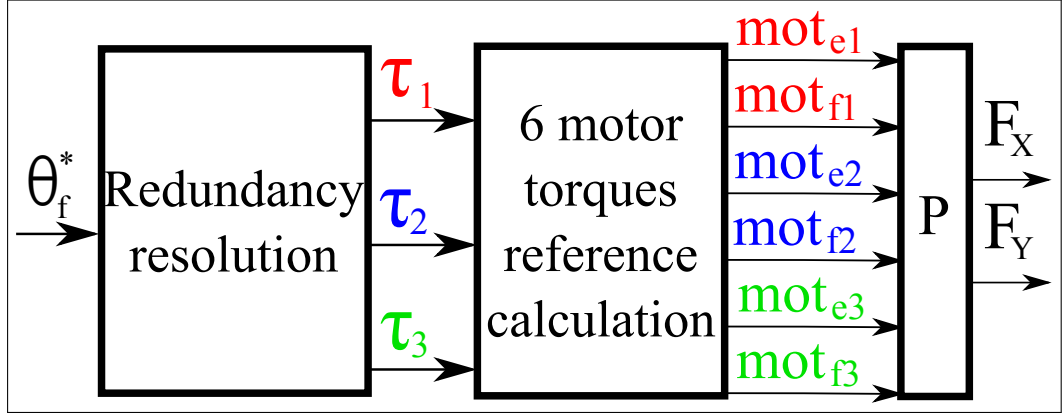
Figure 6.14: Feedforward control block diagram

Fig. 5.1(a) – e_1, f_1, e_2, f_2, e_3, f_3 – are calculated as:

$$mot_{e1} = \begin{cases} \tau_1 & \text{if } \tau_1 < 0 \\ 0 & \text{otherwise} \end{cases} \tag{6.1}$$

$$mot_{f1} = \begin{cases} \tau_1 & \text{if } \tau_1 > 0 \\ 0 & \text{otherwise} \end{cases} \tag{6.2}$$

$$mot_{e2} = \begin{cases} K_{tl}\tau_2 & \text{if } \tau_2 < 0 \\ 0 & \text{otherwise} \end{cases} \tag{6.3}$$

$$mot_{f2} = \begin{cases} K_{tl}\tau_2 & \text{if } \tau_2 > 0 \\ 0 & \text{otherwise} \end{cases} \tag{6.4}$$

$$mot_{e3} = \begin{cases} \tau_3 & \text{if } \tau_3 < 0 \\ 0 & \text{otherwise} \end{cases} \tag{6.5}$$

$$mot_{f3} = \begin{cases} \tau_3 & \text{if } \tau_3 > 0 \\ 0 & \text{otherwise} \end{cases} \tag{6.6}$$

$$\tag{6.7}$$

In order to compensate for the inevitable transmission loss in the thrust wires the reference motor torques for joint 2 – mot_{e2} and mot_{f2} – are multiplied by a constant $K_{tl} = 1.33$. Such value is relatively high, due to the low cost of the thrust wires. However, by using more sophisticated thrust wires the transmission loss can be reduced to smaller value, for example to **5%** of the input torque as in [115].

The calculated reference motor torques (mot_{ei} and mot_{fi} for $i = \{1,2,3\}$) are sent to the robot arm as step inputs. The manipulator end effector output force ($\mathbf{F} = [F_x, F_y]^T$) is measured by a force sensor, and its steady state value is taken into account. The end effector output force direction (θ_f) is varied from 0 to $360°$ every $5°$.

6.4   Results

The proposed $\infty - norm$ is compared with the $2 - norm$ in in Section 6.4.1, while the NLPDC is compared to PDC in 6.4.2. The comparison in both cases is realized showing what are the calculated joint actuator input torques, and the calculated and experimentally measured end effector maximum output force at BiWi.

Four configuration of BiWi are considered:

- Configuration I: $\theta_1 = -60°$ and $\theta_2 = 120°$

- Configuration II: $\theta_1 = -45°$ and $\theta_2 = 90°$

- Configuration III: $\theta_1 = -30°$ and $\theta_2 = 60°$

- Configuration IV: $\theta_1 = -25°$ and $\theta_2 = 50°$

6.4.1 $2 - norm$ vs. $\infty - norm$

The maximum output force at the end effector of BiWi is calculated and experimentally measured using the $2 - norm$ and the $\infty - norm$ approaches.

The results are shown in Fig. 6.15 for configurations I and II, and in Fig. 6.16 for configurations III and IV. The desired force direction at the end effector (θ_f^*) varies from 0 to $360°$ every $5°$.

The experimental results agree with the calculated values, and show that the maximum output force at the end effector is greater, when using the $\infty - norm$ approach.

The joint actuator input patterns calculated using the $\infty - norm$ approach are continuous in respect to θ_f as shown in Fig. 6.15 for configurations I and II, and in Fig. 6.16 for configurations III and IV. Therefore, the three switching conditions used for the redundancy resolution in the $\infty - norm$ approach do not result in torque reference discontinuities, which could cause instability to the system.
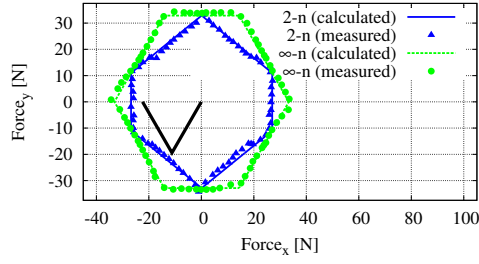
(a) Maximum output force
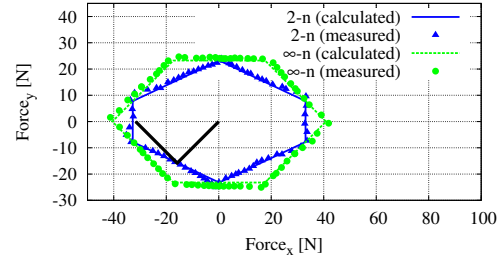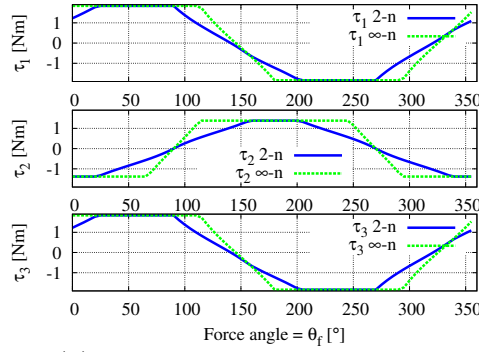
(d) Maximum output force

(b) Joint actuator torque inputs
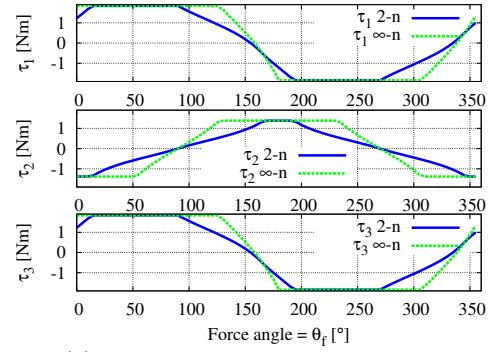
(e) Joint actuator torque inputs
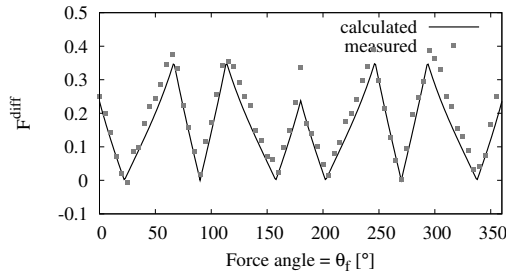
(c) Difference in maximum output force
$\theta_1 = -60°$ and $\theta_2 = 120°$
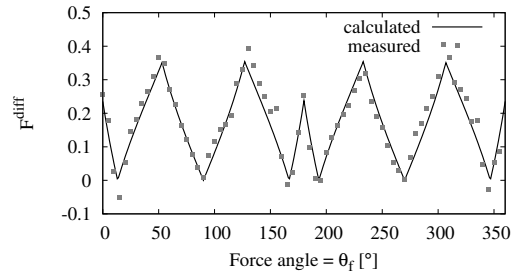
(f) Difference in maximum output force
$\theta_1 = -45°$ and $\theta_2 = 90°$

Figure 6.15: $\infty-norm$ vs. $2-norm$: measured maximum output force (top), joint actuator torque inputs (middle), and difference in maximum output force (bottom), for configurations I (left) and II (right).

The relative difference in maximum output force magnitude is expressed by:

$$F^{diff} = \frac{|F^m_{\infty-n}| - |F^m_{2-n}|}{|F^m_{2-n}|} \tag{6.8}$$

The value of F^{diff} is always positive, indicating that the maximum end effector output force obtained using the $\infty-norm$ approach is always greater (or

(a) Maximum output force

(d) Maximum output force

(b) Joint actuator torque inputs

(e) Joint actuator torque inputs

(c) Difference in maximum output force
$\theta_1 = -30°$ and $\theta_2 = 60°$

(f) Difference in maximum output force
$\theta_1 = -25°$ and $\theta_2 = 50°$
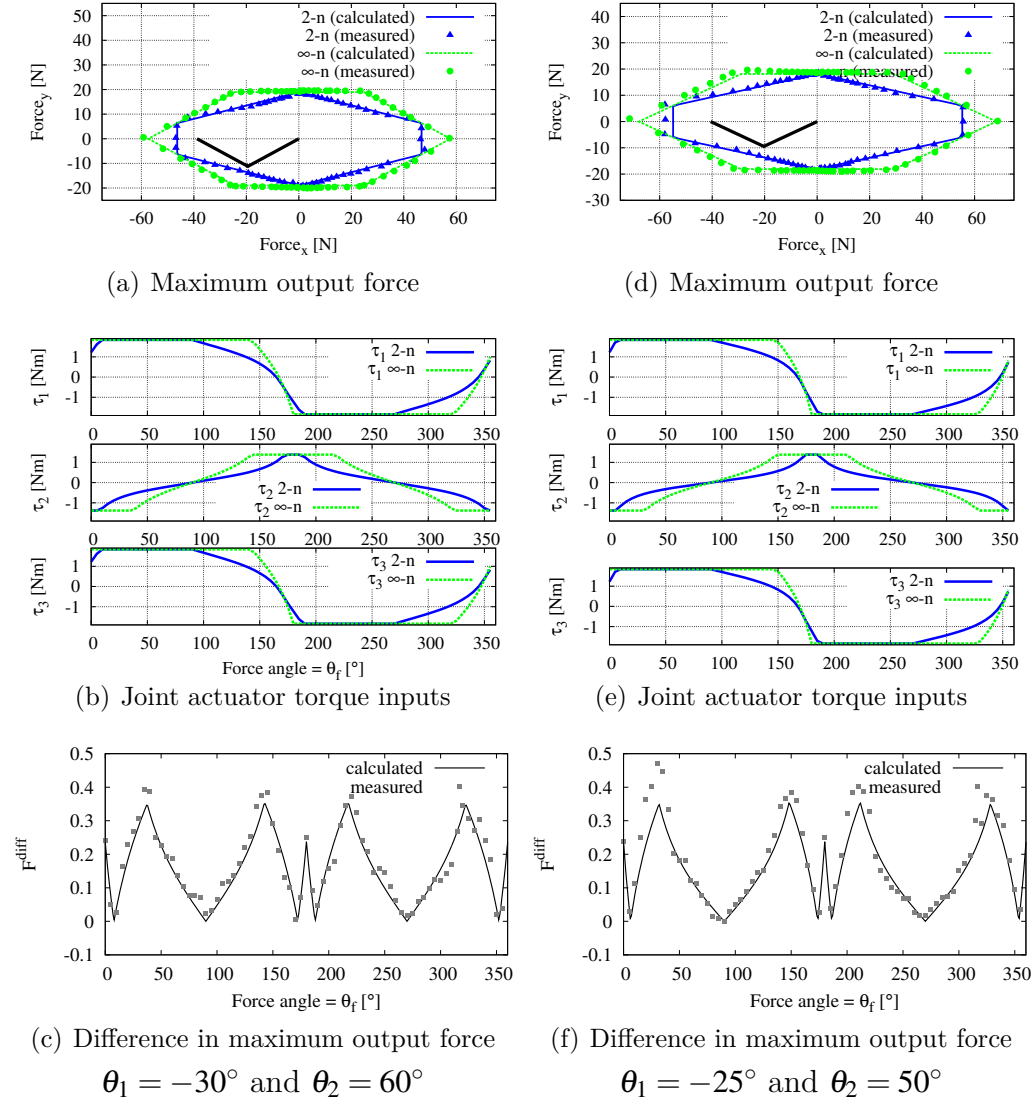
Figure 6.16: $\infty-norm$ vs. $2-norm$: measured maximum output force (top), joint actuator torque inputs (middle), and difference in maximum output force (bottom), for configurations III (left) and IV (right).

equal) to the one obtained using the $2-norm$ approach. The maximum F^{diff} is about 0.35 for all the four configuration. The greater maximum output force represents the main advantage of the proposed $\infty-norm$ approach in respect to the $2-norm$ approach.

6.4.2 PDC vs. NLPDC

The joint actuator torque input patterns calculated using PDC and NLPDC are shown in Fig. 6.17 for the four configurations. In both the approaches the
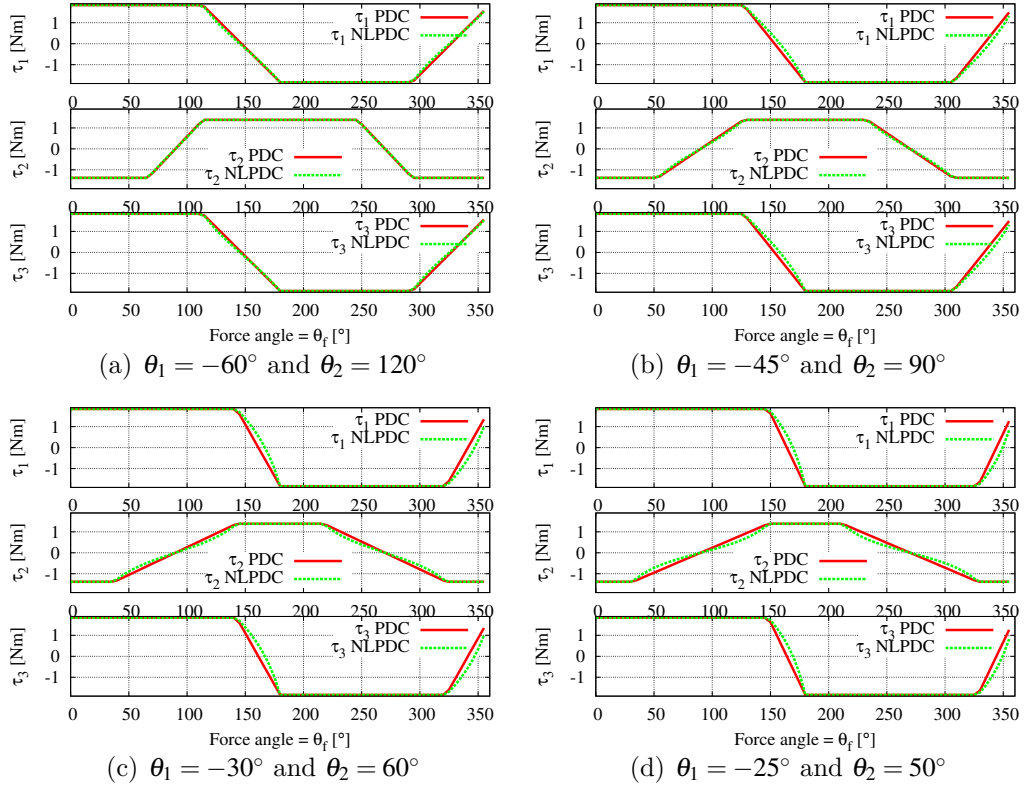
Figure 6.17: Joint actuator torque input patterns calculated using PDC and NLPDC

joint actuator input torque patterns are continuous in respect to the output force angle (θ_f). Therefore, the six switching conditions in both approaches do not cause torque reference discontinuities, which could cause instability to the system.

The maximum output force at the end effector of BiWi, calculated using the joint actuator input torque patterns of Fig. 6.17, is shown in Fig. 6.18. The desired force direction at the end effector (θ_f^*) varies from 0 to 360° every 5°. The joint actuator torque input patterns determined using the NLPDC produces no error in calculation of end effector output force. On the other hand, for the PDC approach the error in output force is small in configuration I, but it increases significantly when the arm moves towards configuration IV.

(a) $\theta_1 = -60°$, $\theta_1 = 120°$

(b) $\theta_1 = -45°$, $\theta_1 = 90°$

(c) $\theta_1 = -30°$, $\theta_1 = 60°$
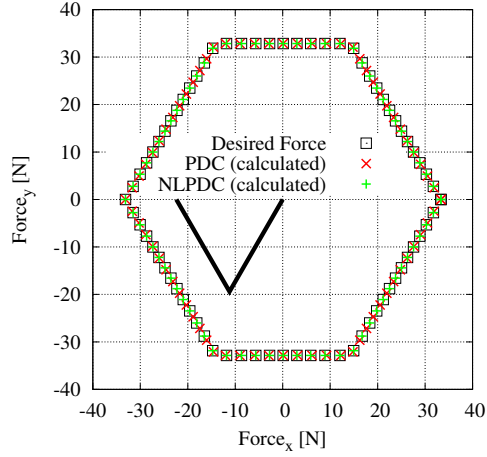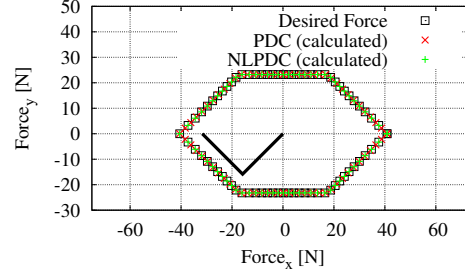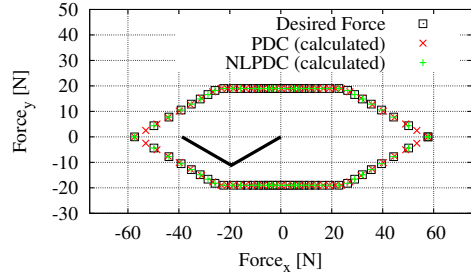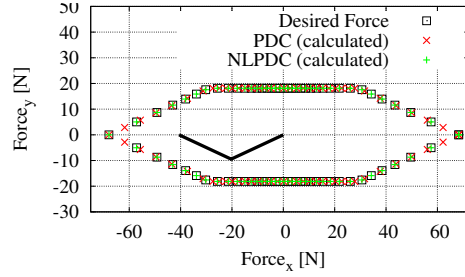
(d) $\theta_1 = 25°$, $\theta_1 = 50°$

Figure 6.18: Calculated maximum output force at the end effector of BiWi using PDC and NLPDC

The measured maximum output force at the end effector of BiWi, using the joint actuator torque input of Fig. 6.17, is shown in Fig. 6.19 for the four configurations. The experimental results show a greater error in output force for the PDC approach, as illustrated in Fig. 6.20, where it is shown the relative error of output force magnitude for the calculation and experimental measurement, respectively defined as

$$f_{cal}^{err} = \frac{|\boldsymbol{F}^{calculated}| - |\boldsymbol{F}^m|}{|\boldsymbol{F}^m|} \tag{6.9}$$

and

$$f_{mea}^{err} = \frac{|\boldsymbol{F}^{measured}| - |\boldsymbol{F}^m|}{|\boldsymbol{F}^m|} \tag{6.10}$$

where:

(a) $\theta_1 = -60°$, $\theta_1 = 120°$

(b) $\theta_1 = -45°$, $\theta_1 = 90°$

(c) $\theta_1 = -30°$, $\theta_1 = 60°$

(d) $\theta_1 = 25°$, $\theta_1 = 50°$
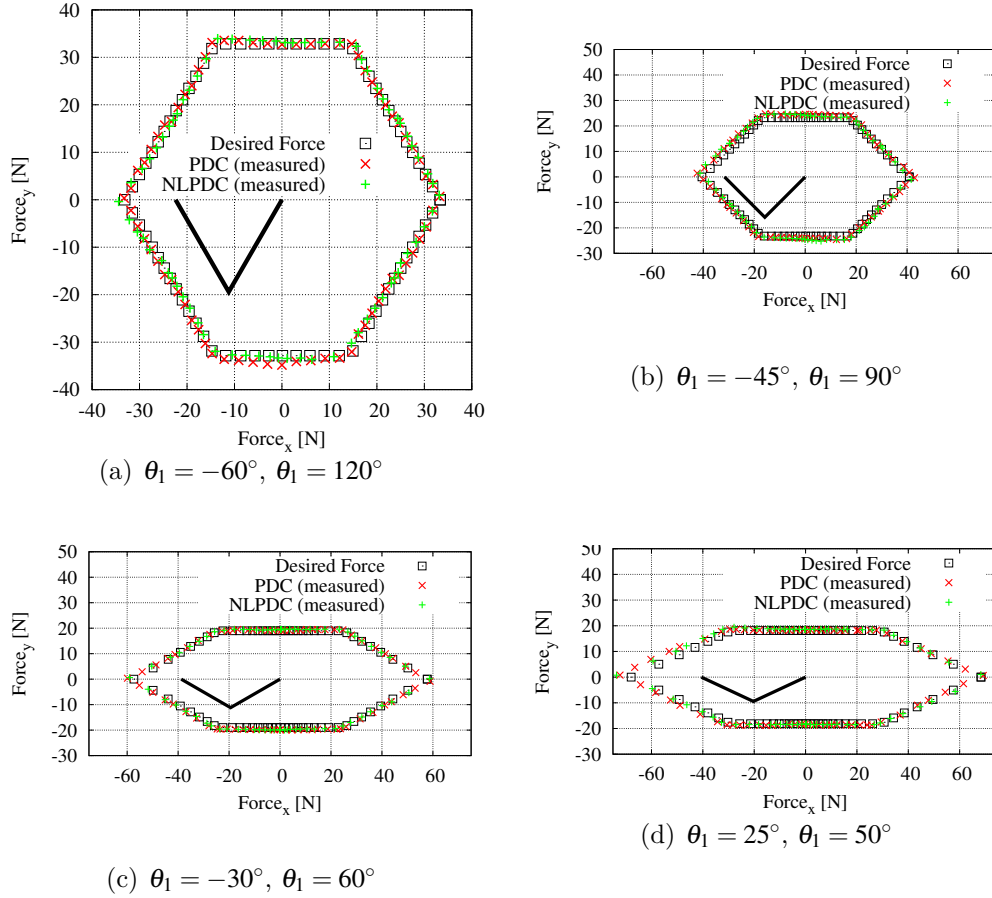
Figure 6.19: Measured maximum output force at the end effector of BiWi using PDC and NLPDC

- $\boldsymbol{F}^{calculated}$ is derived from (5.9), (5.10), (5.12), (5.1), (5.2), and (5.3), together with Tab. 5.2 for the PDC, and Tab. 5.3 for the NLPDC, respectively

- $\boldsymbol{F}^m$ is the maximum output force that can be obtained on direction θ_f^*.

The measured relative error of output force magnitude do not show significant difference between PDC and NLPDC approaches in configuration I, where $f_{mea}^{err} \approx 0.04$. Such error is is due to sensor noise and inevitable modeling errors, and in the case of the PDC approach increases when the arm moves towards singular configurations. In configuration IV, f_{mea}^{err} for the PDC approach has peaks of about 0.25, which is a significant error, and must be taken into account in the control of bi-articualrly actuated robot arms.

(a) $\theta_1 = -60°$, $\theta_1 = 120°$

(b) $\theta_1 = -45°$, $\theta_1 = 90°$

(c) $\theta_1 = -30°$, $\theta_1 = 60°$

(d) $\theta_1 = 25°$, $\theta_1 = 50°$
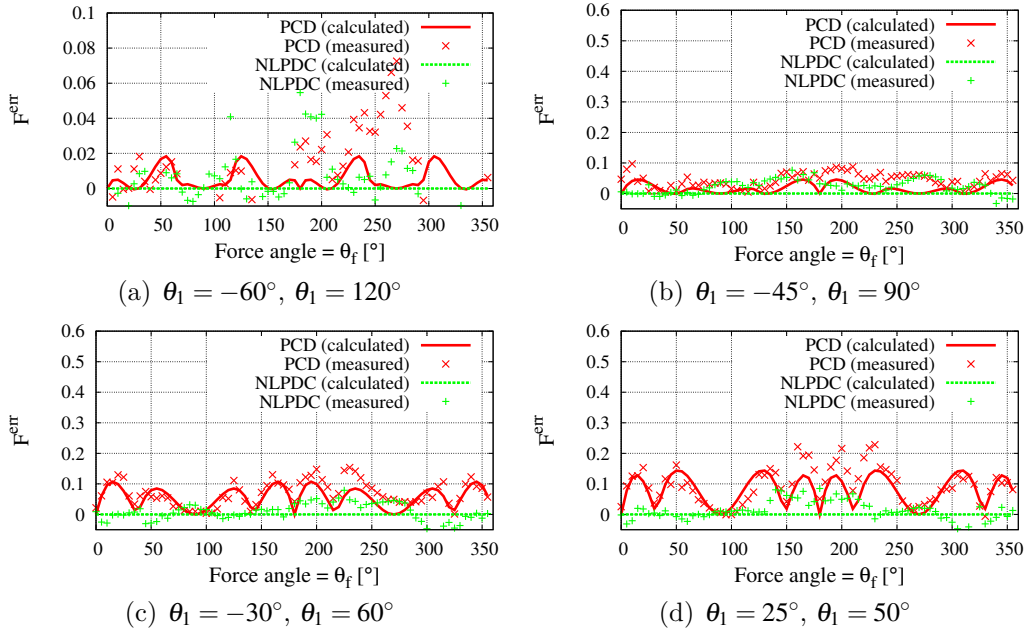
Figure 6.20: Relative error of output force magnitude f_{cal}^{err} and f_{mea}^{err} using PDC and NLPDC

6.5 Discussion on Bi-Articular Actuation

Biologically inspired robot arms such as the ones driven by bi-articular actuators present usually more actuators than joints, resulting in actuator redundancy.

The two proposed approaches to resolve actuator redundancy for robot arms driven by bi-articular actuators — $\infty - norm$ and NLPDC — are compared with three traditional approaches — PDC, $2 - norm$, and Linear Programming — by theoretical and experimental analysis.

A biologically inspired robot arm named **BiWi** — **Bi**-articularly actuated and **Wi**-re driven robot arm — is proposed as an experimental apparatus. BiWi is actuated by six motors arranged so to reproduce the human musculoskeletal system characteristics in term of force production. The wire based transmission system allows the reduction of link inertia thanks to the placement of motors away from the links, and the increase of energy efficiency and safety. The combination of antagonistic actuators and wire transmission allow a perfect decoupling between mono- and bi-articular actuators joint torques, resulting in a homogeneous distribution of force the end effector in respect to force direction. The experimental measurements were conducted on the basis of a feedforward control strategy.

6.5.1   Type of solution

Both the traditional $2-norm$ and the proposed $\infty-norm$ approaches determine the three joint actuator torques τ_1, τ_2, τ_3 that produce an end effector output force ($\boldsymbol{F}$). The maximum end effector output force $\boldsymbol{F}^m$ that can be produced on a desired direction $\boldsymbol{\theta}_f^*$ can not be directly calculated, an iterative algorithm is used. For both the approaches a closed form solution to calculate the three joint actuator torques τ_1, τ_2, τ_3 given an end effector output force $\boldsymbol{F}$ is derived. The closed form solution of the $2-norm$ approach is based on three linear functions, one for every joint actuator torque input τ_1, τ_2, τ_3. The closed form solution of the $\infty-norm$ approach is based on three piecewise functions, one for every joint actuator torque input τ_1, τ_2, τ_3. Every piecewise function is made of three linear functions that depend on the value of the joint torque T_1 and T_2. The three piecewise linear functions are defined and continuous in all the domain $\boldsymbol{D} = (T_1, T_2)$.

The PDC, Linear Programming, and NLPDC approaches determine the six muscle force inputs that produce the maximum end effector output force $\boldsymbol{F}^m$ on a desired direction $\boldsymbol{\theta}_f^*$. The six muscle force inputs calculated with these three approaches can be combined to calculate the three joint actuator torques τ_1, τ_2, τ_3 If an end effector output force ($\boldsymbol{F}$) lower than the maximum one ($\boldsymbol{F}^m$) is required, the six muscle force inputs have to be linearly scaled by the relationship between $\boldsymbol{F}$ and $\boldsymbol{F}^m$.

The PDC approach has a closed form solution based on three piecewise functions, one for every joint actuator torque input τ_1, τ_2, τ_3. Every piecewise function is made of six linear functions that depend on the value of the output force direction $\boldsymbol{\theta}_f$. These six piecewise functions are defined and continuous in all the domain $\boldsymbol{\theta}_f \in [0, 360°]$. There is no closed form solution for the Linear Programming approach, therefore an iterative algorithm should be used to determine the joint actuator torque input τ_1, τ_2, τ_3 that produce the maximum end effector output force $\boldsymbol{F}^m$ given a desired force direction $\boldsymbol{\theta}_f^*$.

The NLPDC approach has a closed form solution based on three piecewise functions, one for every joint actuator torque input τ_1, τ_2, τ_3. Every piecewise function is made of six non linear functions that depend on the value of the output force direction $\boldsymbol{\theta}_f$. These six piecewise functions are defined and continuous in all the domain $\boldsymbol{\theta}_f \in [0, 360°]$.

6.5.2   Relationship between Desired Output Force and Desired Actuators Joint Torque Inputs

Given a desired force direction $\boldsymbol{\theta}_f^*$, both the proposed approaches — $\infty-norm$ and NLPDC — and the Linear Programming approach determine the same

joint actuator torque input $\tau = [\tau_1, \tau_2, \tau_3]^T$ that produce the maximum end effector output force $\boldsymbol{F}^m$.

From the comparison between the $\infty - norm$ approach to the $2 - norm$ approach emerges that:

- Under the same maximum joint actuator torques, the proposed approach allows to obtain a greater output force at the end effector (up to 35%), especially in force output direction peculiar for application which interact with humans such as rehabilitation robots, as well as for jumping/waking robots.

- The calculation are confirmed by experimental results

From the comparison between the NLPDC approach and the PDC approach emerges that:

- Given a desired output force at the end effector, the NLPDC approach produces no error in calculation of joint actuator torque inputs that produce the desired output force. On the other hand the PDC approach produces non-zero error in such calculation.

- The relative error of output force magnitude (F^{err}) has no significant difference when the angle between links 1 and 2 (θ_2) is about 120°. However, F^{err} increases when the arm moves towards singular configurations. For $\theta_2 = 25°$, F^{err} has peaks of about 0.25 for the PDC approach.

- The output error in the PDC depends on three factors — the desired force direction (θ_f^*), the angle between the links (θ_2), and on the link length ratio — and can increase exponentially when the manipulator moves towards singular configurations [100].

- The calculation are confirmed by experimental results.

6.5.3   Generalization to more links and muscles

The PDC the NLPDC approaches are specific for two-link manipulators with six actuators, every one with arbitrary maximum joint torque.

The $\infty - norm$ approach is suitable for for two-link manipulators with three joint actuators, two mono-articular and one bi-articular, every one with arbitrary maximum joint torque. This include the case of six actuators paired in three antagonistic pairs, if the two antagonistic actuators of every pair have the same maximum joint torque.

On the other hand, the $2 - norm$ and Linear Programming approaches can be used for any number of links and actuators. The Linear Programming allows anyway to obtain the maximum output force, but requires an iterative algorithm to find a solution. As the joints and muscles increases the computation needed by the iterative algorithm increases as well. The $2 - norm$ approach can generate a direct solution, however the maximum output force is limited to a lower value than the one achievable with the Linear Programming method.

6.5.4 Summary table

The comparison between the five approaches for actuator redundancy resolution of robot arms driven by bi-articular actuators is summarized in Tab. 6.5.4. The symbol "◯" stands for good, the "△" for not so good, the "X" for not possible. Where there is a "(?)" it means that a further investigation can determine a possible solution.

Table 6.3: Redundancy resolution approaches comparison

	PDC	$2 - n$	LP	$\infty - n$	NLPDC
$\boldsymbol{F^m}$	△	△	◯	◯	◯
$\boldsymbol{F}$ to $\boldsymbol{\tau}$ closed form solution	△	◯	X	◯	◯
Computation	◯	◯	△	◯	◯
Linear	◯	◯	◯	◯	X
$\boldsymbol{F^m}$ to $\boldsymbol{\tau}$ closed form solution	△	X	X	X	◯
Design stiffness & torque independently	X	△	(?)	△	◯
2 joints and 6 muscles	△	◯	◯	△	◯
3 or more joints	(?)	◯	◯	(?)	(?)
7 or more actuators	(?)	◯	◯	(?)	(?)

As results from Tab. 6.5.4:

- For a two-link manipulator the combination of $\infty - norm$ and NLPDC is the best.

- For more than two links and six muscles LP is the best.

Chapter 7

Conclusions and Future Works

7.1 Conclusions

Power assist devices are used for three main reasons: increasing performances such as muscle strength and endurance for workers in health-care centers and hospitals, wild land firefighters, disaster relief workers, soldiers, heavy labour factories, and in any other emergency situations; supporting elderly and disabled people; providing support in rehabilitation processes and physical training.

Although big progress have been done, there are still three main challenging aspects which need more investigation and innovative solutions to improve: safety for the user and the surrounding environment, a comfortable and user-friendly human-robot interaction, and performances such as response speed, end effector force production and energy efficiency.

Most of the ongoing researches focus on power assist robot hardware and control design with a pure engineering approach, neglecting the inspiration from nature. Biologically inspired robotics is a process that goes beyond merely copying what nature shows at first sight. It involves three phases:

1. Observation and understanding nature

2. Design robots not copying from nature, but embedding and resembling the desired nature functionalities

3. Implementation and development

Understanding humans and animal functionalities and the following implementation on robot applications has shown to improve robot performances in terms of robustness, safety, and flexibility in a variety of complex dynamic tasks.

In order to increase safety, robustness, time response, and precision in output force for power assist robots, in this work we are **inspired by biological motion control and actuation mechanisms**. These two inspirational mechanisms are:

1. **Variable impedance control strategy**: humans and animals highly vary impedance of their body to stabilize unstable dynamics.

2. **Bi-articular muscles**: bi-articular muscles — muscles that span two joints — play a fundamental role for mechanical energy transfer, impedance modulation and stabilization of human and animal dynamics.

Based on human Variable Impedance control strategy, a new approach to force control for power assist devices — Force Sensor-less Power Assist Control (FSPAC) with Variable Impedance — is proposed.

The proposed FSPAC with Variable impedance is successfully implemented on an experimental door actuated by either a linear motor (low friction system) or by a rotational motor and a ballscrew (high friction system). A comparison with traditional FSPAC is carried out. The superiority of the proposed FSPAC with Variable Impedance in respect to the traditional FSPAC with Constant Impedance, in terms of safety, robustness and smoothness in assistance is experimentally shown.

Regarding the design of bi-articularly actuated robots, our focus is on the resolution of the redundancy actuation resulting from the presence of more actuators than joints; two new approaches — the Infinity Norm and the Non Linear Phase Different Control (NLPDC) — are proposed.

A human-like actuated robot named **BiWi** — **Bi**-articularly actuated and **Wi**-re driven robot arm — is developed and used as an experimental apparatus to compare the two proposed redundancy resolution approaches with the three traditional approaches — Phase Different Control (PDC), Pseudo inverse matrix, and Linear Programming.

The proposed infinity norm approach allows the arm to produce greater end effector force compared the traditional pseudo-inverse matrix approach. The proposed infinity norm approach is suitable for system with three inputs and two outputs, as for example parallel manipulators with a redundant DOF [131] or Pen-based force display for precision manipulation in virtual environments [11]. The NLPDC approach increases the output force precision compared to the PDC approach, and requires less computation compared with the Linear Programming approach. Moreover, the NLPDC allows the independent design of common and different modes for robot arms actuated by three pairs of antagonistic actuators, consisting of four mono- and two bi-articular actuators couple in antagonistic pairs.

In summary, the proposed control approaches — **FSPAC with Variable Impedance**, and actuator redundancy resolution methods based on **Infinity norm** and **NLPDC** — dramatically contribute to improve safety, robustness, smoothness in human-robot interaction and performances such as speed response, maximum and precision end effector force production for power assist robots.

7.2 Future Works

The proposed FSPAC with Variable Impedance control has shown great improvements in safety, robustness and smoothness in power assistance. In the future, a more systematic approach to design the Velocity Dependant Triangular Gain (VD-TG), as well as further simplification of the velocity dependant gain design, are investigated to generalize and simplify even more the design of the Variable Impedance controller for power assist design.

The proposed infinity norm approach for resolution of systems with three inputs and two outputs has shown great advantage in terms of greater achievable output values. The extension of the closed form solution of the infinity norm approach to systems with four inputs and three outputs will be investigated. Systems with 4 inputs and three output are the more and more rising interest electric vehicle actuated by 4 in-wheel motors, such as Kanon [26]. Determining a closed form solution based on infinity norm for such systems will lead to the possibility to design electric vehicles with smaller actuators and better performances. Furthermore, a unified approach for defining the desired inputs of redundant systems, including the infinity norm for maximization of output, $2 - norm$ and $1 - norm$ for input minimization, will lead to the design of high performance and high efficient systems.

Appendix A

Proof of Closed Form Solution for the 2-Norm Approach

The problem expressed by (5.21) is written for a simpler notation as:

$$
\begin{aligned}
\min \quad & \sqrt{\frac{(x)^2}{(mx)^2} + \frac{(y)^2}{(my)^2} + \frac{(z)^2}{(mz)^2}} \\
\text{s.t.} \quad & T_1 = x + z \\
& T_2 = y + z
\end{aligned}
\tag{A.1}
$$

where T_1 and T_2 are the desired joint torques (known), and x, y, z are the desired actuator joint torques τ_1, τ_2, τ_3 (unknown), respectively. $mx = \tau_1^m$, $my = \tau_2^m$, and $mz = \tau_3^m$.

Taking into account the 3 dimensional space $\mathbb{R}^3$, the solution (x, y, z) which satisfy $\sqrt{\frac{(x)^2}{(mx)^2} + \frac{(y)^2}{(my)^2} + \frac{(z)^2}{(mz)^2}}$ has to meet the following three requirements:

1. To be on the line defined by

$$
T_1 = x + z \tag{A.2}
$$

$$
T_2 = y + z \tag{A.3}
$$

2. To be on the ellipsoid surface defined by:

$$
\frac{x^2}{mx^2} + \frac{y^2}{my^2} + \frac{z^2}{mz^2} = k \tag{A.4}
$$

where k is a constant.

3. The plane passing through the line defined by (A.2) and (A.3) has to be tangent to the ellipsoid defined by (A.4). Hence:

$$\frac{1}{mx^2}\frac{\partial x^2}{\partial x} + \frac{1}{my^2}\frac{\partial y^2}{\partial y} + \frac{1}{mz^2}\frac{\partial z^2}{\partial z} = 0 \tag{A.5}$$

Therefore, the solution of the problem (A.1) is:

$$\begin{cases} x = \frac{(T_1-T_2)mx^2mz^2+T_1mx^2my^2}{mx^2my^2+mx^2mz^2+my^2mz^2} \\ y = \frac{T_2mx^2my^2+(T_2-T_1)my^2mz^2}{mx^2my^2+mx^2mz^2+my^2mz^2} \\ z = \frac{T_1my^2mz^2+T_2mx^2mz^2}{mx^2my^2+mx^2mz^2+my^2mz^2} \end{cases} \tag{A.6}$$

Appendix B

Proof of Closed Form Solution for the Infinity-Norm Approach

The problem expressed by (5.40) is written for a simpler notation as:

$$
\begin{aligned}
\min \quad & \max\left\{\frac{|x|}{mx}, \frac{|y|}{my}, \frac{|z|}{mz}\right\} \\
\text{s.t.} \quad & T_1 = x + z \\
& T_2 = y + z
\end{aligned}
\tag{B.1}
$$

where T_1 and T_2 are the desired joint torques (known), and x, y, z are the desired actuator joint torques τ_1, τ_2, τ_3 (unknown), respectively. $mx = \tau_1^{max}$, $my = \tau_2^{max}$, and $mz = \tau_3^{max}$.

A closed form solution of (B.1) is determined in the following.

The searched solution has to satisfy at least one of the three equations $\frac{|x|}{mx} = \frac{|y|}{my}$, $\frac{|y|}{my} = \frac{|z|}{mz}$, $\frac{|x|}{mx} = \frac{|z|}{mz}$. In fact, when one of three variable's absolute value decreases at least one of the other two increases. Therefore for any solution of the system with $\frac{|x|}{mx} \neq \frac{|y|}{my} \neq \frac{|z|}{mz}$ it is possible to decrease the higher value among the three so to be equal to at least one of the other two. Therefore the searched solution is one among the following six:

1. $\frac{x}{mx} = -\frac{y}{my}$

$$
\begin{cases}
x + z = T_1 \\
y + z = T_2 \\
\frac{x}{mx} = -\frac{y}{my}
\end{cases}
\Rightarrow
\begin{cases}
x = (T_1 - T_2)\frac{mx}{my+mx} \\
y = (T_2 - T_1)\frac{my}{my+mx} \\
z = T_2 - (T_2 - T_1)\frac{my}{my+mx}
\end{cases}
\tag{B.2}
$$

2. $\frac{y}{my} = \frac{z}{mz}$

$$
\begin{cases}
x + z = T_1 \\
y + z = T_2 \\
\frac{y}{my} = \frac{z}{mz}
\end{cases}
\Rightarrow
\begin{cases}
x = T_1 - T_2\frac{mz}{my+mz} \\
y = T_2\frac{my}{my+mz} \\
z = T_2\frac{mz}{my+mz}
\end{cases}
\tag{B.3}
$$

3. $\frac{x}{mx} = \frac{z}{mz}$

$$\begin{cases} x+z = T_1 \\ y+z = T_2 \\ \frac{x}{mx} = \frac{z}{mz} \end{cases} \Rightarrow \begin{cases} x = T_1 \frac{mx}{mz+mx} \\ y = T_2 - T_1 \frac{mz}{mz+mx} \\ z = T_1 \frac{mz}{mz+mx} \end{cases} \tag{B.4}$$

4. $\frac{x}{mx} = \frac{y}{my}$

$$\begin{cases} x+z = T_1 \\ y+z = T_2 \\ \frac{x}{mx} = \frac{y}{my} \end{cases} \Rightarrow \begin{cases} x = (T_2 - T_1)\frac{mx}{my-mx} \\ y = (T_2 - T_1)\frac{my}{my-mx} \\ z = T_2 - (T_2 - T_1)\frac{my}{my-mx} \end{cases} \tag{B.5}$$

5. $\frac{y}{my} = -\frac{z}{mz}$

$$\begin{cases} x+z = T_1 \\ y+z = T_2 \\ \frac{y}{my} = -\frac{z}{mz} \end{cases} \Rightarrow \begin{cases} x = T_1 - T_2 \frac{mz}{mz-my} \\ y = -T_2 \frac{my}{mz-my} \\ z = T_2 \frac{mz}{mz-my} \end{cases} \tag{B.6}$$

6. $\frac{x}{mx} = -\frac{z}{mz}$

$$\begin{cases} x+z = T_1 \\ y+z = T_2 \\ \frac{x}{mx} = -\frac{z}{mz} \end{cases} \Rightarrow \begin{cases} x = -T_1 \frac{mx}{mz-mx} \\ y = T_2 - T_1 \frac{mz}{mz-mx} \\ z = T_1 \frac{mz}{mz-mx} \end{cases} \tag{B.7}$$

Let us define:

$$c_1 = \frac{mz - mx}{mz + my} \tag{B.8}$$

$$c_2 = \frac{mz + my}{mz + mx} \tag{B.9}$$

$$c_3 = \frac{mz - my}{mz + mx} \tag{B.10}$$

These values depend only on the hardware characteristics of the arm, therefore are constant.

Among the six possible solutions the searched one is directly selected on the basis of T_1 and T_2 as follows (the variable subscript represents the respective equation number):

- if ($T_1 \leq c_1 T_1$ and $T_2 \geq c_3 T_1$) or ($T_1 > c_1 T_2$ and $T_2 < c_3 T_1$):

$$
\begin{cases}
|z_{(B.2)}| \leq |x_{(B.2)}| = |y_{(B.2)}| \\
|x_{(B.2)}| \leq |x_{(B.3)}| \\
|y_{(B.2)}| \leq |y_{(B.4)}| \\
|x_{(B.2)}| \leq |x_{(B.5)}| \\
|y_{(B.2)}| \leq |y_{(B.5)}| \\
|x_{(B.2)}| \leq |x_{(B.6)}|, \text{ if } mz \geq my \\
|y_{(B.2)}| \leq |y_{(B.6)}|, \text{ if } mz < my \\
|x_{(B.2)}| \leq |x_{(B.7)}|, \text{ if } mx \geq mz \\
|y_{(B.2)}| \leq |y_{(B.7)}|, \text{ if } mx < mz
\end{cases}
\tag{B.11}
$$

  Therefore solution is (B.2). In this case, τ_1 in (5.44), τ_2 in (5.45), and τ_3 in (5.46), are equal to x in (B.2), y in (B.2), and z in (B.2), respectively.

- if ($T_1 \geq c_1 T_2$ and $T_2 \geq c_2 T_1$) or ($T_1 < c_1 T_2$ and $T_2 < c_2 T_1$):

$$
\begin{cases}
|x_{(B.3)}| \leq |y_{(B.3)}| = |z_{(B.3)}| \\
|z_{(B.3)}| \leq |z_{(B.2)}| \\
|y_{(B.3)}| \leq |y_{(B.4)}| \\
|y_{(B.3)}| \leq |y_{(B.5)}|, \text{ if } my \geq mx \\
|z_{(B.3)}| \leq |z_{(B.5)}|, \text{ if } my < mx \\
|y_{(B.3)}| \leq |y_{(B.6)}| \\
|z_{(B.3)}| \leq |z_{(B.6)}| \\
|y_{(B.3)}| \leq |y_{(B.7)}|, \text{ if } mx \geq mz \\
|z_{(B.3)}| \leq |z_{(B.7)}|, \text{ if } mx < mz
\end{cases}
\tag{B.12}
$$

  Therefore solution is (B.3). In this case, τ_1 in (5.44), τ_2 in (5.45), and τ_3 in (5.46), are equal to x in (B.3), y in (B.3), and z in (B.3), respectively.

- if $(T_2 \leq c_2 T_1$ and $T_2 \geq c_3 T_1)$ or $(T_2 > c_2 T_1$ and $T_2 < c_3 T_1)$:

$$
\begin{cases}
|y_{(B.4)}| \leq |x_{(B.4)}| = |z_{(B.4)}| \\
|z_{(B.4)}| \leq |z_{(B.2)}| \\
|x_{(B.4)}| \leq |x_{(B.3)}| \\
|x_{(B.4)}| \leq |x_{(B.5)}|, \text{ if } mx \geq my \\
|z_{(B.4)}| \leq |z_{(B.5)}|, \text{ if } mx < my \\
|x_{(B.4)}| \leq |x_{(B.6)}|, \text{ if } my \geq mz \\
|z_{(B.4)}| \leq |z_{(B.6)}|, \text{ if } my < mz \\
|x_{(B.4)}| \leq |x_{(B.7)}| \\
|x_{(B.4)}| \leq |x_{(B.7)}|
\end{cases}
\tag{B.13}
$$

Therefore solution is (B.4). In this case, τ_1 in (5.44), τ_2 in (5.45), and τ_3 in (5.46), are equal to x in (B.4), y in (B.4), and z in (B.4), respectively.

Appendix C

Calculation of Joint Actuator Input Torques for 2-Norm and Infinity Norm Approaches

Given a desired force angle θ_f and a redundancy resolution approach ($2-norm$ or $\infty-norm$), the desired joint actuator torques (τ_1, τ_2, and τ_3) producing the maximum force in direction θ_f, while respecting the torque limits (τ_1^m, τ_2^m, and τ_3^m) are calculated using the following algorithm. For $\theta_f = k$:

1. Set $i = 0$, and $|\mathbf{F}|_i = 0.001$

2. Calculate $\mathbf{T}_i$ using the Jacobian (5.12)

3. Given $\mathbf{T}_i$, calculate the necessary $(\tau_1)_i$, $(\tau_2)_i$ and $(\tau_3)_i$ using either the $2-norm$ approach ((5.22), (5.23), and (5.24)) or the $\infty-norm$ approach ((5.44), (5.45), (5.46))

4. If $\left(|(\tau_1)_i| > \tau_1^m\right)$ or $\left(|(\tau_2)_i| > \tau_2^m\right)$ or $\left(|(\tau_3)_i| > \tau_3^m\right)$
   then $(\tau_1)_i = (\tau_1)_{i-1}$, $(\tau_2)_i = (\tau_2)_{i-1}$, $(\tau_3)_i = (\tau_3)_{i-1}$
   else $|\mathbf{F}| = |\mathbf{F}| + 0.001$, $i = i+1$, and repeat from step 2

5. The calculated $(\tau_1)_i$, $(\tau_2)_i$, and $(\tau_1)_i$ are used as input reference torques.
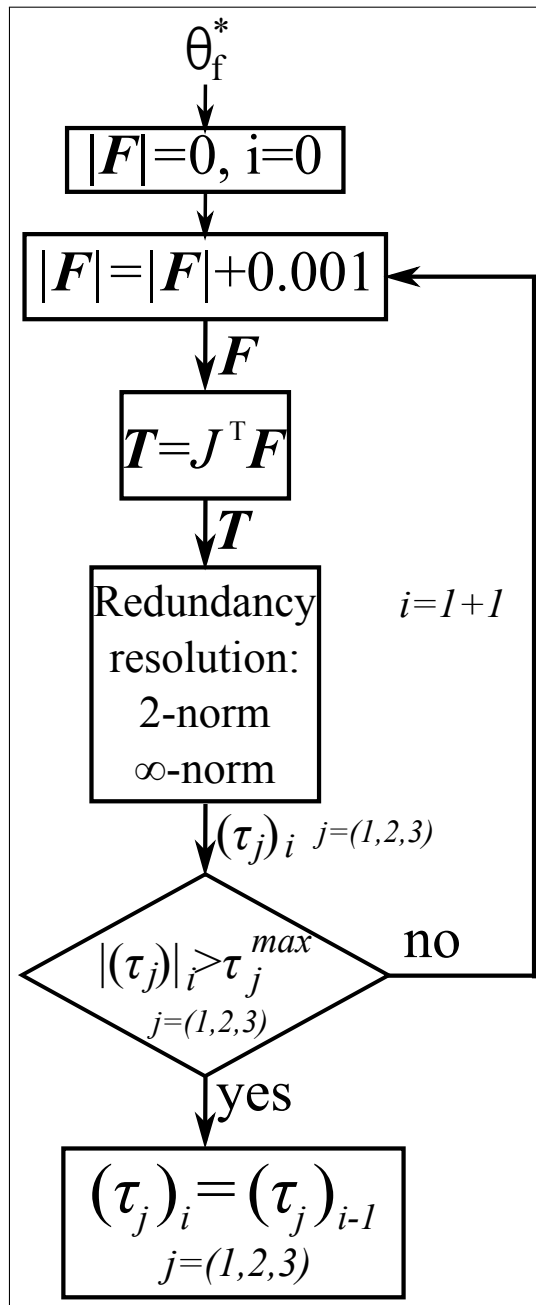
Figure C.1: Calculation of desired actuator joint input torques for the $2-$*norm* and $\infty-$*norm* approaches

Appendix D

Proof of Non Linear Phase Different Control Approach

Coordinates of point A and B in Fig. D.1 are:
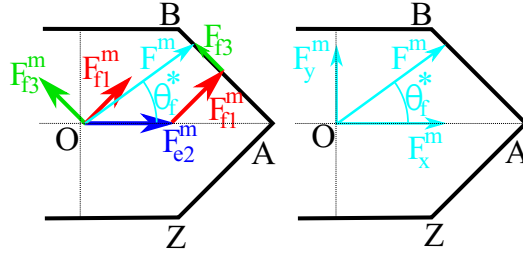
Figure D.1: Force vectors producing $\boldsymbol{F}^m$ (left). $\boldsymbol{F}_x^m$ and $\boldsymbol{F}_y^m$ (right)

$$\begin{bmatrix} A_X \\ A_y \end{bmatrix} = \frac{1}{|J|} \begin{bmatrix} d-c \\ -b+a \end{bmatrix} \begin{bmatrix} (f_1^m + f_3^m)r \\ (f_2^m + f_3^m)r \end{bmatrix} \tag{D.1}$$

$$\begin{bmatrix} B_X \\ B_y \end{bmatrix} = \frac{1}{|J|} \begin{bmatrix} d-c \\ -b+a \end{bmatrix} \begin{bmatrix} (f_1^m + f_3^m)r \\ (e_2^m + f_3^m)r \end{bmatrix} \tag{D.2}$$

Given a desired output force angle $\boldsymbol{\theta}_f^*$, the value of the force $\boldsymbol{F}^m = [F_x^m, F_y^m]^T$ is on the line represented by:

$$F_y^m = F_x^m \tan(\boldsymbol{\theta}_f^*) \tag{D.3}$$

By using the equation of a line though points A and B together with (D.3):

$$(B_x - A_x)(F_x^m \tan(\theta_f^*) - A_y) + (A_y - B_y)(F_x^m - A_x) = 0 \tag{D.4}$$

Resolving (D.4) in respect to F_x^m, using (D.1), (D.2), with the opportune simplifications follows:

$$F_x^m = \frac{(-f_1^m - e_2^m)r}{(d-c)\tan(\theta_f^*) + b - a} \tag{D.5}$$

The torque required at joints 1 and 2 to produce the output force $\boldsymbol{F}$ is calculated using (5.12), (D.3), and (D.5):

$$\begin{bmatrix} T_1 \\ T_2 \end{bmatrix} = J^T \begin{bmatrix} F_x^m \\ F_x^m \tan(\boldsymbol{\theta}_f^*) \end{bmatrix} = \begin{bmatrix} \frac{(-f_1^m - e_2^m)r(a + c\tan(\boldsymbol{\theta}_f^*))}{(d-c)\tan(\boldsymbol{\theta}_f^*) + b - a} \\ \frac{(-f_1^m - e_2^m)r(b + d\tan(\boldsymbol{\theta}_f^*))}{(d-c)\tan(\boldsymbol{\theta}_f^*) + b - a} \end{bmatrix} \tag{D.6}$$

The muscle activation level $m_3^{\alpha\beta}$ is found subtracting the torque produce by the muscle activation level $f_1^m r$ to T_1:

$$m_3^{\alpha\beta} = \frac{(-f_1^m - e_2^m)(a + c\tan(\boldsymbol{\theta}_f^*))}{(d-c)\tan(\boldsymbol{\theta}_f^*) + b - a} - f_1^m \tag{D.7}$$

Using the same method the values of $m_2^{\beta\gamma}$, $m_1^{\gamma\delta}$, $m_3^{\delta\varepsilon}$, $m_2^{\varepsilon\zeta}$, $m_1^{\zeta\alpha}$ are determined.

Appendix E

Non-Redundant Bi-Articularly Actuated Robot Arms

Bi-articular actuation in a redundant configuration has numerous advantages, as the dramatical increase in range of end effector impedance which can be achieved without feedback [39], and the ability to produce a homogeneous maximum output force at the end effector [25]. However, such important advantages are due to the use of bi-articular actuators in addition to the traditional mono-articular one. Therefore, drawbacks as design complexity and cost are present.

In the following we investigate the role of bi-articular actuators for robot arms equipped with as many actuators as joints. Hence, even if the bi-articular actuator is present, there is no actuator redundancy. A planar robot arm with two links and two actuators is taken into account, in two different actuator configurations:

1. Configuration mono-mono: two mono-articular actuators, each actuator produces a torque about each joint.

2. Configuration mono-bi: a mono-articular actuator produces torque about the shoulder joint, and a bi-articular one produces the same torque about both shoulder and elbow joints.

The robot arm in mono-mono and mono-bi configurations is shown in Fig. E.1(a) and in Fig. E.1(b), respectively. T_1 and T_2 are the joint torques. τ_1 and τ_2 are the torques produced on joints 1 and 2 by actuators 1 and 2 respectively, while τ_3 is the torque produced at the same time about joint 1 and 2 by the bi-articular actuator.

(a) Robot arm in mono-mono configuration   (b) Robot arm in mono-bi configuration
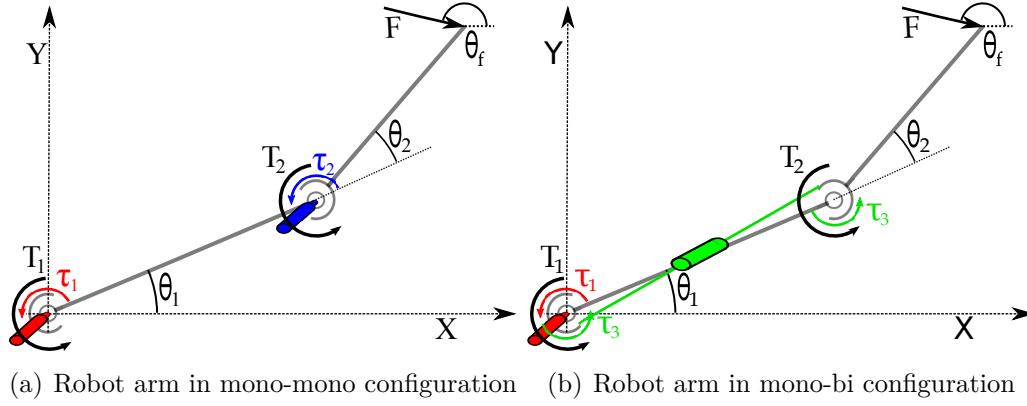
Figure E.1: Robot arm in two actuation configurations

Statics Analysis

The statics of mono-mono configuration are expressed by:

$$T_1 = \tau_1 \tag{E.1}$$
$$T_2 = \tau_2 \tag{E.2}$$

The statics of mono-bi configuration are expressed by:

$$T_1 = \tau_1 + \tau_3 \tag{E.3}$$
$$T_2 = \tau_3 \tag{E.4}$$

For both the configurations of Fig. E.1(a) and Fig E.1(b) the relationship between force at the end effector and joint torques is expressed by:

$$\begin{bmatrix} T_1 \\ T_2 \end{bmatrix} = J^T \begin{bmatrix} F_x \\ F_y \end{bmatrix} \tag{E.5}$$

where

$$J = \begin{bmatrix} -l_1\sin(\theta_1) - l_2\sin(\theta_1 + \theta_2) & -l_2\sin(\theta_1 + \theta_2) \\ l_1\cos(\theta_1) + l_2\cos(\theta_1 + \theta_2) & l_2\cos(\theta_1 + \theta_2) \end{bmatrix} \tag{E.6}$$

The main difference for the two configuration are the maximum joint torques T_1^m and T_2^m. In mono-mono configuration the maximum joint torques are:

$$-\tau_1^m \leq T_1^m \leq \tau_1^m \tag{E.7}$$
$$-\tau_2^m \leq T_2^m \leq \tau_2^m \tag{E.8}$$

In mono-bi configuration the maximum joint torques are:

$$-\tau_1^m - \tau_3^m \leq T_1^m \leq \tau_1^m + \tau_3^m \tag{E.9}$$

$$-\tau_3^m \leq T_2^m \leq \tau_3^m \tag{E.10}$$

From (E.10) results that, if the required actuator torques τ_1 and τ_3 have opposite sign T_1 is smaller in mono-bi configuration. On the contrary T_1 in mono-bi configuration is greater than in mono-mono configuration when τ_1 and τ_3 have same sign.

The sign relationship between τ_1 and τ_3 depends on the robot arm posture (θ_1 and θ_2 and on the desired force direction at the end effector (θ_f). As a consequence the maximum output force at the end effector has a different shape in the two actuators configurations.

Experimental Setup

Joint actuator torques inputs are calculated using the two algorithms in Fig. E.2(a) and Fig. E.2(b) for the mono-mono and mono-bi configurations, respectively. As for the torque saturation conditions, in the mono-mono configuration the following algorithm is used:

$$\begin{aligned}
&\tau_i^* = T_i^* \\
&\text{if } \tau_i^* > \tau_i^m, \ \tau_i^* = \tau_i^m \\
&\text{if } \tau_i^* < -\tau_i^m, \ \tau_i^* = -\tau_i^m
\end{aligned} \tag{E.11}$$

where $i \in \{1, 2\}$.

While in the mono-bi configuration the following algorithm is used:

$$\begin{aligned}
&\tau_3^* = T_2^* \\
&\text{if } \tau_3^* > \tau_3^m, \ \tau_3^* = \tau_3^m \\
&\text{if } \tau_3^* < -\tau_3^m, \ \tau_3^* = -\tau_3^m \\
&\tau_1^* = T_1^* - \tau_3^* \\
&\text{if } \tau_1^* > \tau_1^m, \ \tau_1^* = \tau_1^m \\
&\text{if } \tau_1^* < -\tau_1^m, \ \tau_1^* = -\tau_1^m
\end{aligned} \tag{E.12}$$

From the actuator joint torques input, the motor reference torques are calculated using (6.1) (6.2) (6.3) (6.4) (6.5) (6.6).

The maximum output force in the two actuation configurations is calculated and measured for BiWi robot arm (6.2). In the experiment the arm posture is varied. Three different joint angle configurations are taken into account:

1. $\theta_1 = -135°$ and $\theta_2 = 90°$

(a) Feedforward control block diagram for mono-mono configuration

(b) Feedforward control block diagram for mono-bi configuration
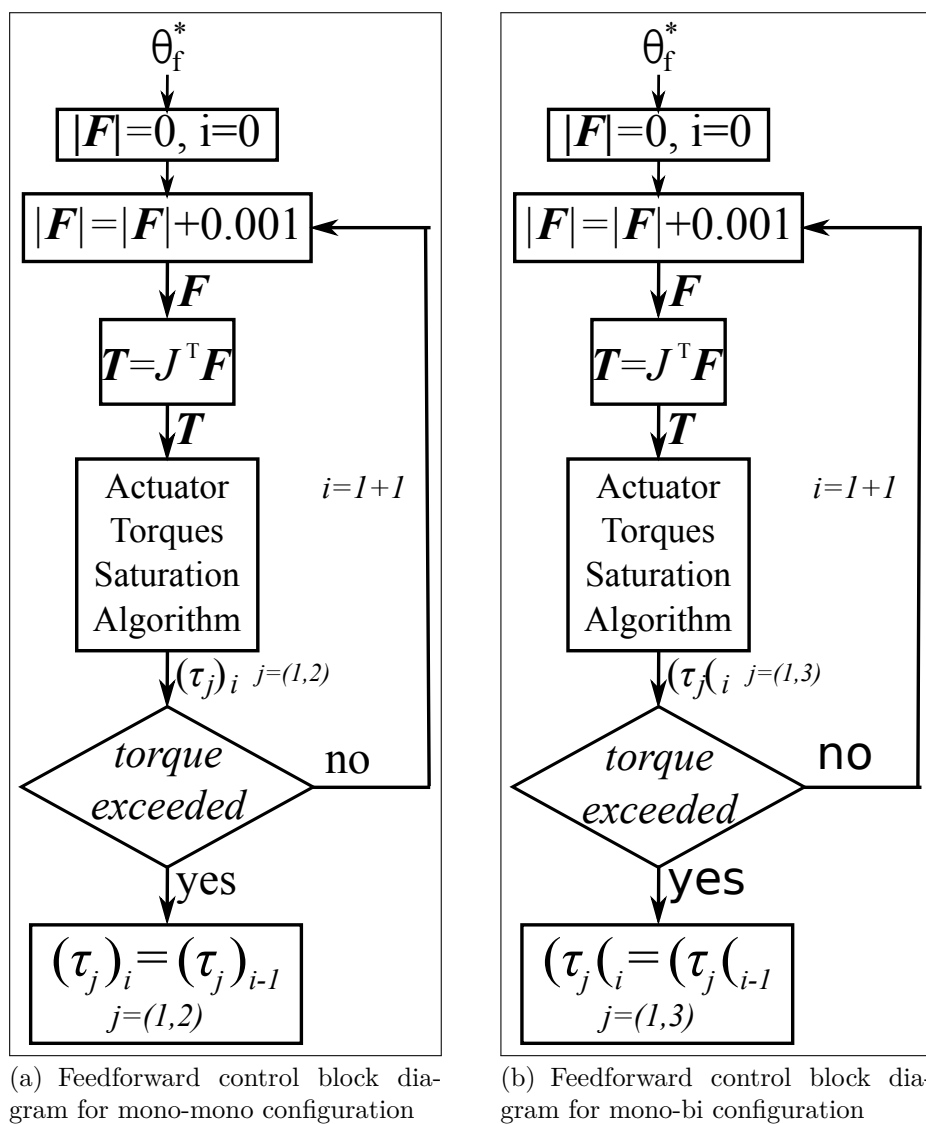
Figure E.2: Feedforward control block diagram for mono-mono and mono-bi configurations

2. $\theta_1 = -120°$ and $\theta_2 = 60°$

3. $\theta_1 = -104.5°$ and $\theta_2 = 29°$

The output force is measured for the output force direction (θ_f) varying from 0 to 360° every 10°. The maximum actuator joint torques are set to $\tau_1 = \tau_2 = \tau_3 = 1.5\ Nm$. The motor torque references are sent as step inputs,

the manipulator end effector output force $\boldsymbol{F} = [F_x, F_y]^T$ is measured by a force sensor, and its steady state value is taken into account.

Results

Maximum output force experimentally measured using BiWi are shown in Fig. E.3. The maximum force at the end effector in the direction perpendicu-
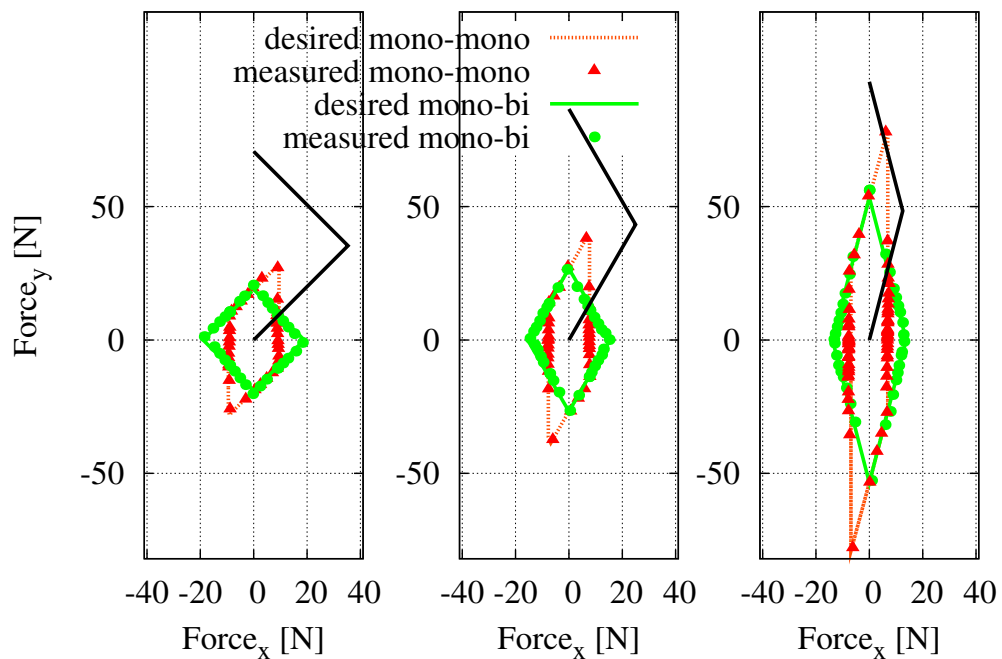
Figure E.3: Experimentally measured maximum output force at the end effector

lar to ground is the same in the two cases. On the other hand, the maximum force in the horizontal direction is bigger in the mono-bi configuration.

In order to investigate the role of bi-articular actuators for non-redundant manipulators in dynamic conditions the following simulation is performed. A two-link planar with $l_1 = l_2 = 1\ m$ is considered (Fig. E.4).

The arm initial position is $x(t_0) = 1\ m$, $y(t_0) = 0$. The desired final position is $x(t_f) = 1.8\ m$, $y(t_f) = 0$. The arm in the initial and desired final position is shown in Fig. E.4.

A straight trajectory in the Cartesian space is designed using a cubic
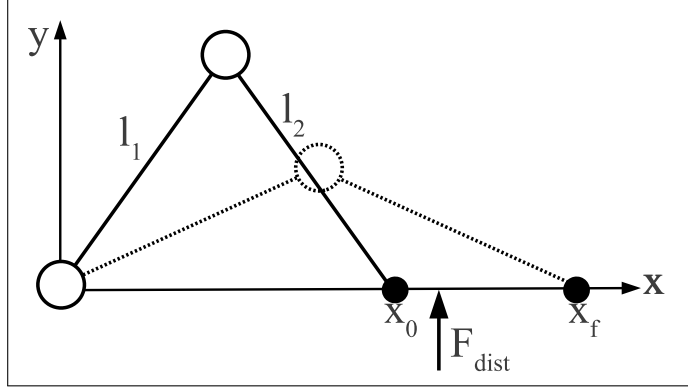
Figure E.4: Arm in initial and desired final position

spline:

$$\begin{cases} x(t) = x_0 + \frac{3}{t_f^2}(x_f - x_0)t^2 - \frac{2}{t_f^3}(x_f - x_0)t^3 \\ y(t) = 0 \end{cases} \tag{E.13}$$

where t is the time, $t_0 = 0$, $t_f = 5$ seconds.

A disturbance force with magnitude $F_x^{dist} = 0$, and $F_y^{dist} = 3.5$ N is applied at $t = 3$ s for a length of 0.5 seconds at the end effector. Further parameters used in the simulation are shown in Tab. E.

Table E.1: Simulation parameters

Parameter	value
Length link 1	1 $[m]$
Lenght link 2	1 $[m]$
Mass 1	5 $[Kg]$
Mass 2	5 $[Kg]$
COM 1	0.5 $[m]$
COM 2	0.5 $[m]$
Momentum of Inertia 1	2.25 $[Kg/m^2]$
Momentum of Inertia 2	2.25 $[Kg/m^2]$
Damping Coefficient Joint 1	0.01 $[Ns/m]$
Damping Coefficient Joint 2	0.01 $[Ns/m]$
$\tau_1^m = \tau_2^m = \tau_3^m$	1 Nm

Fig. E.5 shows the control block diagram used in the simulation. P includes all the robot arm dynamics. Joint position control is realized by a PID controller. The tracking performances of the arm in Fig. E.4 are evaluated

in the two actuator configurations mono-mono and mono-bi. The actuator torque saturation algorithms are (E.11) for the mono-mono configuration and (E.12) for the mono-bi configuration.
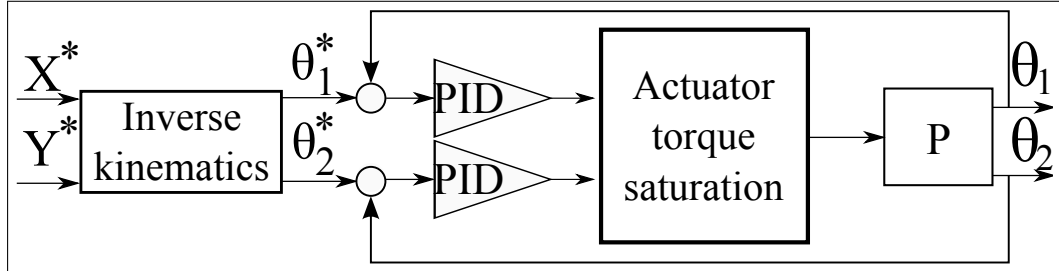
Figure E.5: Control block diagram used in the dynamics simulation

The tracking performances of the arm are shown in Fig. E.6. In particular, desired joint angular positions (θ_1^* and θ_2^*), actual joint angular positions (θ_1 and θ_2), angular position errors (θ_1^{err} and θ_2^{err}), desired joint torques (T_1^* and T_2^*) and actual joint torques (T_1 and T_2) are shown.

These results show that in the mono-mono configuration the system is unstable, as the angular position error θ_1^{err} in Fig. E.6(b) does not converge to 0. On the other hand, in the mono-bi configuration the position errors θ_1^{err} and θ_2^{err} converge to 0 (Fig. E.6(f)). Therefore the arm can reach the final desired position.

In dynamic conditions, the greater maximum force in the horizontal direction results in a greater capability of disturbance rejection to forces directed horizontally respect to the ground for jumping/walking robots. As a consequence the presence of bi-articular actuators improve the balance capability of jumping/walking robots.

mono-mono configuration   **mono-bi configuration**

(a) Desired and actual joint angles   (e) Desired and actual joint angles

(b) Angular position error of the joint angles (f) Angular position error of the joint angles

(c) Desired joint torques   (g) Desired joint torques

(d) Actual Joint torques   (h) Actual Joint torques
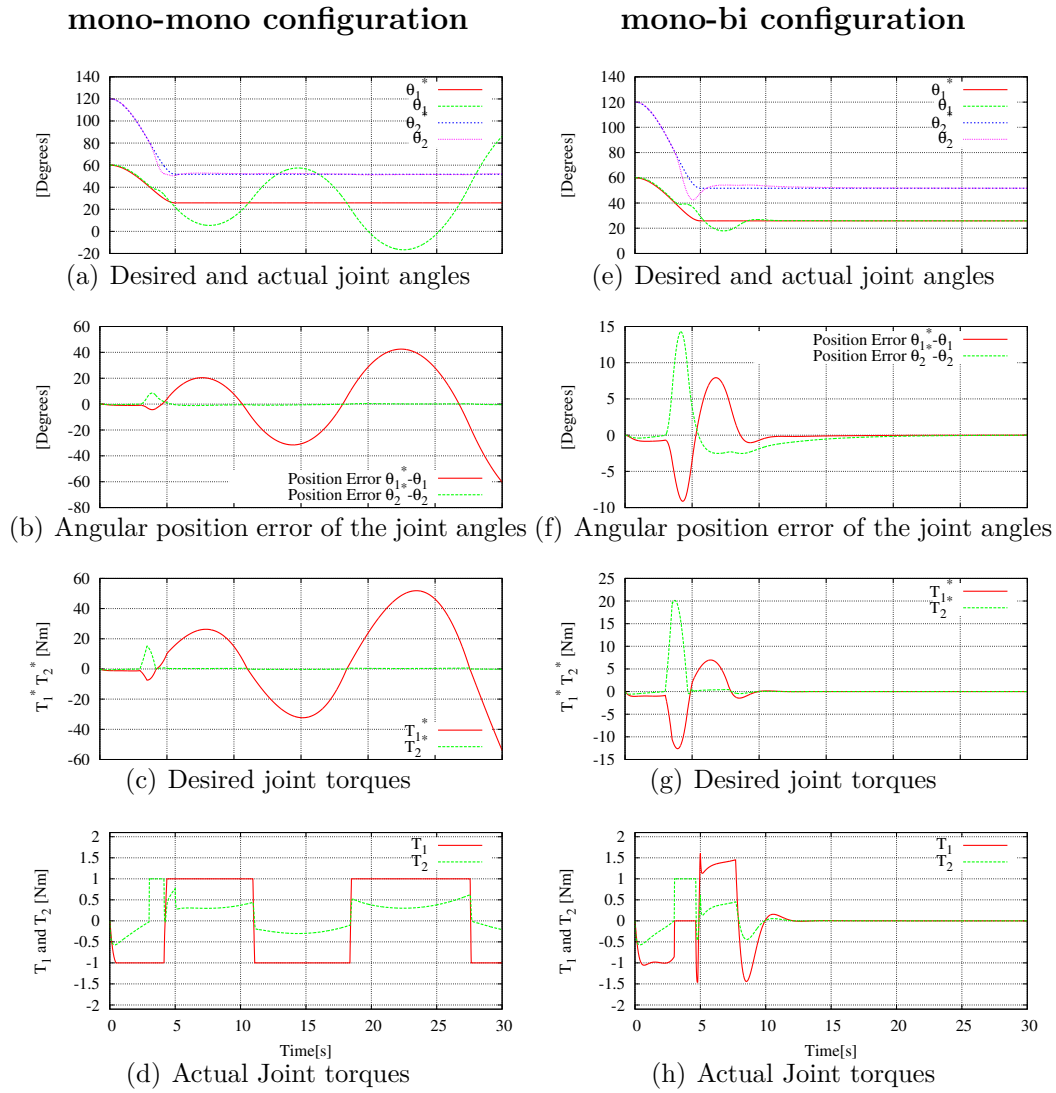
Figure E.6: Tracking performances mono-mono (left) and mono-bi (right) in configurations

Bibliography

[1] L.M. Aksman, C.R. Carignan, and D.L. Akin. Force estimation based compliance control of harmonically driven manipulators. In *Robotics and Automation, 2007 IEEE International Conference on*, pages 4208–4213, 2007.

[2] Adamantios Arampatzis, Gert-Peter Brüggemann, and Verena Metzler. The effect of speed on leg stiffness and joint kinetics in human running. *Journal of Biomechanics*, 32(12):1349–1353, December 1999.

[3] J. Babic and J. Lenarcic. Optimization of biarticular gastrocnemius muscle in humanoid jumping robot simulation. *International Journal of Humanoid Robotics*, 3(2):219, 2006.

[4] J. Babic, B. Lim, D. Omrcen, J. Lenarcic, and FC Park. A biarticulated robotic leg for jumping movements: Theory and experiments. *Journal of mechanisms and robotics*, 1(1), 2009.

[5] S.K. Banala, Seok Hun Kim, S.K. Agrawal, and J.P. Scholz. Robot assisted gait training with active leg exoskeleton (ALEX). *Neural Systems and Rehabilitation Engineering, IEEE Transactions on*, 17(1):2–8, 2009.

[6] A. Bicchi and G. Tonietti. Fast and "soft-arm" tactics [robot arm design]. *Robotics & Automation Magazine, IEEE*, 11(2):22–33, 2004.

[7] J.A. Blaya and H. Herr. Adaptive control of a variable-impedance ankle-foot orthosis to assist drop-foot gait. *Neural Systems and Rehabilitation Engineering, IEEE Transactions on*, 12(1):24–31, 2004.

[8] Maarten F. Bobbert and Gerrit Jan van Ingen Schenau. Coordination in vertical jumping. *Journal of Biomechanics*, 21(3):249–262, 1988.

[9] E. B Brokaw, T. Murray, T. Nef, and P. S Lum. Retraining of interjoint arm coordination after stroke using robot-assisted time-independent functional training. 43:299–316, 2011.

[10] M. Buehler and D. McMordle. *Towards Pronking With a Hexapod Robot.* Storming Media, 2001.

[11] P. Buttolo and B. Hannaford. Pen-based force display for precision manipulation in virtual environments. In *Virtual Reality Annual International Symposium, 1995. Proceedings.*, pages 217–224. IEEE, March 1995.

[12] C. Carignan, J. Tang, and S. Roderick. Development of an exoskeleton haptic interface for virtual task training. In *Intelligent Robots and Systems, 2009. IROS 2009. IEEE/RSJ International Conference on*, pages 3697–3702, 2009.

[13] Stefano Chiaverini, Giuseppe Oriolo, and Ian Walker. Kinematically redundant manipulators. In *Springer Handbook of Robotics*, pages 245–268. 2008.

[14] Dongil Choi and Jun-Ho Oh. Human-friendly motion control of a wheeled inverted pendulum by reduced-order disturbance observer. In *Robotics and Automation, 2008. ICRA 2008. IEEE International Conference on*, pages 2521–2526, 2008.

[15] N. Costa and D.G. Caldwell. Control of a biomimetic "Soft-actuated" 10DoF lower body exoskeleton. In *Biomedical Robotics and Biomechatronics, 2006. BioRob 2006. The First IEEE/RAS-EMBS International Conference on*, pages 495–501, 2006.

[16] P.R. Culmer, A.E. Jackson, S. Makower, R. Richardson, J.A. Cozens, M.C. Levesley, and B.B. Bhakta. A control strategy for upper limb robotic rehabilitation with a dual robot system. *Mechatronics, IEEE/ASME Transactions on*, 15(4):575–585, 2010.

[17] Monica A. Daley. Biomechanics: Running over uneven terrain is a No-Brainer. *Current Biology*, 18(22):R1064–R1066, November 2008.

[18] Monica A. Daley, James R. Usherwood, Gladys Felix, and Andrew A. Biewener. Running over rough terrain: guinea fowl maintain dynamic stability despite a large unexpected change in substrate height. *J Exp Biol*, 209(1):171–187, January 2006.

[19] Claire T. Farley and Octavio González. Leg stiffness and stride frequency in human running. *Journal of Biomechanics*, 29(2):181–186, February 1996.

[20] Daniel P. Ferris, Keith E. Gordon, Gregory S. Sawicki, and Ammanath Peethambaran. An improved powered ankle-foot orthosis using proportional myoelectric control. *Gait & Posture*, 23(4):425–428, June 2006.

[21] Daniel P. Ferris, Kailine Liang, and Claire T. Farley. Runners adjust leg stiffness for their first step on a new running surface. *Journal of Biomechanics*, 32(8):787–794, August 1999.

[22] Daniel P. Ferris, Micky Louie, and Claire T. Farley. Running in the real world: adjusting leg stiffness for different surfaces. *Proceedings of the Royal Society of London. Series B: Biological Sciences*, 265(1400):989 –994, June 1998.

[23] S. Floyd, T. Keegan, J. Palmisano, and M. Sitti. A novel water running robot inspired by basilisk lizards. In *Intelligent Robots and Systems, 2006 IEEE/RSJ International Conference on*, pages 5430–5436, 2006.

[24] S. Floyd and M. Sitti. Design and development of the lifting and propulsion mechanism for a biologically inspired water runner robot. *Robotics, IEEE Transactions on*, 24(3):698–709, 2008.

[25] Tomohiko Fujikawa, Tooru Oshima, Minayori Kumamoto, and Nobuyasu Yokoi. Output force at the endpoint in human upper extremities and coordinating activities of each antagonistic pairs of muscles. *Transactions of the Japan Society of Mechanical Engineers. C*, 65(632):1557–1564, 1999.

[26] H. Fujimoto and Y. Yamauchi. Advanced motion control of electric vehicle based on lateral force observer with active steering. In *Industrial Electronics (ISIE), 2010 IEEE International Symposium on*, pages 3627–3632, 2010.

[27] Y. Fujimoto, T. Kominami, and H. Hamada. Development of a Spirally-Shaped linear actuator. In *Industry Applications Society Annual Meeting, 2008. IAS '08. IEEE*, pages 1–5, 2008.

[28] Yasutaka Fujimoto, Issam A. Smadi, and Yuki Wakayama. Development of musculoskeletal biped robot driven by Direct-Drive actuators. In *Proc. IEEE International Conference on Mechatronics (ICM)*, 2011.

[29] K. Fujisaki, Y. Saito, and A. Umemura. Study on power assisting rehabilitation robotics arm operated by handicapped person. In *Proceedings of the Third Asia International Symposium on Mechatronics*, 2008.

[30] Senshi Fukashiro, Thor F. Besier, Rod Barrett, Jodie Cochrane, Akinori Nagano, and David G. Lloyd. Direction control in standing horizontal and vertical jumps. *International Journal of Sport and Health Science*, 3(Special_Issue_2005):272–279, 2005.

[31] H. Fukusho, T. Sugimoto, and T. Koseki. Control of a straight line motion for a two-link robot arm using coordinate transform of bi-articular simultaneous drive. In *Advanced Motion Control, 2010 11th IEEE International Workshop on*, pages 786–791, 2010.

[32] Hiroaki Gomi and Rieko Osu. Task-Dependent viscoelasticity of human multijoint arm and its spatial characteristics for interaction with environments. *J. Neurosci.*, 18(21):8965–8978, November 1998.

[33] R.A.R.C. Gopura and K. Kiguchi. Development of a 6DOF exoskeleton robot for human Upper-Limb motion assist. In *Information and Automation for Sustainability, 2008. ICIAFS 2008. 4th International Conference on*, pages 13–18, 2008.

[34] K. P. Granata, D. A. Padua, and S. E. Wilson. Gender differences in active musculoskeletal stiffness. part II. quantification of leg stiffness during functional hopping tasks. *Journal of Electromyography and Kinesiology*, 12(2):127–135, April 2002.

[35] Sten Grimmer, Michael Ernst, Michael Gunther, and Reinhard Blickhan. Running on uneven ground: leg adjustment to vertical steps and self-stability. *J Exp Biol*, 211(18):2989–3000, September 2008.

[36] J.W. Grizzle, J. Hurst, B. Morris, Hae-Won Park, and K. Sreenath. MABEL, a new robotic bipedal walker and runner. In *American Control Conference, 2009. ACC '09.*, pages 2030–2036, 2009.

[37] J. Heaston, D. Hong, I. Morazzani, Ping Ren, and G. Goldman. STriDER: Self-Excited tripedal dynamic experimental robot. In *Robotics and Automation, 2007 IEEE International Conference on*, pages 2776–2777, 2007.

[38] A.L. Hof. The force resulting from the action of mono- and biarticular muscles in a limb. *Journal of Biomechanics*, 34(8):1085–1089, August 2001.

[39] Neville Hogan. Impedance control: An approach to manipulation: Part III—Applications. *Journal of Dynamic Systems, Measurement, and Control*, 107(1):17–24, March 1985.

[40] Neville Hogan. The mechanics of multi-joint posture and movement control. *Biological Cybernetics*, 52(5):315–331, 1985.

[41] T Horita, P V Komi, C Nicol, and H Kyröläinen. Interaction between pre-landing activities and stiffness regulation of the knee joint musculoskeletal system in the drop jump: implications to performance. *European Journal of Applied Physiology*, 88(1-2):76–84, November 2002. PMID: 12436273.

[42] Koh Hosoda, Yuki Sakaguchi, Hitoshi Takayama, and Takashi Takuma. Pneumatic-driven jumping robot with anthropomorphic muscular skeleton structure. *Autonomous Robots*, 28(3):307–316, December 2009.

[43] I W Hunter and R E Kearney. Dynamics of human ankle stiffness: variation with mean ankle torque. *Journal of Biomechanics*, 15(10):747–752, 1982. PMID: 7153227.

[44] S Hyon, T Emura, and T Mita. Dynamics-based control of a one-legged hopping robot. *Proceedings of the Institution of Mechanical Engineers, Part I: Journal of Systems and Control Engineering*, 217(2):83–98, January 2003.

[45] S. H Hyon and T. Mita. Development of a biologically inspired hopping robot-Kenken. In *IEEE International Conference on Robotics and Automation, 2002. Proceedings. ICRA '02*, volume 4, pages 3984– 3991 vol.4. IEEE, 2002.

[46] F. Iida, J. Rummel, and A. Seyfarth. Bipedal walking and running with spring-like biarticular muscles. *Journal of Biomechanics*, 41(3):656–667, 2008.

[47] Tomoya Inaba and Toshiro Noritsugu. Analysis and control of model to develop support device using biarticular muscle with rubber artificial muscles. *Transactions of the Japan Society of Mechanical Engineers Series C*, 77(778):2323–2335, 2011.

[48] M. Ishii, K. Yamamoto, and K. Hyodo. Stand-Alone wearable power assist Suit–Development and availability–. *Journal ref: Journal of Robotics and Mechatronics*, 17(5):575–583, 2005.

[49] R Jacobs and G J van Ingen Schenau. Control of an external force in leg extensions in humans. *The Journal of Physiology*, 457(1):611 –626, November 1992.

[50] Ron Jacobs, Maarten F. Bobbert, and Gerrit Jan van Ingen Schenau. Mechanical output from individual muscles during explosive leg extensions: The role of biarticular muscles. *Journal of Biomechanics*, 29(4):513–523, April 1996.

[51] Y. Jeong, Y. Lee, K. Kim, Y. S Hong, and J. O Park. A 7 DOF wearable robotic arm using pneumatic actuators. In *Proceedings of the 32nd ISR (International Symposium on Robotics)*, volume 19, page 21, 2001.

[52] K. Kadota, M. Akai, K. Kawashima, and T. Kagawa. Development of Power-Assist robot arm using pneumatic rubber muscles with a balloon sensor. In *The 18th IEEE International Symposium on Robot and Human Interactive Communication, 2009. RO-MAN 2009*, pages 546–551. IEEE, October 2009.

[53] Kazuo Kiguchi, Mohammad Habibur Rahman, Makoto Sasaki, and Kenbu Teramoto. Development of a 3DOF mobile exoskeleton robot for human upper-limb motion assist. *Robotics and Autonomous Systems*, 56(8):678–691, August 2008.

[54] Sangbae Kim, M. Spenko, S. Trujillo, B. Heyneman, D. Santos, and M.R. Cutkosky. Smooth vertical surface climbing with directional adhesion. *Robotics, IEEE Transactions on*, 24(1):65–74, 2008.

[55] Seyoung Kim and Sukyung Park. Leg stiffness increases with speed to modulate gait frequency and propulsion energy. *Journal of Biomechanics*, 44(7):1253–1258, April 2011.

[56] Y. Kimura, Sehoon Oh, and Y. Hori. Novel robot arm with bi-articular driving system using a planetary gear system and disturbance observer. In *Advanced Motion Control, 2010 11th IEEE International Workshop on*, pages 296–301, 2010.

[57] C. A. Klein and C. H Huang. Review of pseudoinverse control for use with kinematically redundant manipulators. *IEEE Transactions on Systems, Man, and Cybernetics*, 13:245–250, 1983.

[58] Theresa J. Klein, Tuan M. Pham, and M. Anthony Lewis. On the design of walking machines using biarticulate actuators. In *Advances In Mobile Robotics - Proceedings of the Eleventh International Conference on Climbing and Walking Robots and the Support Technologies for Mobile Machines*, pages 229–237, Coimbra, Portugal, 2008.

[59] S. Komada and K. Ohnishi. Force feedback control of robot manipulator by the acceleration tracing orientation method. *Industrial Electronics, IEEE Transactions on*, 37(1):6–12, 1990.

[60] Minayori Kumamoto, Toru Oshima, and Tomohisa Yamamoto. Control properties induced by the existence of antagonistic pairs of bi-articular muscles – mechanical engineering model analyses. *Human Movement Science*, 13(5):611–634, October 1994.

[61] F. Lacquaniti, M. Carrozzo, and N. A. Borghese. Time-varying mechanical behavior of multijointed arm in man. *Journal of Neurophysiology*, 69(5):1443 –1464, May 1993.

[62] Ho Seong Lee and M. Tomizuka. Robust motion controller design for high-accuracy positioning systems. *Industrial Electronics, IEEE Transactions on*, 43(1):48–55, 1996.

[63] T. Lenzi, S. De Rossi, N. Vitiello, A. Chiri, S. Roccella, F. Giovacchini, F. Vecchi, and M.-C. Carrozza. The neuro-robotics paradigm: NEURARM, NEUROExos, HANDEXOS. In *Engineering in Medicine and Biology Society, 2009. EMBC 2009. Annual International Conference of the IEEE*, pages 2430–2433, 2009.

[64] M. Anthony Lewis and T. J Klein. Achilles: A robot with realistic legs. In *IEEE Biomedical Circuits and Systems Conference (BIOCAS)*, 2008.

[65] C. Mavroidis, J. Nikitczuk, B. Weinberg, G. Danaher, K. Jensen, P. Pelletier, J. Prugnarola, R. Stuart, R. Arango, M. Leahey, et al. Smart portable rehabilitation devices. *Journal of neuroengineering and rehabilitation*, 2(1):18, 2005.

[66] J McIntyre, F A Mussa-Ivaldi, and E Bizzi. The control of stable postures in the multijoint arm. *Experimental Brain Research. Experimentelle Hirnforschung. Expérimentation Cérébrale*, 110(2):248–264, July 1996. PMID: 8836689.

[67] Thomas A. McMahon and George C. Cheng. The mechanics of running: How does stiffness couple with speed? *Journal of Biomechanics*, 23(Supplement 1):65–78, 1990.

[68] F. Mobasser and K. Hashtrudi-Zaad. A model-independent force observer for teleoperation systems. In *Mechatronics and Automation, 2005 IEEE International Conference*, volume 2, pages 964–969 Vol. 2, 2005.

[69] E. Z Moore and M. Buehler. Stable stair climbing in a simple hexapod robot. 2001.

[70] E. Z. Moore, D. Campbell, F. Grimminger, and M. Buehler. Reliable stair climbing in the simple hexapod'RHex'. In *Robotics and Automation, 2002. Proceedings. ICRA'02. IEEE International Conference on*, volume 3, page 2222–2227, 2002.

[71] Chet T. Moritz and Claire T. Farley. Passive dynamics change leg mechanics for an unexpected surface during human hopping. *Journal of Applied Physiology*, 97(4):1313 –1322, October 2004.

[72] FA Mussa-Ivaldi, N Hogan, and E Bizzi. Neural, mechanical, and geometric factors subserving arm posture in humans. *J. Neurosci.*, 5(10):2732–2743, October 1985.

[73] Takahiko Nakamura, Zhidong Wang, Kazunari Saito, and Kazuhiro Kosuge. Wearable antigravity muscle support system utilizing human body dynamics. *Advanced Robotics*, 20:1237–1256, November 2006.

[74] Richard R. Neptune, David J. Clark, and Steven A. Kautz. Modular control of human walking: A simulation study. *Journal of Biomechanics*, 42(9):1282–1287, June 2009.

[75] N. Neville, M. Buehler, and I. Sharf. A bipedal running robot with one actuator per leg. In *Robotics and Automation, 2006. ICRA 2006. Proceedings 2006 IEEE International Conference on*, pages 848–853, 2006.

[76] R. Niiyama, A. Nagakubo, and Y. Kuniyoshi. Mowgli: A bipedal jumping and landing robot with an artificial musculoskeletal system. In *Robotics and Automation, 2007 IEEE International Conference on*, pages 2546–2551, 2007.

[77] R. Niiyama, S. Nishikawa, and Y. Kuniyoshi. Athlete robot with applied human muscle activation patterns for bipedal running. In *Humanoid Robots (Humanoids), 2010 10th IEEE-RAS International Conference on*, pages 498–503, 2010.

[78] T. Noritsugu and T. Tanaka. Application of rubber artificial muscle manipulator as a rehabilitation robot. *Mechatronics, IEEE/ASME Transactions on*, 2(4):259–267, 1997.

[79] S. Oh and Y. Hori. Development of Two-Degree-of-Freedom control for robot manipulator with biarticular muscle torque. In *American Control Conference*, 2009.

[80] Sehoon Oh and Y. Hori. Generalized discussion on design of force-sensor-less power assist control. In *Advanced Motion Control, 2008. AMC '08. 10th IEEE International Workshop on*, pages 492–497, 2008.

[81] Sehoon Oh, Y. Kimura, and Y. Hori. Force control based on biarticular muscle system and its application to novel robot arm driven by planetary gear system. In *Intelligent Robots and Systems (IROS), 2010 IEEE/RSJ International Conference on*, pages 4360–4365, 2010.

[82] Sehoon Oh, Y. Kimura, and Y. Hori. Reaction force control of robot manipulator based on biarticular muscle viscoelasticity control. In *Advanced Intelligent Mechatronics (AIM), 2010 IEEE/ASME International Conference on*, pages 1105–1110, 2010.

[83] Sehoon Oh, Valerio Salvucci, Yasuto Kimura, and Yoichi Hori. Development of simplified statics of robot manipulator and optimized muscle troque distribution based on the statics. In *American Control Conference (ACC)*, 2011.

[84] Y. Ohba, M. Sazawa, K. Ohishi, T. Asai, K. Majima, Y. Yoshizawa, and K. Kageyama. Sensorless force control for injection molding machine using reaction torque observer considering torsion phenomenon. *Industrial Electronics, IEEE Transactions on*, 56(8):2955–2960, 2009.

[85] Y Ohta, H Yano, R Suzuki, M Yoshida, N Kawashima, and K Nakazawa. A two-degree-of-freedom motor-powered gait orthosis for spinal cord injury patients. *Proceedings of the Institution of Mechanical Engineers, Part H: Journal of Engineering in Medicine*, 221(6):629–639, January 2007.

[86] T. Oshima, T. Fujikawa, O. Kameyama, and M. Kumamoto. Robotic analyses of output force distribution developed by human limbs. In *Robot and Human Interactive Communication, 2000. RO-MAN 2000. Proceedings. 9th IEEE International Workshop on*, pages 229–234, 2000.

[87] T. Oshima, N. Momose, K. Koyanagi, T. Matsuno, and T. Fujikawa. Jumping mechanism imitating vertebrate by the mechanical function of bi-articular muscle. In *Mechatronics and Automation, 2007. ICMA 2007. International Conference on*, pages 1920–1925, 2007.

[88] R.V. Patel, H.A. Talebi, J. Jayender, and F. Shadpey. A robust position and force control strategy for 7-DOF redundant manipulators. *Mechatronics, IEEE/ASME Transactions on*, 14(5):575–589, 2009.

[89] J.E. Pratt, B.T. Krupp, C.J. Morse, and S.H. Collins. The RoboKnee: an exoskeleton for enhancing strength and endurance during walking. In *Robotics and Automation, 2004. Proceedings. ICRA '04. 2004 IEEE International Conference on*, volume 3, pages 2430–2435 Vol.3, 2004.

[90] Boris I. Prilutsky and Vladimir M. Zatsiorsky. Tendon action of two-joint muscles: Transfer of mechanical energy between joints during jumping, landing, and running. *Journal of Biomechanics*, 27(1):25–34, January 1994.

[91] Denis Rancourt and Neville Hogan. Stability in Force-Production tasks. *Journal of Motor Behavior*, 33(2):193–204, June 2001.

[92] R. Richardson, A. Jackson, P. Culmer, B. Bhakta, and M. C. Levesley. Pneumatic impedance control of a 3-d.o.f. physiotherapy robot. *Advanced Robotics*, 20(12):1321–1339, December 2006.

[93] M. Roos, S. I Yamamoto, E. Fransen, O. Ekeberg, T. Komeda, and M. Tasuku. Modeling and controlling a gait training system utilizing a biarticular muscle model. In *Japan Society of Mechanical Engineers Symposium on Welfare Engineering*, volume 2006, page 234–235, 2006.

[94] Y. Saito, K. Kikuchi, H. Negoto, T. Oshima, and T. Haneyoshi. Development of externally powered lower limb orthosis with bilateral-servo actuator. In *Rehabilitation Robotics, 2005. ICORR 2005. 9th International Conference on*, pages 394–399, 2005.

[95] Valerio Salvucci, Yasuto Kimura, Sehoon Oh, and Yoichi Hori. BiWi: Bi-Articularly actuated and wire driven robot arm. In *IEEE International Conference on Mechatronics (ICM)*, 2011.

[96] Valerio Salvucci, Yasuto Kimura, Sehoon Oh, and Yoichi Hori. Experimental verification of infinity norm approach for force maximization of manipulators driven by bi-articular actuators. In *American Control Conference (ACC)*, 2011.

[97] Valerio Salvucci, Yasuto Kimura, Sehoon Oh, and Yoichi Hori. Experimental verification of infinity norm approach for precise force control of manipulators driven by bi-articular actuators. In *International Federation of Automatic Control (IFAC)*, 2011.

[98] Valerio Salvucci, Sehoon Oh, and Yoichi Hori. Force sensor-less power assist control with variable gain for ball screw door applications. In *The Robotics Society of Japan, RSJ*, 2009.

[99] Valerio Salvucci, Sehoon Oh, and Yoichi Hori. Force Sensor-Less power assist control for low friction systems. In *Advanced Motion Control, 11th IEEE International Workshop on*, pages 290–295, 2010.

[100] Valerio Salvucci, Sehoon Oh, and Yoichi Hori. Infinity norm approach for output force maximization of manipulators driven by bi-articular actuators. In *6th Europe-Asia Congress on Mechatronics EAM, Proceedings of*, 2010.

[101] Valerio Salvucci, Sehoon Oh, and Yoichi Hori. A new approach for torque sharing of robotic arms equipped with bi-articular actuators. In *International Symposium on Application of Biomechanical Control Systems to Precision Engineering, ISAB*, 2010.

[102] D. Santos, B. Heyneman, Sangbae Kim, N. Esparza, and M.R. Cutkosky. Gecko-inspired climbing behaviors on vertical and overhanging surfaces. In *Robotics and Automation, 2008. ICRA 2008. IEEE International Conference on*, pages 1125–1131, 2008.

[103] U. Saranli and D.E. Koditschek. Back flips with a hexapedal robot. In *Robotics and Automation, 2002. Proceedings. ICRA '02. IEEE International Conference on*, volume 3, pages 2209–2215, 2002.

[104] Uluc Saranli, Martin Buehler, and Daniel E. Koditschek. RHex: a simple and highly mobile hexapod robot. *The International Journal of Robotics Research*, 20(7):616 –631, July 2001.

[105] C. Schmitt, P. Métrailler, A. Al-Khodairy, R. Brodard, J. Fournier, M. Bouri, and R. Clavel. A study of a knee extension controlled by a closed loop functional electrical stimulation. In *Proceedings, 9th An. conf. of the IFESS, Bournemouth*, 2004.

[106] Luc P. J. Selen, David W. Franklin, and Daniel M. Wolpert. Impedance control reduces instability that arises from motor noise. *The Journal of Neuroscience*, 29(40):12606 –12616, October 2009.

[107] A. Seyfarth, F. Iida, R. Tausch, M. Stelzer, O. von Stryk, and A. Karguth. Towards bipedal jogging as a natural result of optimizing walking speed for passively compliant Three-Segmented legs. *The*

International Journal of Robotics Research, 28(2):257 –265, February 2009.

[108] Y. Shibata, S. Imai, T. Nobutomo, T. Miyoshi, and S. Yamamoto. Development of body weight support gait training system using antagonistic bi-articular muscle model. In *2010 Annual International Conference of the IEEE Engineering in Medicine and Biology Society (EMBC)*, pages 4468–4471. IEEE, September 2010.

[109] Y. Shibata, M. Takagi, T. Miyoshi, R. Aoyama, S. Yamamoto, and Y. Kawakami. Development of gait training system using bi-articular muscle model. In *Symposium on Fluid Power*, volume 2008, 2008.

[110] S. Shimizu, N. Momose, T. Oshima, and K. Koyanagi. Development of robot leg which provided with the bi-articular actuator for training techniques of rehabilitation. In *Robot and Human Interactive Communication, 2009. RO-MAN 2009. The 18th IEEE International Symposium on*, pages 921–926, 2009.

[111] Ahmad Zaki Shukor and Yasutaka Fujimoto. Modelling and control of redundant robot manipulator using spiral motor. In *6th Europe-Asia Congress on Mechatronics EAM, Proceedings of*, pages 59–65, 2010.

[112] Ahmad Zaki Shukor and Yasutaka Fujimoto. Workspace control of biarticular manipulator. In *IEEE International Conference on Mechatronics (ICM), proceedings of*, 2011.

[113] Jeroen B.J. Smeets. Bi-articular muscles and the accuracy of motor control. *Human Movement Science*, 13(5):587–600, October 1994.

[114] Takahiro Sugimoto, Hiroyuki Fukusho, and Takafumi Koseki. A proposal of maximizing method of output force and acceleration for a manipulator with kinematic and muscular redundancy using linear programming method and its engineering verification. *Journal of the Robotics Society of Japan*, 2011.

[115] Y. Suzuki, K. Sugawara, and K. Ohnishi. Achievement of precise force control for a tendon-driven rotary actuator with thrust wires and a PE line. In *IECON 2010 - 36th Annual Conference on IEEE Industrial Electronics Society*, pages 1430–1435, 2010.

[116] K. Tadano, M. Akai, K. Kadota, and K. Kawashima. Development of grip amplified glove using bi-articular mechanism with pneumatic

artificial rubber muscle. In *2010 IEEE International Conference on Robotics and Automation (ICRA)*, pages 2363–2368. IEEE, May 2010.

[117] Y. Tanaka and T. Tsuji. Analysis of human hand impedance regulation ability. In *Cybernetics and Intelligent Systems, 2004 IEEE Conference on*, volume 2, pages 987–992, 2004.

[118] Y. Tanaka, T. Tsuji, and M. Kaneko. Task readiness impedance in human arm movements for virtual ball-catching task. In *Industrial Electronics Society, 2003. IECON '03. The 29th Annual Conference of the IEEE*, volume 1, pages 478–483 vol.1, 2003.

[119] N. G Tsagarakis and Darwin G Caldwell. Development and control of a Soft-Actuated exoskeleton for use in physiotherapy and training. *Autonomous Robots*, 15:21–33, July 2003. ACM ID: 792589.

[120] T. Tsuji. A model of antagonistic triarticular muscle mechanism for lancelet robot. In *2010 11th IEEE International Workshop on Advanced Motion Control*, pages 496–501. IEEE, March 2010.

[121] Toshio Tsuji, Pietro G. Morasso, Kazuhiro Goto, and Koji Ito. Human hand impedance characteristics during maintained posture. *Biological Cybernetics*, 72(6):475–485, May 1995.

[122] A. Umemura, Y. Saito, and K. Fujisaki. A study on power-assisted rehabilitation robot arms operated by patient with upper limb disabilities. In *IEEE International Conference on Rehabilitation Robotics, 2009. ICORR 2009*, pages 451–456. IEEE, June 2009.

[123] A. Umemura, Y. Saito, and T. Haneyoshi. The rigidity of the biarticular robotic arm with a planetary gear. In *Advanced Motion Control, 2010 11th IEEE International Workshop on*, pages 490–495, 2010.

[124] T. Umeno and Y. Hori. Robust speed control of DC servomotors using modern two degrees-of-freedom controller design. *Industrial Electronics, IEEE Transactions on*, 38(5):363–368, 1991.

[125] Gerrit Jan Van Ingen Schenau. From rotation to translation: Constraints on multi-joint movements and the unique action of bi-articular muscles. *Human Movement Science*, 8(4):301–337, August 1989.

[126] Gerrit Jan van Ingen Schenau. Proposed actions of bi-articular muscles and the design of hindlimbs of bi- and quadrupeds. *Human Movement Science*, 13(5):665–681, October 1994.

[127] Arthur J. van Soest, Arend L. Schwab, Maarten F. Bobbert, and Gerrit Jan van Ingen Schenau. The influence of the biarticularity of the gastrocnemius muscle on vertical-jumping achievement. *Journal of Biomechanics*, 26(1):1–8, January 1993.

[128] G.D. White, R.M. Bhatt, C.P. Tang, and V.N. Krovi. Experimental evaluation of dynamic redundancy resolution in a nonholonomic wheeled mobile manipulator. *Mechatronics, IEEE/ASME Transactions on*, 14(3):349–357, 2009.

[129] K. Yoshida, N. Hata, S. Oh, and Y. Hori. Extended manipulability measure and application for robot arm equipped with bi-articular driving mechanism. In *Industrial Electronics, 2009. IECON '09. 35th Annual Conference of IEEE*, pages 3083–3088, 2009.

[130] K. Yoshida, T. Uchida, and Y. Hori. Novel FF control algorithm of robot arm based on bi-articular muscle principle - emulation of muscular viscoelasticity for disturbance suppression and path tracking. In *Industrial Electronics Society, 2007. IECON 2007. 33rd Annual Conference of the IEEE*, pages 310–315, 2007.

[131] Xiaocong Zhu, Guoliang Tao, Bin Yao, and Jian Cao. Adaptive robust posture control of parallel manipulator driven by pneumatic muscles with redundancy. *Mechatronics, IEEE/ASME Transactions on*, 13(4):441–450, 2008.

[132] M. Zinn, O. Khatib, B. Roth, and J.K. Salisbury. Playing it safe [human-friendly robots]. *Robotics & Automation Magazine, IEEE*, 11(2):12–21, 2004.

[133] A.B. Zoss, H. Kazerooni, and A. Chu. Biomechanical design of the berkeley lower extremity exoskeleton (BLEEX). *Mechatronics, IEEE/ASME Transactions on*, 11(2):128–138, 2006.

List of Publications

Journals

1. **V. Salvucci**, Y. Kimura, S. Oh, and Y. Hori, "Force Maximization of Bi-articularly Actuated Manipulators Using Infinity Norm", IEEE/ASME Transaction on Mechatronics, 2011 [Submitted].

2. **V. Salvucci**, Y. Kimura, S. Oh, and Y. Hori, "Non-linear Phase Different Control for Precise Output Force of Bi-Articularly Actuated Manipulators" *Advanced Robotics*, 2011. [Submitted]

3. **V. Salvucci**, T. Sugimoto, Y. Kimura, S. Oh, T. Koseki, and Y. Hori, "Comparing Methods for Resolving Actuator Redundancy in Robots with Animal-like Musculoskeletal Actuation Structure", IEEE/ASME Transaction on Mechatronics, 2011 [To be submitted to Special Issue on "Bio-Inspired Mechatronics" in TMECH].

International Conferences

1. **V. Salvucci**, Y. Kimura, S. Oh, and Y. Hori, "Experimental Verification of Infinity Norm Approach for Precise Force Control of Manipulators Driven by Bi-articular Actuators", in International Federation of Automatic Control (IFAC), 2011 [To be presented].

2. S. Oh, **V. Salvucci**, Y. Kimura, and Y. Hori, "Mathematical and Experimental Verification of Efficient Force Transmission by Biarticular Muscle Actuator", in International Federation of Automatic Control (IFAC), 2011 [To be presented].

3. **V. Salvucci**, Y. Kimura, S. Oh, and Y. Hori, "Experimental Verification of Infinity Norm Approach for Force Maximization of Manipulators Driven by Bi-Articular Actuators", in American Control Conference (ACC), 2011.

4. S. Oh, **V. Salvucci**, Y. Kimura, and Y. Hori, "Development of Simplified Statics of Robot Manipulator and Optimized Muscle Torque Distribution Based on the Statics", in American Control Conference (ACC), 2011.

5. **V. Salvucci**, S. Oh, and Y. Hori, "Disturbance Rejection Improvement in Non-Redundant Robot Arms using Bi-articular Actuators", in Industrial Electronics (ISIE), IEEE International Symposium on, 2011.

6. **V. Salvucci**, Y. Kimura, S. Oh, and Y. Hori, "BiWi: a Bi-Articularly Actuated and Wire Driven Robotic Arm", in IEEE International Conference on Mechatronics (ICM), 2011.

7. **V. Salvucci**, S. Oh, and Y. Hori, "Infinity Norm Approach for Precise Force Control Of Manipulators Driven by Bi-articular Actuators", in 36th Annual Conference of the IEEE Industrial Electronics Society, IECON, 2010, pp. 1908-1913.

8. **V. Salvucci**, S. Oh, and Y. Hori, "Infinity Norm Approach for Output Force Maximization of Manipulators Driven by Bi-articular Actuators", in 6th Europe-Asia Congress on Mechatronics EAM, Proceedings of, 2010.

9. **V. Salvucci**, S. Oh, and Y. Hori, "A New Approach for Torque Sharing of Robotic Arms Equipped with Bi-articular Actuators", in International Symposium on Application of Biomechanical Control Systems to Precision Engineering, ISAB, 2010.

10. **V. Salvucci**, S. Oh, and Y. Hori, "New Approach to Force Sensor-Less Power Assist Control for High Friction and High Inertia Systems", in Industrial Electronics (ISIE), IEEE International Symposium on, pp. 3559-3564, 2010.

11. **V. Salvucci**, S. Oh, and Y. Hori, "Force Sensor-Less Power Assist Control for Low Friction Systems", in Advanced Motion Control, 11th IEEE International Workshop on, 2010, pp. 290-295.

Domestic Conferences

1. **V. Salvucci**, S. Oh, and Y. Hori, "Optimal Actuator Torques Distribution for Bi-articular Driven Manipulators", in The Robotics Society of Japan, RSJ, 2010.

2. **V. Salvucci**, S. Oh, and Y. Hori, "Force Sensor-less Power Assist Control with Variable Gain for Ball Screw Door Applications", in The Robotics Society of Japan, RSJ, 2009.